NASA Technical Paper 1695

Development and Validation of a Hybrid-Computer Simulator for a Transonic Cryogenic Wind Tunnel

Jerry J. Thibodeaux and S. Balakrishna

SEPTEMBER 1980

NASA

NASA Technical Paper 1695

Development and Validation of a Hybrid-Computer Simulator for a Transonic Cryogenic Wind Tunnel

Jerry J. Thibodeaux
Langley Research Center
Hampton, Virginia

S. Balakrishna
Old Dominion University
Norfolk, Virginia

NASA
National Aeronautics
and Space Administration

Scientific and Technical
Information Branch

1980

SUMMARY

Experience during the past 6 years of operation of the Langley 0.3-Meter Transonic Cryogenic Tunnel has shown that there are problems associated with the operation and control of such tunnels. One problem has been an inability to provide long-term accurate control of test parameters. Additionally, the time required for transition from one test condition to another has proven to be excessively long. Due to the high degree of process cross-coupling between the independent control variables, man-in-the-loop operation has proven to be much less efficient than desirable in terms of liquid-nitrogen and electrical-power usage. For these reasons, studies have been undertaken at the Langley Research Center to model the cryogenic-wind-tunnel process, to validate the model by the use of experimental data, and to construct an interactive tunnel simulator with the validated model. Additionally, this model has been used to design closed-loop feedback control laws for regulation of the temperature and pressure parameters.

The global mathematical model that has been developed consists of coupled, nonlinear differential governing equations based on an energy-state concept of the physical cryogenic phenomena. Although the fundamental process is quite stable, the tendency for continuous drifting from balanced equilibrium energy conditions is prevalent. The process equations, the simulation responses, and the experimental data are provided here for future reference. Also included are the control laws and simulator responses using these closed-loop feedback schemes.

INTRODUCTION

Historically, capital and operating costs have tended to keep transonic wind tunnels small, and the many problems encountered at high pressures have tended to keep operating pressures low. The net result has been that existing (ambient temperature) tunnels operate at Reynolds numbers which are far too low to insure proper simulation of the flow experienced in flight, particularly with regard to shock—boundary-layer interactions encountered on modern high-subsonic and transonic aircraft.

Of the various ways of increasing Reynolds number that have been tried or proposed for transonic tunnels, cooling the test gas to cryogenic temperatures (150 K or lower) appears to be the best solution in terms of model, balance, and sting loads, as well as capital and operating costs (ref. 1). Personnel at the NASA Langley Research Center (LaRC) have been studying the application of the cryogenic-tunnel concept to various types of high Reynolds number transonic tunnels since the autumn of 1971 and, through extensive theoretical and experimental studies, have successfully demonstrated both the validity and practicality of the concept. As a result of this work, the first major transonic tunnel especially designed to take full advantage of cryogenic operation is now under construction at LaRC. This tunnel, the National Transonic

Facility (NTF), will provide an order of magnitude increase in Reynolds number capability over existing tunnels in the United States when it becomes operational in 1982.

It can be shown that for equal test Reynolds numbers and for any arbitrary maximum operating pressure, a cryogenic tunnel uses less total energy, and therefore costs less to operate, than an ambient temperature tunnel doing the same amount of testing. Even so, the operation of large cryogenic tunnels will be very expensive in absolute terms. For example, the NTF, when operating at its maximum Reynolds number of 120×10^6 at transonic speeds, will use liquid nitrogen (LN_2) at the rate of approximately 454 kg/sec (1000 lb/sec). Although the average LN_2 usage rate in the NTF will be much less than 454 kg/sec, it is still highly desirable, if not essential, that the tunnel be operated in an efficient automatic manner in order to minimize LN_2 consumption.

Experience with the Langley 0.3-Meter Transonic Cryogenic Tunnel (0.3-m TCT) (ref. 2) demonstrated the need for automatic control systems if the full potential of the cryogenic tunnel is to be realized. Although the basic cryogenic process is stable, there is a strong tendency for drifting from preset test conditions because of the heat-transfer effects created by imperfect tunnel insulation. Additionally, due to the high degree of process cross-coupling between independent control variables (temperature, pressure, and drive-fan speed) and the desired test conditions (Mach number, Reynolds number, and dynamic pressure), man-in-the-loop operation has proven to be much less efficient than desired in terms of LN_2 and electrical-power usage.

In order to meet the specific control needs of the 0.3-m TCT as well as to study the control requirements of cryogenic tunnels in general, a study has been undertaken at LaRC to develop and validate a mathematical model of 0.3-m TCT process, to utilize the model in a hybrid-computer simulation to design temperature- and pressure-feedback control laws, and to evaluate the adequacy of these control schemes by analysis of closed-loop data. The results of this study are reported herein.

SYMBOLS

A	area, m^2 or percent
b	pressure-loss coefficient
c_m	specific heat capacity of metal, J/kg-K
c_p	specific heat capacity of gas at constant pressure, J/kg-K
c_v	specific heat capacity of gas at constant volume, J/kg-K
D	dimensionality constant
E	total energy, J
h	specific enthalpy, J/kg

K	gain
K_M	$= 597(1 - 0.3M)p^{-0.035}$
M	Mach number
$\dot{m}$	mass flow rate, kg/sec
N	fan speed, rpm
p	total pressure, atm (1 atm = 101.3 kPa)
$\dot{Q}$	heat flow, J/sec
r	pressure ratio
s	Laplace variable
T	total temperature, K
t	time, sec
U	internal energy, J
u	specific internal energy, J/kg
V	volume, m^3
W	mass, kg
y	heat-transfer coefficient, J/sec-K
α	cooling capacity of gaseous nitrogen, J/kg
β	cooling capacity of liquid nitrogen, J/kg
γ	ratio of specific heats
η	fan efficiency
θ	thermal mass, J/kg
τ	transport time lag, sec

Subscripts:

a	acoustic
c	tunnel circuit
e	exit

F	fan
G	gas
i	inlet
L	liquid
m	metal
p	plenum
set	set point value

The use of a dot over a quantity denotes the derivative of the quantity with respect to time.

MATHEMATICAL MODEL OF THE LANGLEY 0.3-METER TRANSONIC CRYOGENIC TUNNEL

The development of a control-compatible model of the 0.3-m TCT (shown schematically in fig. 1) has been discussed in detail in reference 3. The fundamental principles, assumptions, and equations of this modeling effort are presented in the appendix of this paper. These governing equations provide a simple, single lumped-parameter multivariable process model of the 0.3-m TCT. Control analysis of the mass-energy interaction existing between the mass of gas in the tunnel and the control input parameters was used to develop the dynamic model from which the real-time interactive simulator was assembled. This resulted in a concept of energy control of the tunnel by manipulation of the process states.

The basic thermodynamic equation for determining the time rate of change of the total energy of the gas (ignoring potential and kinetic energy) is

$\dot{E}$ = Heat from the tunnel metal + Heat of compression from the fan

+ Heat from injection of LN_2 + Heat from exhaust of gaseous nitrogen (GN_2)

or

$$\dot{E} = \frac{\partial}{\partial t}(W_G c_v T) = -\int^{\text{Surface}} \dot{Q}_m + \dot{Q}_F + \dot{m}_L h_L - \dot{m}_G c_p T \qquad (1)$$

with heat energy added to the gas being positive.

After mathematical manipulation, adding the transport delays involved in the measurements, and using the definitions $\dot{Q}_m = \frac{W_m c_m T s}{1 + t_m s}$, $\alpha = (c_p - c_v)T$, and $\beta \cong h_L - c_p T$ from reference 3, the temperature dynamics of the tunnel can be written

$$\frac{\partial T}{\partial t}\left(\frac{1 + t_G s}{1 + t_m s}\right) = \frac{(\beta + \alpha)}{\theta} \dot{m}_L e^{-\tau_L s} - \left(\frac{\alpha}{\theta}\right)\dot{m}_G e^{-\tau_G s} + \frac{\dot{Q}_F}{\theta} e^{-\tau_F s} \tag{2}$$

where $\theta = W_G c_v + W_m c_m$.

From the ideal gas law, the pressure of a confined gas is proportional to the mass of the gas and its temperature, $p = K_1 W_G T$. After taking the appropriate derivatives and making substitutions, the time rate of change of pressure may be expressed as

$$\frac{\partial p}{\partial t} = \frac{p}{T}\frac{\partial T}{\partial t} + \frac{p}{W_G}\frac{\partial W_G}{\partial t} \tag{3}$$

After substitutions and manipulation, the pressure dynamics for the tunnel can be written

$$\dot{p} = \frac{\partial p}{\partial t} = \frac{p}{W_G}\dot{m}_L e^{-\tau_L s} - \frac{p}{W_G}\dot{m}_G e^{-\tau_G s} + \frac{p}{T}\dot{T} + DbMp\frac{\partial M}{\partial t} \tag{4}$$

where $b = 0.197\left(1 - \frac{7pM}{T}\right)$. Equations (2) and (4) permit the description of the temperature and pressure response characteristics of the gas in the tunnel due to the tunnel control inputs.

Other important relationships necessary for modeling the 0.3-m TCT are given as follows. The form of the equations used here reflects the specific physical characteristics of the 0.3-m TCT and the various elements used for measurement and control of the test conditions.

Mach number:

$$M = \frac{N e^{-\tau_a s}}{K_M \sqrt{T}(1 + t_p s)} \tag{5}$$

where

K_M $= 597(1 - 0.3M)p^{-0.035}$

t_p plenum time constant

τ_a acoustic time lag

Tunnel circuit time:

$$t_c = \frac{0.0149V}{AM\sqrt{T}}\left(1 + 250\,\frac{p}{T^2}\right)(1 + 0.2M^2)^3 \tag{6}$$

LN_2 flow rate:

$$\dot{m}_L = K_L A_L = 3.47\sqrt{p_L - p}\,A_L \qquad (0 \leqq A_L \leqq 100\%) \tag{7}$$

GN_2 flow rate: (Since K_G is a function of p, two relationships are applicable for GN_2 flow rate.)

$$\dot{m}_G = K_G\,\frac{p}{\sqrt{T}}\,A_G = 2.18\,\frac{p}{\sqrt{T}}\,A_G \qquad \begin{pmatrix} p > 1.5 \text{ atm} \\ 0 \leqq A_G \leqq 100\% \end{pmatrix}$$

$$\dot{m}_G = K_G\,\frac{p}{\sqrt{T}}\,A_G = \left[2 - \left(\frac{1.5}{p}\right)^{1.7}\right]21.8\,\frac{p}{\sqrt{T}}\,A_G \qquad \begin{pmatrix} 1 \leqq p \leqq 1.5 \text{ atm} \\ 0 \leqq A_G \leqq 100\% \end{pmatrix} \tag{8}$$

Mass of gas in tunnel:

$$W_G = 341.4\,\frac{pV}{T}\left(1 + 250\,\frac{p}{T^2}\right)\left(1 - 0.033M^{1.5}\right) \tag{9}$$

Fan pressure ratio:

$$r = 1 + \left[0.197\left(1 - \frac{7pM}{T}\right)\right]M^2 \tag{10}$$

Metal enthalpy:

$$h = 2.75T^2 - 0.0026T^3 \tag{11}$$

Fan dynamics:

$$\frac{N}{N_{set}} = \frac{1}{0.2s^2 + 0.56s + 1} \tag{12}$$

Cooling capacities:

$$\beta = -\left(121 + 2p + \frac{66}{T} - \frac{391p}{T} + 1.04T\right) \cong h_L - c_pT$$

$$\alpha = (c_p - c_v)T \tag{13}$$

Fan heat:

$$\dot{Q}_F = \frac{K_F p M^3 \sqrt{T}}{(1 + 0.2M^2)^3} \tag{14}$$

where

$$K_F \triangleq \frac{6965Ac_pb}{\eta}\left(\frac{\gamma - 1}{\gamma}\right)$$

These equations describe the lumped-parameter mathematical model of the 0.3-m TCT shown in the sketch in figure 1 and the photograph in figure 2. The location of the three control inputs, the sensor locations, and some of the physical characteristics of the tunnel are shown in figure 1. The multivariable model used for developing the simulator is presented in figure 3 in matrix form. The model outputs (temperature rate, Mach number, and pressure rate) are related to the inputs (LN_2 injection-valve area, fan speed, and GN_2 exhaust-valve area) through the complex dynamics of the system. Examination of the model shows it to be highly coupled and nonlinear in nature. If coupling between the variables were not present, that is, if there were no off-diagonal matrix terms, variation of the LN_2 injection-valve area, the drive-fan speed,

or the GN_2 exhaust-valve area would result in independent changes in the total temperature, test-section Mach number, and total pressure, respectively.

The valve-area openings in the matrix control the mass flow rates of liquid and gaseous nitrogen through the process dynamics to affect rates of change in temperature and pressure. First-order changes in Mach number are controlled by changing the speed of the drive fan. An important feature of this model is the large contribution to the process dynamics made by the energy stored in the metal of the tunnel and by the GN_2 heat-transfer time constant (which varies significantly as a function of test-section Mach number, pressure, and temperature). The importance of these factors will become evident during the examination of tunnel response data in a subsequent section of this paper.

Transport time delays have been included in the model to account for the mean time between initiating the various control inputs and measuring the resultant changes in the test conditions. For example, the transport time delay associated with the input of LN_2 is the lag corresponding to the transit time from the LN_2 injection valves to just ahead of the screen section where temperature is measured by a thermocouple.

Simulation of the 0.3-m TCT

At the beginning of this study, it was decided to develop a computer simulator of the 0.3-m TCT to give hands-on interactive capability for the process and control studies. Furthermore, it was anticipated that a simulator of this type would be valuable for evaluating various operating techniques as well as for the training of tunnel operator personnel. Consequently, the computer selected for the modeling and simulation effort was a hybrid computer system which permits manual interaction along with high-speed digital computation.

Solution of the system process equations was undertaken on the hybrid-computer system shown in figure 4. Basically, the computer consists of a central digital processor unit and an analog computer electrically interfaced for data exchange. The rate of update between the digital and analog computer systems is 25 Hz.

Because of the nonlinearity and the time dependency of the model, computations were segregated into two parts. All nonlinear computations were performed digitally but integration of process equations took place continuously in the analog side of the computer system. Shown in figure 5 is a functional block diagram of the hybrid-computer simulation. Ten inputs from the analog computer unit (after analog-to-digital conversion) are used in the digital computer to compute the equations shown in figure 5. The computation in the digital computer results in 11 outputs appropriately scaled and converted to analog signals for input to the integrating analog side of the hybrid system. The loop diagrams of the model dynamics and simulation control along with the digitally controlled attenuators which allow the nonlinear digital calculations to be introduced into the analog computer are presented in figure 6. Tunnel temperature dynamics (fig. 6(a)) are obtained from integration of the temperature rate whereas tunnel gas temperature T is used to derive the metal temperature by using the inverse of the metal time constant $1/t_m$. The metal-

to-gas heat flow signal $T_m - T$ is used to derive $-\dot{T}$ in a looped manner. Measured gas temperature for display and closed-loop controller use is created by digital data provided through the digital attenuators.

Pressure, fan, and Mach number dynamics (fig. 6(b)) are derived by the integration of scaled pressure rate $10\dot{p}$. A coupling term $\dot{N}$ has been included to generate the influence of fan acceleration on the rate of change of pressure. Fan-speed modeling is effected by an acceleration-limited second-order transfer function. Fan revolutions per minute and Mach number display information for the simulator operator panel are acquired after appropriate scaling with analog potentiometers.

Figure 6(c) shows details of the patching necessary to create and control the 3-sec pulse inputs used to study the tunnel-model behavior from balanced conditions after various disturbances. Also shown in this figure are the valve-area display signals for the operator console panel, which will be described later.

The last analog diagram used by the hybrid-computer simulator and shown in figure 6(d) is the closed-loop feedback control law for the temperature and pressure loops. Proportional and integral (PI) type controllers and the gain schedules for the respective variables are displayed. Voltage clipping was necessary to prevent negative voltages since the valve-opening area can only be positive.

It was recognized early in this work that experimental data were required to validate the process model. As a result, the first phase of work was to obtain data for dynamic response of temperature, pressure, and Mach number to changes of the input variables throughout the tunnel operational envelope. Figure 7 is a photograph of the control panel of the 0.3-m TCT as it was at the time of these response tests. Principal control inputs are LN_2 injected rate, GN_2 exhaust rate, and fan speed. Both the LN_2 and GN_2 flow rates are manually controlled by commands to specially designed digital valves. These digital valves are revolutionary advances in the state of the art of fluid control and measurement. Multiple-venting control ports, each fitted with an accurately precalibrated, binary-weighted venturi, allow selection of 256 or more discrete flow rates. Thus, for the 8-bit digital valves used in the 0.3-m TCT, fluid flow rate can be controlled to within 1 part in 256 (2^8) with extreme repeatability. Because each control port is bistable (either fully open or fully closed), there is no valve deadband or overshoot which can be experienced with conventional analog valves. Also, each port can be modularly replaced or serviced without removing the whole valve from its location. Figure 8 is a schematic of the commercially available digital exhaust valve.

Inputs to the injection or exhaust systems were realized by pulsing a selected element of the appropriate digital valve. For these tests, the 6.25 percent of full-flow element was cycled. Mach number dynamics were determined by means of a 100-rpm step change in speed of the drive-fan motor. Total temperature, total pressure, and Mach number as well as the three input commands were recorded at a rate of 40 samples per second for the tunnel conditions (given in table I), which span the entire operational range of the 0.3-m TCT. The photograph of the tunnel (fig. 2) shows the LN_2 injection

valves (upper right), the fan section (lower right), and the piping leading to the digital exhaust valve (center left).

Operator Control and Display Panel

In addition to studies of the process dynamic behavior, an important reason for the simulation was to achieve man-in-the-loop interaction so that 0.3-m TCT operational techniques could be investigated. Also, with such a simulator operator training could be accomplished at an insignificant cost compared with training in the tunnel. After appropriate scaling and electrical hookup to the analog patchboard, an operator display and control panel (shown in fig. 9) was made available for the hybrid-computer simulation. Operator inputs are made through potentiometers which control the simulated liquid- and gaseous-nitrogen valve openings and the fan speed. The temperature, pressure, and Mach number digital displays permit realistic simulation of tunnel operation including operator imposition of constraints such as maximum cool-down rate or metal-to-gas temperature difference. Displays not provided on the simulator control panel but present on the tunnel control panel include liquid-nitrogen pump pressure, drive-fan motor power, and digital-valve status indicator lights.

Recording Instrumentation

The technique used to record the experimental data acquired from the 0.3-m TCT was straightforward and consisted of simply patching analog parameter outputs to a remotely located recording system. Data were directly digitized at a rate of 40 samples per second, converted into engineering units, and placed on computer files so that computer plots could be generated and analyzed relative to the simulator results.

The procedure for obtaining the simulator data was not quite as straightforward. Instead of direct digitization, the simulation data had to be first recorded on an FM wide-band recording tape. The recorder is shown in figure 10. The data were then put through a 40-sampler-per-second digitizing process for conversion to engineering-unit tapes which were used to create the computer file data base for simulator validation.

Validation of the 0.3-m TCT Tunnel Simulator

In order to validate the analytical model of the 0.3-m TCT used to develop the real-time cryogenic-tunnel simulator, a number of tests were performed both on the tunnel and the simulator. The results of these separate tests are compared and discussed. Details of the experimental-response tests are presented and the features of the data are correlated with the mathematical terms for validation of the simulator model.

It is well known that linear time-invariant dynamic systems yield transient characteristic responses to deterministic inputs (i.e., sine-wave, step,

ramp, impulse, or doublet inputs). These time-dependent responses can be directly compared with simulated responses. The cryogenic process is obviously time invariant, and though it is nonlinear, the tunnel characteristics can be easily analyzed by assuming linear behavior for small perturbations around an equilibrium point. Because the cryogenic-tunnel process has open-loop integrating temperature and pressure dynamics, step-input disturbances from equilibrium were deemed unsatisfactory since saturation of responses would result. Also, for the actual tunnel, sinusoidal disturbances are difficult to realize except for fan-speed inputs. Consequently, easily generated mass impulse inputs were selected for creation of transient responses for both the 0.3-m TCT and the simulator. An additional argument for impulse inputs is that responses can be analyzed with regression analysis techniques for parameter identification even when the responses are corrupted by measurement noise.

During the response tests, both the 0.3-m TCT and the 0.3-m TCT simulator were established at specified equilibrium conditions by open-loop adjustment of the three control inputs and then subjected to impulse disturbances of LN_2 mass injection, GN_2 mass exhaust, and drive-fan speed. The disturbances were applied serially with sufficient time allowed between impulses to allow transients to decay and equilibrium to be reestablished.

The amplitudes and duration of the perturbations were selected so that changes in the tunnel conditions would be in excess of system noise. Thus, a 6.25-percent increment in the LN_2 valve full-open area, a 6.25-percent increment in the GN_2 valve full-open area, and a 100-rpm decrease in drive-fan speed were chosen as the input perturbation amplitudes. Each of these inputs was imposed for a period of approximately 3 sec. This pulse duration corresponds to 3/4 to 4 tunnel-circuit time periods, depending on test conditions. Typically, these pulse inputs create changes in temperature of 0.5 K to 6.0 K, changes in pressure of 0.017 to 0.102 atm, and changes in Mach number of 0.006 to 0.030. The dynamic responses of the experimental data and the simulation data are compared in figures 11 to 37 for the various test conditions selected to cover the full range of operation of the 0.3-m TCT.

Inspection of the data shows that the records for the simulator responses are practically noise free whereas the tunnel data exhibit some measurement and recording noise. The Mach number traces show a larger level of noise because Mach number is calculated from two pressure records, each of which has its own noise component. One particular problem encountered in obtaining the experimental data from the 0.3-m TCT was a 10- to 20-percent random drift from the nominal value in the LN_2 pump pressure. This prevented accurate measurement of the mass flow of the LN_2 injected into the tunnel.

Once equilibrium was established, perturbation of the 6.25-percent element of the LN_2 valve admitted an additional mass of LN_2 into the tunnel circuit, typically between 0.5 and 1.5 kg per pulse. Perturbation of the 6.25-percent element of the GN_2 valve exhausted an additional mass of GN_2 to the atmosphere, typically between 0.2 and 1.0 kg per pulse.

ANALYSIS OF TUNNEL AND SIMULATOR

Transient Responses

Figures 11, 28, and 29 are provided as typical impulse responses alphabetically subdivided so that various features and characteristics of the temperature, pressure, and Mach number trajectories can be identified and explained. Prior to any intentional system disturbance the equilibrium conditions for the cases studied were established. The segment ABCD defines the portion of the response influenced by the perturbation to the LN_2 valve area. The segment EFG defines the portion of the response influenced by the perturbation to the GN_2 valve area. The segment HJK defines the portion of the response influenced by the perturbation of the drive-fan speed. Correlation of these dynamic records with the model mathematics was performed to provide better comprehension and insight into why specific results are obtained. This is done in the following sections for the three control inputs.

LN_2 Pulse Input

Temperature response.- Refer to the temperature trace of figure 11. Prior to A the tunnel was placed in a balanced mass and energy condition such that the rates of change of pressure and temperature were zero ($\dot{p} = \dot{T} = 0$), the liquid-mass inflow was equal to the gaseous-exhaust outflow ($\dot{m}_L = \dot{m}_G$), and temperature, pressure, and Mach number were constant. During segment AC, LN_2 mass flow rate is increased by $\Delta\dot{m}_L$ due to the increase in valve area of 6.25 percent of the full-open valve area during the perturbation. This creates a negative temperature gradient ($\dot{T} < 0$) due to the negative β term in equation (2). As the temperature of the gas in the tunnel rapidly drops, the temperature of the metal in the tunnel shell lags behind and begins releasing stored heat energy to the gas. Eventually the amplitude of the temperature gradient is dynamically reduced as dictated by the lead/lag term of equation (2). Gas temperature (at the measuring station) continues to drop beyond point C. The value $\Delta\dot{m}_L$ returns to zero due to removal of the perturbation and closure of the 6.25-percent element of the LN_2 injection valve. Recovery from the perturbation takes place in the segment CD due to continued heat transfer from the walls to the gas. At point D, most of this heat transfer is completed. It may be noted that there exists an obvious temperature transport delay relative to the commanded input position. This corresponds to that portion of the circuit time constant (see eq. (6)) consistent with the circuit length between the LN_2 injection station and the temperature-measurement station. All temperature data (figs. 11 to 37) display this delay characteristic.

The temperature differential established between C and D by first a negative gradient (due to liquid input) and then a positive gradient (due to wall heat release) can be predicted by reexamination of equation (2). For zero change in exhaust flow and no added heat contribution from a steadily running fan, only LN_2 influences the differential temperature ΔT (or $\dot{T}$). If ΔT is represented by $\frac{(1 + t_m s)}{(1 + t_G s)}\left(\frac{\beta + \alpha}{\theta}\right)\dot{m}_L e^{-\tau_L s}$ and $\frac{1}{\theta}\left(\frac{1 + t_m s}{1 + t_G s}\right)$ is transiently

approximated by $\frac{1}{W_G c_v}$ (since the energy of the $W_m c_m$ term in $\theta = W_G c_v + W_m c_m$ is released only after a long time period), then $\frac{\left(\beta \dot{m}_L e^{-\tau_L s} + \dot{Q}_L\right)}{W_G c_v}$. By using this simplified analysis, the largest value of ΔT should occur when β is largest and W_G is smallest. Equation (9) shows W_G is smallest when pressure is lowest and temperature is highest. For the tunnel conditions tested, W_G is smallest at a pressure of 1.5 atm and a temperature of 275 K. The experimental (tunnel) data presented in figures 11 and 29, for example, confirm that the maximum ΔT does, in fact, occur under conditions of minimum W_G. For the condition of constant temperature, as the mass of the gas in the tunnel increases with increasing pressure, the amplitude of ΔT should decrease correspondingly. Such a decrease in ΔT is shown, for example, in figures 29, 32, and 35. Thus, the smallest ΔT occurs when β is smallest and W_G is largest. For the conditions examined this occurs at 5.0 atm and 100 K. The tunnel data presented in figures 17 to 19 exhibited the smallest values of ΔT as predicted. The magnitude of recorded temperature differentials is somewhat smaller than predicted because of some filtering of the actual temperature measurements due to the response characteristics of the thermocouple used for the temperature sensor.

Pressure response.- Refer again to figure 11. With attention now focused on the pressure trace, the following analysis will explain the pressure behavior of the tunnel. Equation (4) is the tunnel state relationship for the rate of change of operating pressure. With constant values of gaseous exhaust and fan contributions in the pressure rate equation, only the cooling term $\frac{p}{T}\dot{T}$ and the mass term $\frac{p}{W_G}\Delta\dot{m}_L e^{-\tau_L s}$ influence the pressure gradient. For segment AB of the pressure trace, $\dot{p}$ is negative because the cooling term is larger than the mass term. At point B the two terms are equal and opposite. As a result, $\dot{p} = 0$ and the minimum pressure is realized. For the segment BC, the mass term becomes much larger because of the additional liquid-mass input, and despite a negative $\dot{T}$, a positive $\dot{p}$ ensues. Thus, the positive pressure gradient from B to C is due to the dominant heat transfer from the tunnel wall to the test gas. At point C, $\Delta\dot{m}_L$ is reduced to zero by reducing the valve incremental area to zero. Because the wall is warmer than the gas, the net heat flow to the gas causes $\dot{T}$ to become positive in the $\frac{p}{T}\dot{T}$ term. As a result, $\dot{p}$ increases until the heat transfer is complete and a new equilibrium value of p is established.

This initial decrease in pressure due to the liquid input followed by an increase in pressure is characteristic of all conditions tested for the simulator and the tunnel. (See figs. 11 to 37.) The location of the minimum pressure (point B) varies as a function of the test conditions of the tunnel. For gas temperatures of 100 K, the minimum pressure consistently occurs very near the end of the liquid input (point C). (See figs. 11 to 19.) On the other

hand, at a gas temperature of 275 K, the minimum pressure is very near the beginning of the liquid input (point A). This indicates that a much more rapid pressure recovery is established because of the large amount of energy released from the tunnel walls. This is as expected since the metal enthalpy (eq. (11)) at 275 K is eight times the enthalpy at 100 K. At the intermediate gas temperature of 200 K, the minimum pressure varies in location between points A and C. This is due to the different values of the cooling effect experienced because of varying degrees of wall heat release. It should be noted that minimum pressure shifts toward point C as gas-weight increases (i.e., increase in pressure). The data presented in figures 20, 23, and 26 illustrate this for the 200 K case.

An interesting point in the study of the response of tunnel pressure to liquid input is the system behavior at point D. When this point is reached, most of the heat-transfer effects have been completed and tunnel recovery begins. At temperatures of 200 K or 275 K (figs. 20 to 37), the pressure level at point D is much higher than the starting or initial equilibrium pressure whereas at 100 K (figs. 11 to 19) the final pressure is almost the same as the starting pressure. On the other hand, the recovery pressure gradient is not as pronounced at the lower temperature. The higher temperature data indicate that the slope of the recovery gradient increases more negatively as the Mach number increases. (See figs. 20 to 22 and figs. 29 to 31.) These larger negative gradients can be explained with the help of equations (4) and (8). The rate of change of pressure $\dot{p}$ is a function of exhaust-mass flow rate which itself is related to $\frac{p}{\sqrt{T}} A_G$. The exhaust valve area A_G at the higher Mach numbers has to be larger to maintain equilibrium, and therefore when the incremental liquid input is removed, more GN_2 is being exhausted from the tunnel, resulting in larger negative values of $\dot{p}$. Note that there exists essentially no delay in the response of tunnel pressure to changes in LN_2 flow rate.

Mach number response.- The response of Mach number to liquid input can be evaluated by using equation (5), which indicates that Mach number is inversely proportional to the square root of temperature for constant fan speed N. Therefore, when the LN_2 flow rate is increased, temperature falls, the speed of sound decreases, and since flow velocity is constant, the Mach number increases. This situation is illustrated, for example, in figure 11 in the increase in Mach number for segment AC. Coupling between temperature and Mach number is caused by the increase in fan pressure ratio due to the reduced temperature. (See eq. (10).) At point C, the Mach number response has the largest deviation, which can be related to the gas temperature-response amplitude by $\frac{\Delta M}{M} \cong -\frac{\Delta T}{2T}$ (derived from eq. (5)). Figure 11 shows that for a Mach number of 0.3 and a temperature of 100 K the perturbation in liquid flow rate causes a change in Mach number of 0.006. (A computed value of $\Delta T = -4$ K results.) Because of the previously mentioned first-order filtering effects of the thermocouple, the recorded experimental data from the tunnel indicate a ΔT of only about -1.5 K. All of the temperature-response data from the tunnel presented in figures 11

to 37 are subject to this type of filtering. However, there is generally good agreement between tunnel and simulator responses.

In summary, test-section Mach number and pressure responses of the tunnel to an LN_2 input agree quite well with the mathematical model predictions described by the simulator responses for the entire operational envelope. Actual tunnel temperature responses did not duplicate simulator predictions quite so well due to the dynamic characteristics of the thermocouple used for temperature measurements.

GN_2 Exhaust-Pulse Input

Once again in reference to figure 11, the tunnel and simulator responses are examined for an exhaust pulse of about 3 sec. These responses are marked EFG for selected study. Equilibrium conditions have been established prior to point E ($\dot{p} = \dot{T} = 0$, $\dot{m}_L = \dot{m}_G$). As with the perturbation to the LN_2 flow rate, the perturbation to the exhaust-gas flow rate is induced by increasing the valve area by an incremental 6.25 percent of the full-open value. This was done physically for the tunnel and in simulation on the computer for all conditions in table I. In the perturbation process an increase in the exhaust-gas mass flow $\Delta\dot{m}_G$ is produced. As described in equation (4), this results in a negative pressure gradient $\left(\dot{p} = -\frac{p}{W_G}\Delta\dot{m}_G e^{-T_G s}\right)$. Because the exhausting causes a negative temperature gradient ($\dot{T}$) during segment EF, there is a small second-order negative pressure-gradient contribution due to the $\frac{p}{T}\dot{T}$ term in equation (4). By and large however, the pulse causes a linear pressure drop during segment EF. The linear pressure drop consistently repeats for both the tunnel and simulator responses as shown in figures 11 to 37. At point F the incremental valve area is made zero, thereby making $\Delta\dot{m}_G = 0$. Once $\Delta\dot{m}_G$ is made zero, the slope of the pressure gradient $\dot{p}$ is characterized by the steady-state gaseous-mass flow rate $\dot{m}_G$, which is a function of $p/\sqrt{T}$. Thus the largest pressure gradients exist when pressure and temperature are maximum ($p = 5.0$ atm and $T = 275$ K). Examination of the data shows this to be true. In contrast, the smallest pressure gradients occur when $p = 1.5$ atm and $T = 100$ K. During the interval FG, the pressure gradient is a direct function of the gaseous-valve-area opening A_G. During steady state, this valve-area opening is largest at high Mach numbers in order to maintain equilibrium operation. Because of the large opening at high Mach numbers, more GN_2 is being exhausted. When the 6.25-percent incremental valve-area perturbation is removed, the reduction in $\Delta\dot{m}_G$ is greatest at high Mach numbers. For this reason, the pressure recovery during segment FG is fastest at $M = 0.75$ and $M = 0.90$ and slowest at $M = 0.30$.

As expected, in general the perturbations of the exhaust-mass flow rate have more effect on pressure than on either temperature or Mach number. During segment EF, however, a negative $\dot{T}$, which is filtered by the lead/lag term, is found. Equation (2) is the governing equation for this temperature gradient.

When $\Delta\dot{m}_G$ is made zero at point F, $\dot{T}$ becomes positive due to the reduced gas mass exhaustion, thereby establishing a new temperature. The magnitude of ΔT can be transiently approximated by $\frac{\alpha}{W_G c_v} \dot{m}_G e^{-\tau_G s}$ since there is zero change in liquid flow rate and no added heat contribution from a steadily running fan (eq. (2)). Since $\dot{m}_G$ is a function of $p/\sqrt{T}$ (eq. (8)), ΔT is expected to be largest at high pressures and low temperatures. Comparison of figure 11 with figure 29 illustrates this effect quite well.

Fan-Speed Pulse Input

The trajectories marked HJK in figures 11, 28, and 29 correspond to the response of total-pressure, total-temperature, and test-section Mach number dynamics of the cryogenic tunnel to a pertubation in fan speed. As with the other types of pertubations, system equilibrium is established and during segment HJ the fan speed is reduced by 100 rpm. The fan speed decelerates almost linearly as described by the fan dynamics of equation (12). Reduced fan speed results in a pressure-ratio reduction which manifests itself as a decrease in Mach number. Because the fan is accelerated during segment JK back to the original speed, the pressure ratio is increased causing Mach number to return to its original value. The maximum Mach number deviation occurs at point J. This is related to fan speed by $\Delta M = \frac{\Delta N}{\sqrt{T}}$ as indicated in equation (5). Since ΔN is made constant for all runs, the largest Mach number deviation takes place at the lower temperatures. Comparison of figures 11 to 19 with figures 29 to 37 confirms this phenomenon. At 100 K, a typical Mach number change is about 0.034 compared with a 0.020 change at 275 K. Reduced fan heat production due to the speed decrease contributes a secondary influence on the Mach number reduction. The increase in Mach number caused by decreased heat of compression is quite small and cannot be easily separated from the primary effect of the decrease in fan speed. Total-temperature data reflect this by a slight temperature decrease during segment HJ and an increase during segment JK. Equation (2) indicates the influence of fan heat $\dot{Q}_F$ on the temperature gradient. Because fan heat $\frac{K_F p M^3 \sqrt{T}}{(1 + 0.2M^2)^3}$ (eq. (14)) is a contributor to equation (2), the maximum ΔT occurs when p, T, and M are maximum. A comparison of figure 37 (5.0 atm, 275 K, and $M = 0.75$) with figure 11 (1.5 atm, 100 K, and $M = 0.3$) demonstrates this clearly. The transit-time delay previously mentioned is also noticeable in the temperature traces of these records.

Except for figures 12, 25, and 29, the tunnel and simulator responses agree quite well. In figure 12, the oscillatory pressure and temperature responses for the tunnel are due to an inadvertent cycling of one of the smaller exhaust-gas valve elements which is not shown in the figure. Two fan-input commands were made which caused cumulative effects in the tunnel variables shown in figure 25. The second input, which was inadvertently made, is not shown in the figure in order to show only the effects of the inten-

tional input. The large pressure and temperature magnitudes experienced in figure 29 are a result of a 5-sec liquid pulse rather than a 3-sec input.

Quasi-Steady-State Warm-Up and Cool-Down Tests

In addition to the transient-response studies, tests on cool-down and warm-up of the tunnel with excess LN_2 flow and excess fan heating, respectively, were conducted to validate the quasi-steady-state heat-transfer model.

The basic energy equation of the cryogenic-tunnel process is

$$W_G c_v \frac{dT}{dt} + c_v T\left(\dot{m}_L - \dot{m}_G\right) = -\int^{\text{Surface}} \dot{Q}_m + \dot{Q}_F + \dot{m}_L h_L - \dot{m}_G c_p T \qquad (15)$$

where

$$\int^{\text{Surface}} \dot{Q}_m = \frac{W_m c_m T s}{1 + t_m s} = (T - T_m)y$$

In order to validate this heat-transfer model, time histories of the average metal temperature T_m and gas temperature T were recorded for ordered input energy terms. A match between temperature, temperature difference, and time was sought for the tunnel and simulator quasi-steady-state responses.

Cool-down.- The actual cool-down process used for the 0.3-m TCT consists of injecting liquid nitrogen at a constant rate and in a sufficient quantity so that the cooling capacity of the liquid is greater than the heat conducted through the tunnel shell and the heat generated by the fan $\left[\dot{m}_L(h_L - c_p T) >> \dot{Q}_F\right]$. This condition is easily realized by running the tunnel at a very low Mach number while injecting the LN_2. If we neglect the heat conducted through the tunnel walls, this implies that the energy equation can be simplified to

$$W_G c_v \frac{dT}{dt} = -\int^{\text{Surface}} \dot{Q}_m + \dot{m}_L \beta \qquad (16)$$

Both the tunnel and the simulator were brought to an equilibrium condition of 290 K and 1.5 atm while maintaining a constant fan speed of 1200 rpm. Liquid-nitrogen injection pressure was held constant at 6 atm throughout the cool-down. Starting from a condition of equilibrium, the actual cool-down process was started by increasing the LN_2 injection-valve area to 12.5 percent to achieve a 1.02-kg/sec liquid-nitrogen flow rate. Tunnel pressure was maintained constant during the cool-down process by manipulation of the exhaust-

valve area. The temperature of the gas, the average temperature of the metal of the tunnel shell, and the test-section Mach number were recorded during the cool-down. Both metal and gas temperatures were reduced and cool-down was considered complete when the gas reached a temperature of about 105 K. The total amount of LN_2 consumed was also determined and recorded. Figure 38 shows the cool-down profile for both the tunnel and the simulator. As can be seen, both gas and metal temperature trajectories match quite well. An initial gas-to-metal temperature difference of 65 K exists. This difference decreases during the cool-down, with a difference at the end of the cool-down process of only 15 K. The LN_2 consumption to cool the tunnel from 290 K to 100 K was about 1825 kg, whereas the computer simulation for the same cool-down predicted an LN_2 usage of 1800 kg. This close agreement between the simulator prediction and the tunnel data gives confidence that the quasi-steady-state heat-transfer model is accurate.

Warm-up.- For a typical tunnel warm-up, the LN_2 flow is reduced to zero while the tunnel is operated at constant Mach number and pressure. For this study, the warm-up was made after establishing equilibrium conditions with both metal and gas temperatures at 100 K. Since the LN_2 flow rate is zero and GN_2 flow rate is very nearly so, the heat generated by the drive fan is the dominant factor in the warm-up process. Neglecting any heat addition through the tunnel walls, this results in the simplified energy equation

$$W_G c_v \frac{dT}{dt} \cong \dot{Q}_F - \int^{\text{Surface}} \dot{Q}_m \tag{17}$$

where

$$\int \dot{Q}_m = \frac{W_m c_m T s}{1 + t_m s} = (T - T_m) y$$

and

$$\dot{Q}_F = \frac{K_F p M^3 \sqrt{T}}{(1 + 0.2M^2)^3} >> \dot{m}_G c_p T$$

Both tunnel and simulator were set at equilibrium conditions of 100 K and 2 atm. Mach numbers of 0.5, 0.6, and 0.7 were used for the computer simulation in order to show the effect of Mach number on the warm-up profile. Once equilibrium was established, the LN_2 flow was reduced to zero by closing the LN_2 injection valve. Mach number and pressure were maintained constant throughout each warm-up. Figure 39 shows the warm-up profiles predicted by the simulator

for the three different Mach numbers. As expected, the data indicate larger gas-to-metal temperature differences as well as faster warm-up for higher Mach numbers. Figure 40 shows a comparison of an actual 0.3-m TCT warm-up profile and a corresponding simulator warm-up profile at 2 atm and $M = 0.6$. As can be seen, the tunnel warms up slightly slower than predicted by the simulator, but the metal-to-gas temperature differences between the tunnel and simulator agree to within 2 K. These differences between the warm-up profiles are attributed to slight variations in tunnel pressure at the beginning of the warm-up process and perhaps a small error in the constant K_F.

Generally, the behavior of the 0.3-m TCT and the behavior predicted by the computer simulation of the tunnel show good agreement not only in the transient responses, but also in the quasi-steady-state cool-down and warm-up characteristics. This agreement has been found over the entire operational envelope. In view of this agreement, the mathematical model developed to describe the tunnel is assumed to be valid and acceptable for transient, quasi-steady-state, and steady-state performance.

Model Closed-Loop Analysis

Since the beginning of operation of the 0.3-m TCT, the need for improving the quality of data obtained during tunnel tests has become increasingly apparent. A major improvement in the quality of the data can be realized if the test parameters can be held to closer tolerances for longer periods of time. It is reasoned that if inaccurate and inefficient manual operator manipulation for holding and changing the test parameters can be eliminated by the use of advanced control schemes, data quality will significantly improve, with a simultaneous reduction in operating costs. As shown in reference 4, by reducing the run time, one could proportionately reduce the cost of testing because of decreased electrical-power and LN_2 consumption. These arguments all alluded to the implementation of closed-loop control systems, which are inherently faster and more accurate (and generally more reliable) than the human operator. Consequently, proportional-integral-derivative (PID) pressure and temperature control laws were developed and designed for analytical evaluation of the hybrid-computer simulator of the 0.3-m TCT. Figures 41 and 42 show schematic diagrams of the pressure and temperature loops, respectively. Shown in both figures are the equations describing the digital valves and the respective lags associated with the temperature and pressure sensors. Contributions of the various input/output elements are shown with appropriate signs conveying the influence they have on the process loop.

The closed-loop mathematical models of the 0.3-m TCT were operationally analyzed assuming local linearity and no coupling between controls. For purposes of illustration, the pressure loop consists of first-order sensor measurement dynamics with time constant t_2, which determines feedback pressure that is compared with the pressure set-point value. The generated error signal drives the PID controller which, after appropriate gain selection, controls the operation of the nitrogen-gas exhaust value. Root locus analysis of the pressure loop indicates that a gain schedule of $\frac{1}{p\sqrt{T}}$ provides acceptable performance.

A feedback loop similar to that used for pressure control is used for the temperature control with the applicable measurement sensor time constant and digital-valve dynamics. Included in the temperature control loop is a fan power feed-forward term necessary to account for the effect of fan-generated heat on the temperature loop. Root locus analysis of the temperature control loop indicates that a gain scheduling of $\frac{M\sqrt{p}}{T}$ would be satisfactory.

Figure 43 shows data from the hybrid-computer simulator for the closed-loop performance for both low and high tunnel temperatures using only proportional and integral signals within the pressure and temperature controls. Closed-loop data from the simulator were acquired for temperature and pressure set-point changes and finally for fan-speed changes.

In figure 43(a), the temperature set point is reduced by approximately 8 K. The temperature reaches 82 K in about 10 sec and then slowly drifts downward over the next 40 sec. This lag is due to the heat transfer from the tunnel wall. The pressure control maintains pressure to within 0.03 atm and suppresses the fluctuations in pressure due to the temperature disturbance in about 20 sec. It should be noted that Mach number increases because of the reduction in temperature. Following stabilization of the gas temperature at 82 K, the temperature set point is returned to 90 K. The gas temperature reaches 90 K in 5 sec and, since the time spent at the lower temperature was too short to reduce the metal temperature much below 90 K, the gas temperature stabilizes quickly at 90 K. Again the pressure settling time is about 20 sec.

The next disturbance to be evaluated is a pressure set-point change from 2.13 atm to 1.76 atm. An overshoot in the simulated tunnel-pressure process exists but stabilizes quite nicely. Closed-loop temperature oscillations caused by the pressure input settle in about 22 sec whereas Mach number follows the temperature oscillations in opposite fashion. After the pressure stabilizes at 1.76 atm, the pressure set point is returned to 2.13 atm. The relatively slow pressure buildup occurs because it is necessary to increase the mass of gas in the tunnel. The rate of increase is entirely dependent upon the mass flow rate of LN_2 into the tunnel. Closed-loop temperature control for the pressure disturbance is maintained to within 0.5 K and quickly returns to the temperature set-point value.

The last input for closed-loop study consists of a change in drive-fan speed to force a change in Mach number from 0.75 to 0.65 quickly followed by a change in speed to force a change in Mach number from 0.65 to 0.85. Even with the large change in Mach number (0.65 to 0.85), very small temperature and pressure excursions occur, indicating acceptable performance of the temperature and pressure control systems.

Figure 43(b) illustrates the control-system performance for set-point changes at the high temperature of 263 K. Again the pressure and temperature loops perform well, with average settling times of about 20 sec.

Based on these simulator-generated results, the control laws derived on the basis of single-input, single-output analysis provide good closed-loop control of pressure and temperature. Coupling effects between process response and control input are evident, but converge very well using simple loop closures.

CONCLUDING REMARKS

A hybrid-computer simulation of the Langley 0.3-Meter Transonic Cryogenic Tunnel has been developed and fully verified. Comparison of simulation and experimental transient response data exhibited very good agreement throughout the cryogenic-tunnel operational range. Additionally, quasi-steady-state cool-down and warm-up profiles have contributed significantly to the model validation by virtue of the small differences seen between actual and simulated operation. Therefore, it is felt that the single lumped-parameter nonlinear multivariable model has been proven to be globally accurate and reliable in duplicating tunnel temperature, pressure, and Mach number process dynamics. A plethoric compilation of data spanning the tunnel testing range is provided as a data base for future reference.

Proportional-integral control laws designed using the validated mathematical model have been exercised using the hybrid-computer simulator and have been found to be quite satisfactory for control of both the temperature and pressure process responses. As a result, these control laws will be implemented in software for digital microprocessor controllers for temperature and pressure regulation of the Langley 0.3-Meter Transonic Cryogenic Tunnel.

Langley Research Center
National Aeronautics and Space Administration
Hampton, VA 23665
June 23, 1980

APPENDIX

THERMODYNAMIC MODEL OF THE LANGLEY 0.3-m TCT

In this appendix, a dynamic lumped-parameter model is developed for the 0.3-m TCT circuit. The need for a relatively simple model which can be numerically simulated and rapidly executed to permit analytical design and interactive usage excludes an analysis based on nonlinear partial differential equations of fluid flow. Lumped-parameter techniques are applied to produce a low-order model for the dynamics of the process variables at the test-section location in the form of differential-delay/ordinary differential equations.

Temperature Equation

The first law of thermodynamics applied to this analysis can be written as

$$\dot{Q} + \dot{w} = \dot{E}$$

This is an energy equation which states that the change in total system energy E is equal to the heat Q added to and the work w done by the selected system. The energy term consists of the sum of potential energy, kinetic energy, and internal energy. Because the change in elevation as the gas circulates around the tunnel is small, potential-energy contributions were neglected. For the tunnel testing conditions operationally used, the kinetic energy of the circulating gas was found to be a small percentage of the total system energy and was therefore ignored.

Since no work is performed by the circulating cryogenic gas, this term of the general thermodynamic equation is zero. Therefore, it can be seen that heat energy Q is the sole source for change in the level of internal energy of the gas. Mathematically this can be expressed in special form as

$$Q = \frac{\partial U}{\partial t}$$

or

$$\dot{Q} = \frac{\partial (W_G u)}{\partial t} \tag{A1}$$

where

U internal energy, J

u specific internal energy, J/kg

W_G mass of the circulating nitrogen test gas, kg

The left side of the above energy equation is composed of a number of individual sources which collectively contribute to the internal energy of the system. For example, two-way heat transfer exists between the ambient environment and the gas through the imperfectly insulated tunnel metal structure. Heat of compression from the tunnel fan is obtained as the test medium is circulated through the tunnel. Also, energy is added by injection of LN_2 and exhaust of GN_2 during regulation of temperature and pressure conditions within the tunnel. The sign convention selected is such that any energy added to the GN_2 tunnel medium was considered positive.

Expanding equation (A1) by taking the first partial deviative of the right-hand side yields

$$\dot{Q} = W_G \frac{\partial u}{\partial t} + \frac{u \, \partial W_G}{\partial t} \tag{A2}$$

Because $\partial u \triangleq c_v \, \partial T$, equation (A2) becomes

$$\dot{Q} = W_G c_v \frac{\partial T}{\partial t} + u\dot{W}_G$$

or

$$\dot{Q} = W_G c_v \dot{T} = u\dot{W}_G \tag{A3}$$

The term $\dot{W}_G$ is really the time rate of change of the tunnel resident gas and can be expressed as the difference between the injected- and exhausted-nitrogen masses, that is,

$$\dot{W}_G = \dot{m}_L - \dot{m}_G \tag{A4}$$

Substituting this along with the appropriate metal, fan, LN_2, and GN_2 heat energy terms for the left side of equation (A3) gives

$$-\dot{Q}_m + \dot{Q}_F + \dot{m}_L h_L - \dot{m}_G h_G = W_G c_v \dot{T} + u(\dot{m}_L - \dot{m}_G) \tag{A5}$$

After transposing and collecting terms, this equation is

$$\dot{m}_L(h_L - u) - \dot{m}_G(h_G - u) - \dot{Q}_m + \dot{Q}_F = W_G c_v \dot{T} \tag{A6}$$

However, for a perfect gas (which can be assumed for nitrogen), $u = c_v T$ and $h_G = c_p T$. Therefore, the relationship becomes

$$\dot{m}_L(h_L - c_v T) - \dot{m}_G(c_p T - c_v T) - \dot{Q}_m + \dot{Q}_F = W_G c_v \dot{T} \tag{A7}$$

Expressions which are functions of local pressure, temperature, and Mach number are now needed for $\dot{Q}_m$ and $\dot{Q}_F$ in equation (A7). The development of $\dot{Q}_F$ is accomplished in another section of this appendix. A detailed analysis of the derivation of the metal-to-gas heat transfer $\dot{Q}_m$ based on a numerical estimation of the heat-transfer coefficient by Bartz is presented in reference 3. Results of that work indicate that

$$\int_{\text{Surface}} \dot{Q}_m = \frac{W_m c_m \dot{T}}{1 + t_m s} \tag{A8}$$

By using equation (A8) together with equation (A7) and rearranging we get

$$\dot{T}\left(W_G c_v + \frac{W_m c_m}{1 + t_m s}\right) = \dot{m}_L(h_L - c_v T) - \dot{m}_G(c_p - c_v)T + \dot{Q}_F \tag{A9}$$

By defining

$$\alpha = (c_p - c_v)T$$

$$\theta = W_G c_v + W_m c_m$$

and

$$\beta \cong h_L - c_p T = -\left(121 + 2p + \frac{66}{T} - 391\,\frac{p}{T} + 1.04T\right)$$

equation (A9) can be expressed as

$$\dot{T}\left(\frac{\theta + W_G c_v t_m s}{1 + t_m s}\right) = \dot{m}_L(\alpha + \beta) - \dot{m}_G\alpha + \dot{Q}_F$$

or

$$\dot{T}\left(\frac{1 + \dfrac{W_G c_v t_m s}{\theta}}{\dfrac{1 + t_m s}{\theta}}\right) = \dot{m}_L(\alpha + \beta) - \dot{m}_G\alpha + \dot{Q}_F \tag{A10}$$

This becomes

$$\dot{T}\left(\frac{1 + t_G s}{1 + t_m s}\right) = \left(\frac{\alpha + \beta}{\theta}\right)\dot{m}_L - \left(\frac{\alpha}{\theta}\right)\dot{m}_G + \left(\frac{1}{\theta}\right)\dot{Q}_F \tag{A11}$$

where

$$t_G \triangleq \frac{W_G c_v t_m}{\theta}$$

and

$$W_G = 341.4\,\frac{pV}{T}\left(1 + 250\,\frac{p}{T^2}\right)\left(1 - 0.033M^{1.5}\right)$$

Equation (A11) is the fundamental temperature relationship for the model with the exception of transport delays needed for realism. Because transit time is experienced between control input and measurement, pure transport delays are incorporated. Liquid nitrogen is injected downstream of the test section in the 0.3-m TCT, and since this effect is measured in the settling chamber a time delay of $e^{-\tau_L s}$ is used. The fan heat of compression occurs after turn number two in the tunnel, and since it also is measured in the settling chamber a delay of $e^{-\tau_F s}$ is needed. A smaller delay, $e^{-\tau_G s}$, is used for the gas

effects since gas venting is very near the pressure measurement sensor in the settling chamber. By applying these delays and performing a bit of algebra, equation (A11) is now

$$\dot{T} = \left(\frac{\alpha + \beta}{\theta}\right)\left(\frac{1 + t_m s}{1 + t_G s}\right)\dot{m}_L e^{-\tau_L s} - \left(\frac{\alpha}{\theta}\right)\left(\frac{1 + t_m s}{1 + t_G s}\right)\dot{m}_G e^{-\tau_G s}$$

$$+ \left(\frac{1}{\theta}\right)\left(\frac{1 + t_m s}{1 + t_G s}\right)\dot{Q}_F e^{-\tau_F s} \qquad \text{(A12)}$$

The only remaining unknown in equation (A12) is the heat energy generated by the fan while circulating the test gas around the tunnel. This contribution can be represented by

$$\dot{Q}_F = c_p \dot{m}_{F,i} \Delta T \qquad \text{(A13)}$$

If we assume that the mass flow rate at the test section $\dot{m}^*$ is the same as the mass flow rate at the fan inlet (i.e., $\dot{m}^* = \dot{m}_{F,i}$), then the fan-inlet mass flow rate can be expressed as

$$\dot{m}_{F,i} = 6965 \frac{p}{\sqrt{T}} AM(1 + 0.2M^2)^{-3} \qquad \text{(A14)}$$

where p is pressure in atmospheres, A is test-section area in square meters, and T is temperature in kelvins. This expression can be found in any thermodynamic text for the calculation of mass flow rate of an ideal gas through an isentropic nozzle.

The temperature change in equation (A13) at the fan section is found by using the fan pressure-ratio equation for steady, isentropic compressible flow. Mathematically this is

$$r = \frac{p_e}{p_i} = \left(\frac{T_e}{T_i}\right)^{\frac{\gamma}{\gamma - 1}} \qquad \text{(A15)}$$

where $\gamma \triangleq \frac{c_p}{c_v}$, the ratio of specific heats of the gas under consideration. By rearranging this, equation (A15) becomes

$$r = \left(1 + \frac{p_e - p_i}{p_i}\right) = \left(1 + \frac{T_e - T_i}{T_i}\right)^{\frac{\gamma}{\gamma-1}}$$

or

$$r = \left(1 + \frac{\Delta p}{p_i}\right) = \left(1 + \frac{\Delta T}{T_i}\right)^{\frac{\gamma}{\gamma-1}} \tag{A16}$$

Working only with the temperature term in the above we can write

$$r = \left(\frac{T_i + \Delta T}{T_i}\right)^{\frac{\gamma}{\gamma-1}} \tag{A17}$$

Because $\Delta T \triangleq T_e - T_i$, or $T_i = T_e - \Delta T$, equation (A17) can be expressed as

$$r = \left(\frac{T_e - \Delta T + \Delta T}{T_e - \Delta T}\right)^{\frac{\gamma}{\gamma-1}}$$

which, after adding the ΔT terms becomes

$$r = \left(\frac{T_e}{T_e - \Delta T}\right)^{\frac{\gamma}{\gamma-1}} \tag{A18}$$

APPENDIX

Solving equation (A18) for ΔT, we get

$$\Delta T = T_e \left(\frac{r^{\frac{\gamma-1}{\gamma}} - 1}{r^{\frac{\gamma-1}{\gamma}}} \right)$$

which, after assuming a fan efficiency of η, becomes

$$\Delta T = \frac{T_e}{\eta} \left(\frac{r^{\frac{\gamma-1}{\gamma}} - 1}{r^{\frac{\gamma-1}{\gamma}}} \right)$$

or

$$\Delta T = \frac{T_e}{\eta} \left(1 - r^{-\frac{\gamma-1}{\gamma}} \right) \tag{A19}$$

As with any closed-circuit tunnel, the steady-state fan pressure ratio r can be expressed as a function of the integrated pressure-low coefficient and the normalized test-section Mach number. Mathematically,

$$r = 1 + bM^2$$

Introducing this into equation (A19), we get

$$\Delta T = \frac{T_e}{\eta} \left[1 - (1 + bM^2)^{-\frac{\gamma-1}{\gamma}} \right] \tag{A20}$$

APPENDIX

The inner term $(1 + bM^2)^{-\frac{\gamma-1}{\gamma}}$ can be expanded in a first-order Taylor series yielding $1 + \left(-\frac{\gamma - 1}{\gamma}\right)bM^2$. Substitution into equation (A20) gives

$$\Delta T = \frac{T_e}{\eta}\left\{1 - \left[1 + \left(-\frac{\gamma - 1}{\gamma}\right)bM^2\right]\right\}$$

or

$$\Delta T = \frac{T_e}{\eta}\left[\left(\frac{\gamma - 1}{\gamma}\right)bM^2\right] \tag{A21}$$

Placing equations (A14) and (A21) into equation (A13) results in

$$\dot{Q}_F = c_p\left[6965\ \frac{p}{\sqrt{T}}\ AM(1 + 0.2M^2)^{-3}\right]\left[\frac{T_e}{\eta}\left(\frac{\gamma - 1}{\gamma}\right)bM^2\right]$$

Because $T_e = T$ (the total gas temperature), if we let $K_F \triangleq \frac{6965}{\eta}\ Ac_p b\left(\frac{\gamma - 1}{\gamma}\right)$ and cancel like terms, the above can be written as

$$\dot{Q}_F = K_F p M^3 (1 + 0.2M^2)^{-3}\sqrt{T} \tag{A22}$$

From a control standpoint, equation (A22) should be represented in terms of a system input. From a curve fit of tunnel experimental data, a relationship between the system input of revolutions per minute and Mach number is needed. This function was determined to be

$$M = \frac{N}{K_M\sqrt{T}} \tag{A23}$$

where $K_M = 597(1 - 0.3M)p^{-0.035}$. Equation (A23) combined with equation (A22) yields

$$\dot{Q}_F = \frac{K_F}{K_M} pNM^2(1 + 0.2M^2)^{-3} \tag{A24}$$

Finally, the $\dot{T}$ system equation of the matrix in figure 3 can be obtained by substituting equation (A24) and the following valve mass flow rate equations into equation (A12):

$$\dot{m}_L = K_L A_L$$

where $K_L \triangleq 3.47\sqrt{p_L - p}$ and A_L = Injection valve opening in percent, and

$$\dot{m}_G = K_G \frac{p}{\sqrt{T}} A_G$$

where $K_G = \left[2 - \left(\frac{1.5}{p}\right)^{1.7}\right] 21.8$ and A_G = Exhaust valve opening in percent. The equations for $\dot{m}_L$ and $\dot{m}_G$ are equations (7) and (8), respectively.

Mach Number Equation

As previously mentioned, the fan speed and the test-section Mach number are related by the empirical expression

$$N = 597M\sqrt{T}(1 - 0.3M)p^{-0.035} \tag{A25}$$

For any given Mach number, this relationship resulted in a good fit of the 0.3-m TCT data (within ±10 rpm). Because of the plenum volume surrounding the test section, the Mach number is dynamically influenced. Previous testing indicated that this influence is of a first-order type effect because of the net flow into or out of the plenum. Also, there is a slight delay associated with a fan rpm change that is to be interpreted as a test-section Mach number variation. From these two facts, equation (A25) becomes

$$M = \frac{Ne^{-\tau_a s}}{K_M\sqrt{T}(1 + t_p s)} \tag{A26}$$

where

K_M $= 597(1 - 0.3M)p^{-0.035}$

t_p plenum time constant

τ_a acoustic time lag

Equation (A26), which is presented in the text as equation (5), is the second expression of the model matrix in figure 3 and relates the rpm input to the Mach number output.

Pressure Equations

The last dynamic model function used to describe the characteristics of the 0.3-m TCT is the pressure equation. From the ideal gas law (which nitrogen very closely approximates), pressure is related to temperature according to

$$p = K_1 W_G T$$

where W_G is the mass of the gas in kilograms. Simply taking the first partial derivative of this with respect to time yields

$$\frac{\partial p}{\partial t} = K_1 T \frac{\partial W_G}{\partial t} + K_1 W_G \frac{\partial T}{\partial t} + \text{M.E.} \tag{A27}$$

where M.E. denotes momentum effects. But $W_G = \frac{p}{K_1 T}$ and $T = \frac{p}{K_1 W_G}$ will cause equation (A27) to be

$$\frac{\partial p}{\partial t} = \frac{p}{W_G} \frac{\partial W_G}{\partial t} + \frac{p}{T} \frac{\partial T}{\partial t} + \text{M.E.} \tag{A28}$$

Since $\frac{\partial W_G}{\partial t} = \dot{m}_L - \dot{m}_G$, equation (A28) becomes

$$\frac{\partial p}{\partial t} = \frac{p}{W_G}(\dot{m}_L - \dot{m}_G) + \frac{p}{T} \frac{\partial T}{\partial t} + \text{M.E.}$$

or

$$\frac{\partial p}{\partial t} = \frac{p}{W_G}\dot{m}_L - \frac{p}{W_G}\dot{m}_G + \frac{p}{T}\dot{T} + M.E. \tag{A29}$$

The momentum effects are attributed to the fan pressure-ratio changes and pressure losses and were found to be related to the total pressure dynamics according to

$$\frac{\partial p}{\partial t} = DbMp\frac{\partial M}{\partial t}$$

where b is the pressure-loss coefficient and D is a dimensionality constant. If we insert the liquid transport delay, the gaseous transport delay, and the momentum effects, equation (A29) becomes

$$\frac{\partial p}{\partial t} = \frac{p}{W_G}\dot{m}_L e^{-\tau_L s} - \frac{p}{W_G}\dot{m}_G e^{-\tau_G s} + \frac{p}{T}\dot{T} + DbMp\frac{\partial M}{\partial t} \tag{A30}$$

where $b = 0.197\left(1 - \frac{7pM}{T}\right)$. This is equation (4) in the text. Of course, the valve mass flow rate equations are the same, and upon substitution for $\dot{T}$ and arrangement the third matrix equation of figure 3 is derived.

REFERENCES

1. Kilgore, Robert A.; Goodyer, Michael J.; Adcock, Jerry B.; and Davenport, Edwin E.: The Cryogenic Wind-Tunnel Concept for High Reynolds Number Testing. NASA TN D-7762, 1974.

2. Kilgore, Robert A.: Design Features and Operational Characteristics of the Langley 0.3-Meter Transonic Cryogenic Tunnel. NASA TN D-8304, 1976.

3. Balakrishna, S.: Synthesis of a Control Model for a Liquid Nitrogen Cooled, Closed Circuit, Cryogenic Nitrogen Wind Tunnel and Its Validation. NASA CR-162508, 1980.

4. Ray, Edward J.; Ladson, Charles L.; Adcock, Jerry B.; Lawing, Pierce L.; and Hall, Robert M.: Review of Design and Operational Characteristics of the 0.3-Meter Transonic Cryogenic Tunnel. First International Symposium on Cryogenic Wind Tunnels, Proceedings of the Symposium held in the Department of Aeronautics and Astronautics at the University of Southampton, England, Apr. 3-5, 1979, pp. 28.1 - 28.15.

TABLE I.- NOMINAL VALUES OF TUNNEL AND SIMULATOR TEST CONDITIONS

Figure	Total temperature, K	Test-section Mach number	Total pressure, atm
11	100	0.30	1.57
12	100	.60	1.57
13	100	.90	1.57
14	100	.30	3.00
15	100	.60	3.00
16	100	.95	3.07
17	100	.30	5.00
18	100	.60	5.00
19	100	.90	4.93
20	200	.30	1.57
21	200	.60	1.50
22	200	.90	1.57
23	200	.30	2.65
24	200	.60	3.00
25	200	.90	3.00
26	200	.30	5.00
27	200	.60	5.00
28	200	.90	5.00
29	275	.30	1.57
30	275	.60	1.57
31	275	.75	1.57
32	275	.30	3.00
33	274	.60	3.00
34	275	.75	3.00
35	275	.30	5.00
36	275	.60	5.00
37	275	.80	5.00

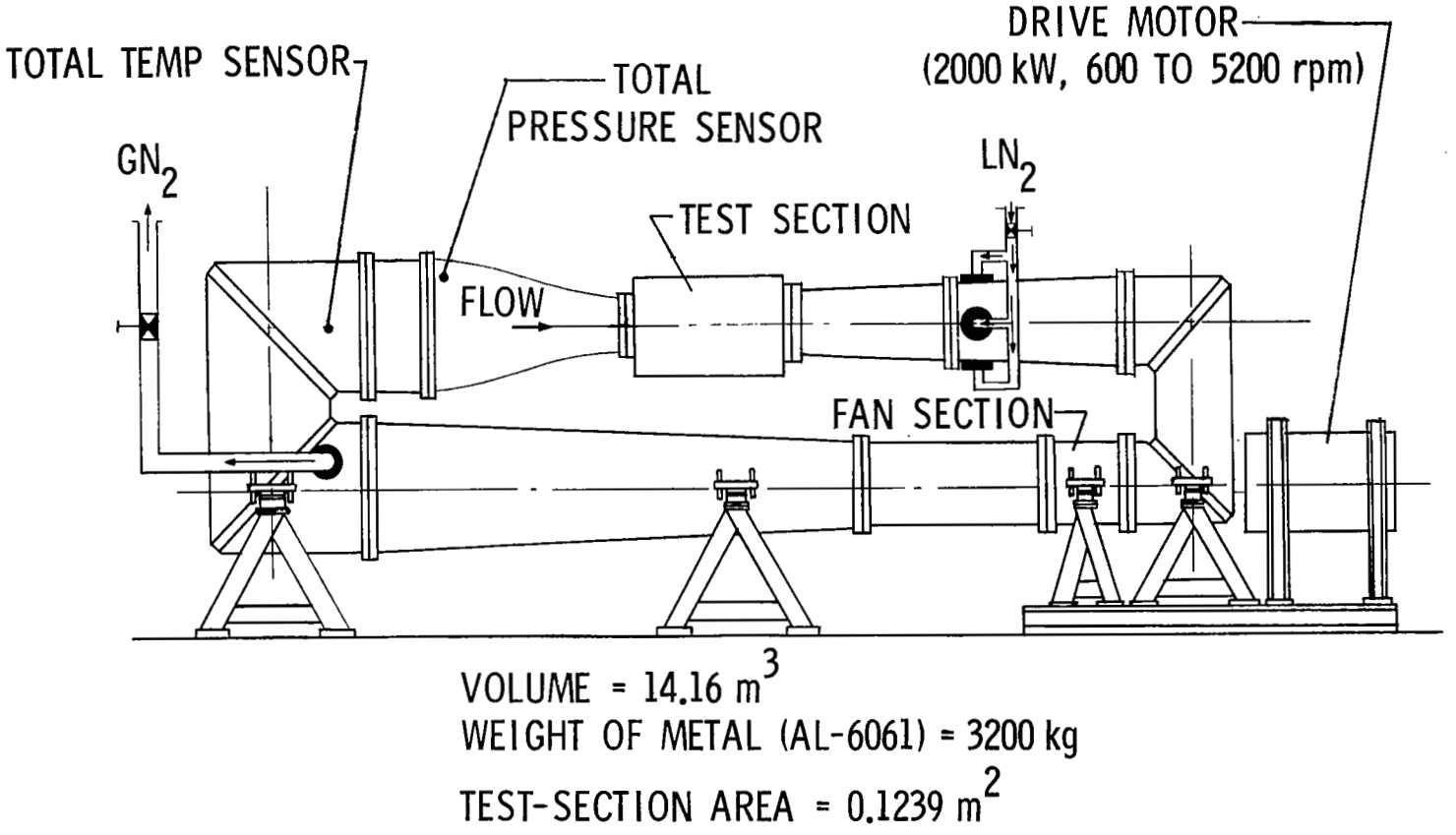

Figure 1.- Schematic of Langley 0.3-Meter Transonic Cryogenic Tunnel.

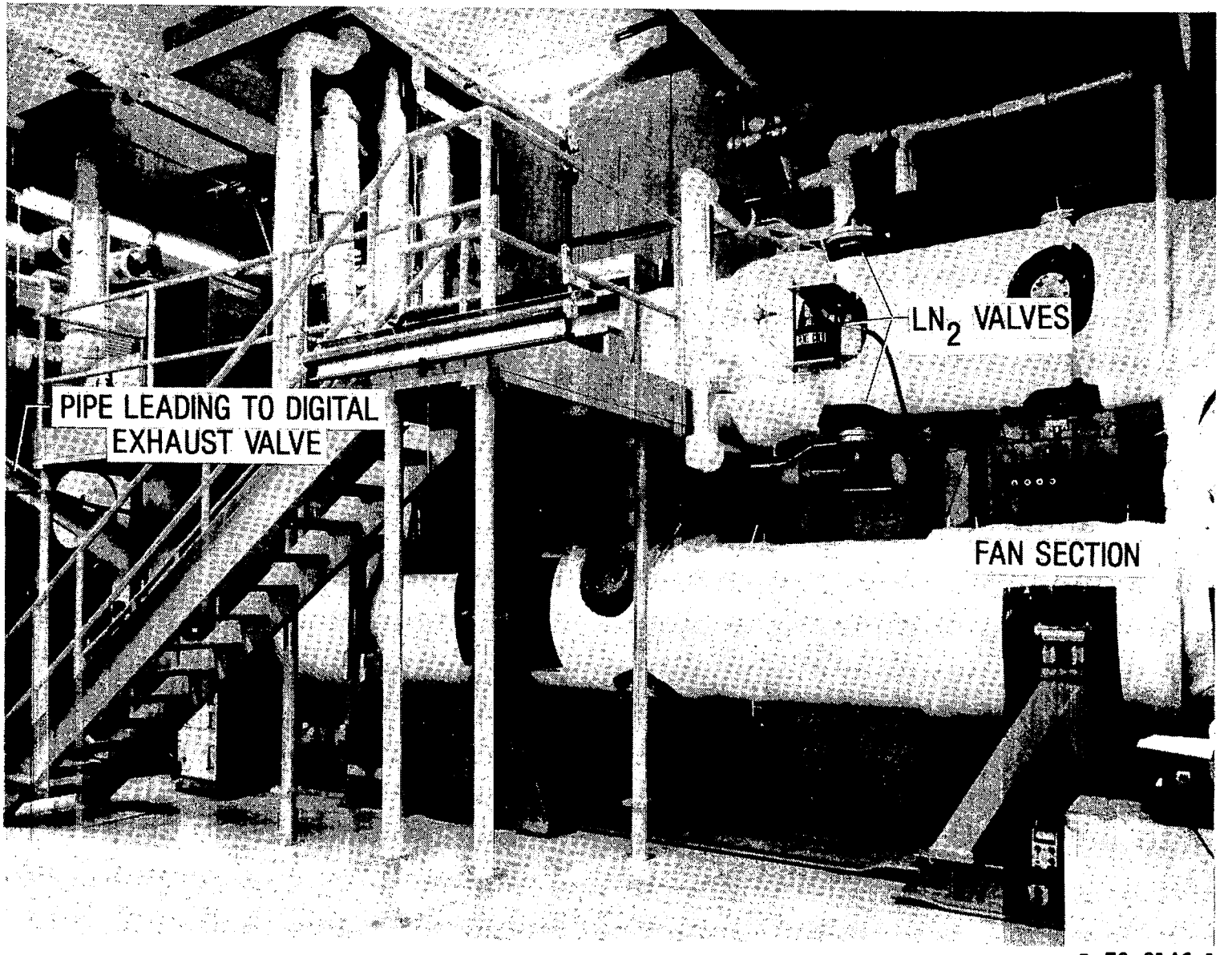

L-79-2146.1

Figure 2.- Photograph of Langley 0.3-Meter Transonic Cryogenic Tunnel.

TUNNEL PROCESS MODEL

$$\begin{bmatrix} \dot{T} \\ M \\ \dot{p} \end{bmatrix} = \begin{bmatrix} K_L\left(\frac{\beta+\alpha}{\theta}\right)\left(\frac{1+t_m s}{1+t_G s}\right)e^{-\tau_L s} & \frac{K_F}{K_M}\left[\frac{pM^2}{\theta(1+0.2M^2)^3}\right]\left(\frac{1+t_m s}{1+t_G s}\right)e^{-\tau_F s} & -K_G\left(\frac{p\alpha}{\sqrt{T}\,\theta}\right)\left(\frac{1+t_m s}{1+t_G s}\right)e^{-\tau_G s} \\ 0 & \frac{e^{-\tau_a s}}{K_M\sqrt{T}(1+t_p s)} & 0 \\ K_L\left\{\frac{p}{W_G}+\left[\frac{p(\beta+\alpha)}{T\theta}\right]\left(\frac{1+t_m s}{1+t_G s}\right)\right\}e^{-\tau_L s} & \frac{K_F}{K_M}\left[\frac{p^2M^2}{T\theta(1+0.2M^2)^3}\right]\left(\frac{1+t_m s}{1+t_G s}\right)e^{-\tau_F s}+\frac{DbpMs}{K_M\sqrt{T}} & -\frac{K_G p}{\sqrt{T}}\left[\frac{p}{W_G}+\left(\frac{p\alpha}{T\theta}\right)\left(\frac{1+t_m s}{1+t_G s}\right)\right]e^{-\tau_G s} \end{bmatrix} \times \begin{bmatrix} A_L \\ N \\ A_G \end{bmatrix}$$

Figure 3.- Lumped-parameter multivariable model of 0.3-m TCT.

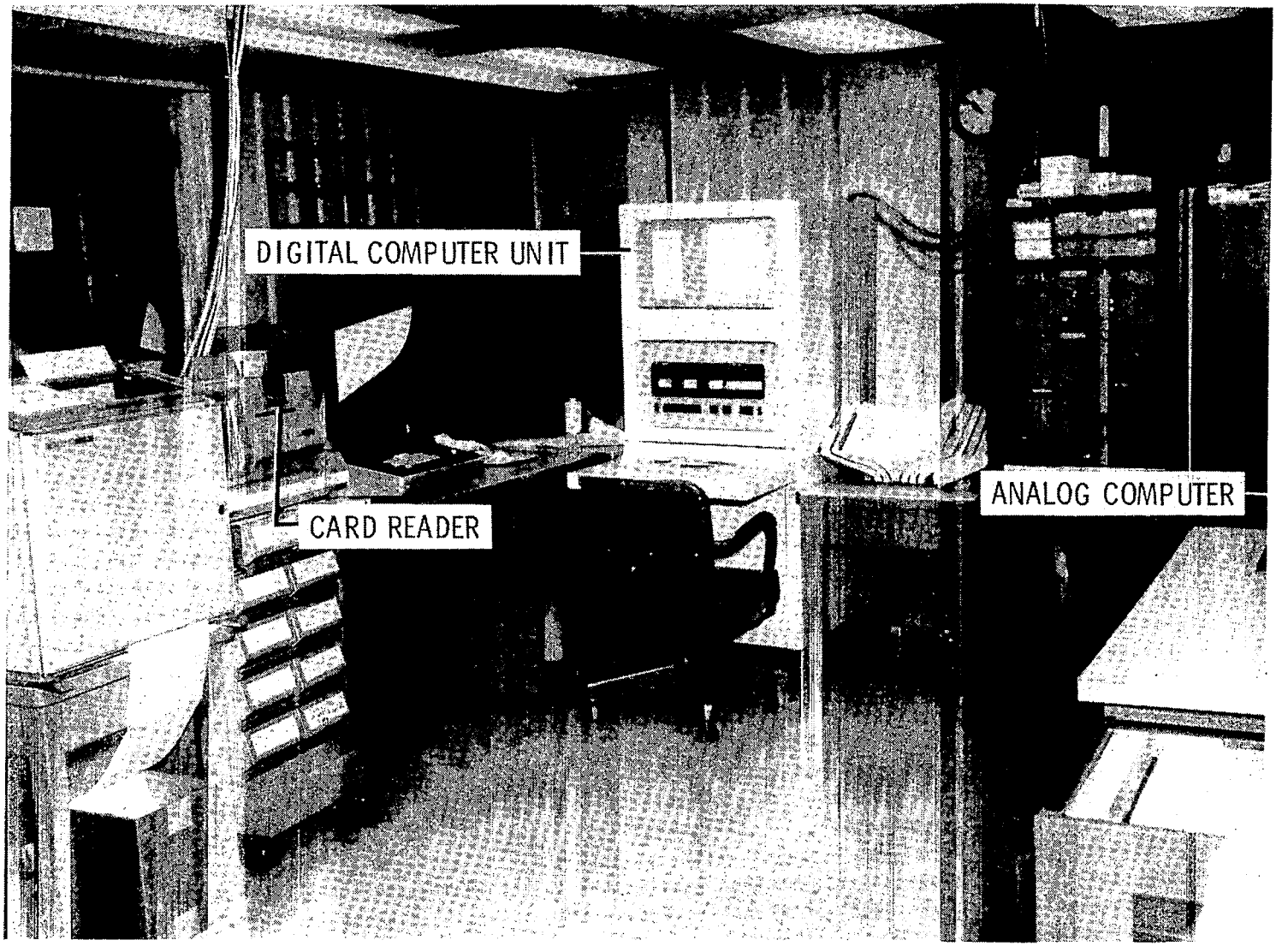

L-79-1665.1

Figure 4.- Hybrid-computer simulation facility.

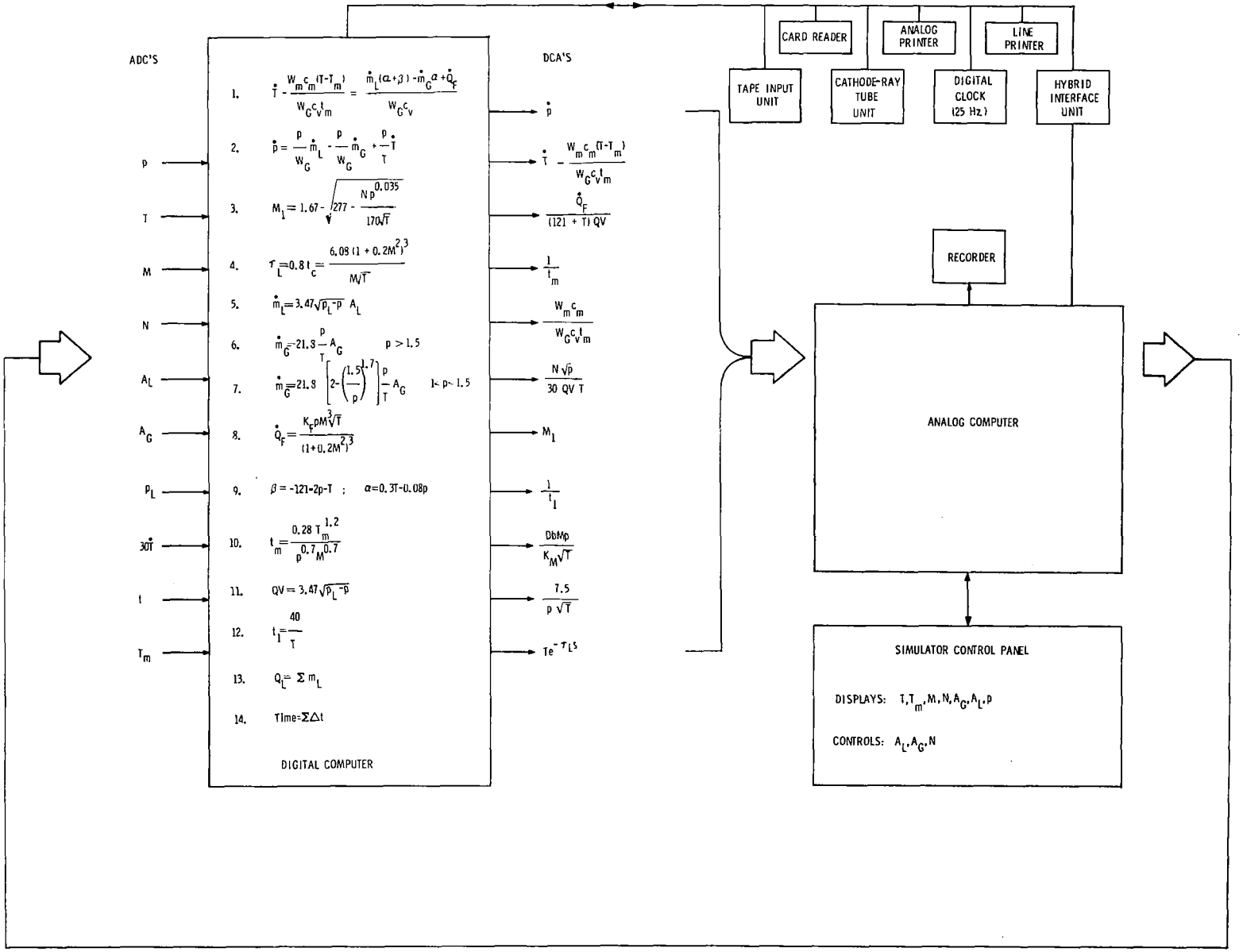

Figure 5.- Block diagram of hybrid-computer simulation.

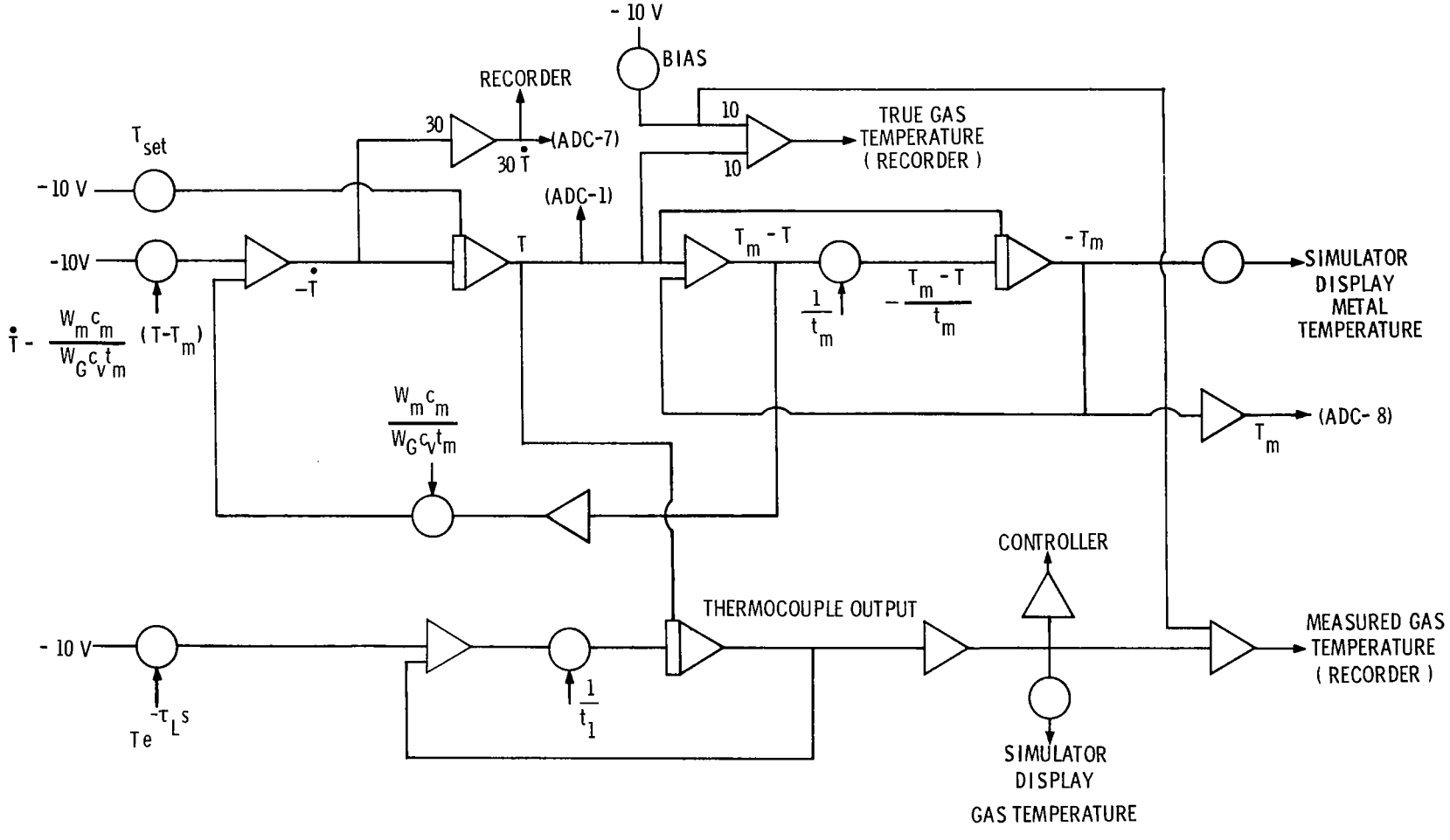

(a) Temperature dynamics.

Figure 6.- Loop diagrams of model dynamics and simulation control.

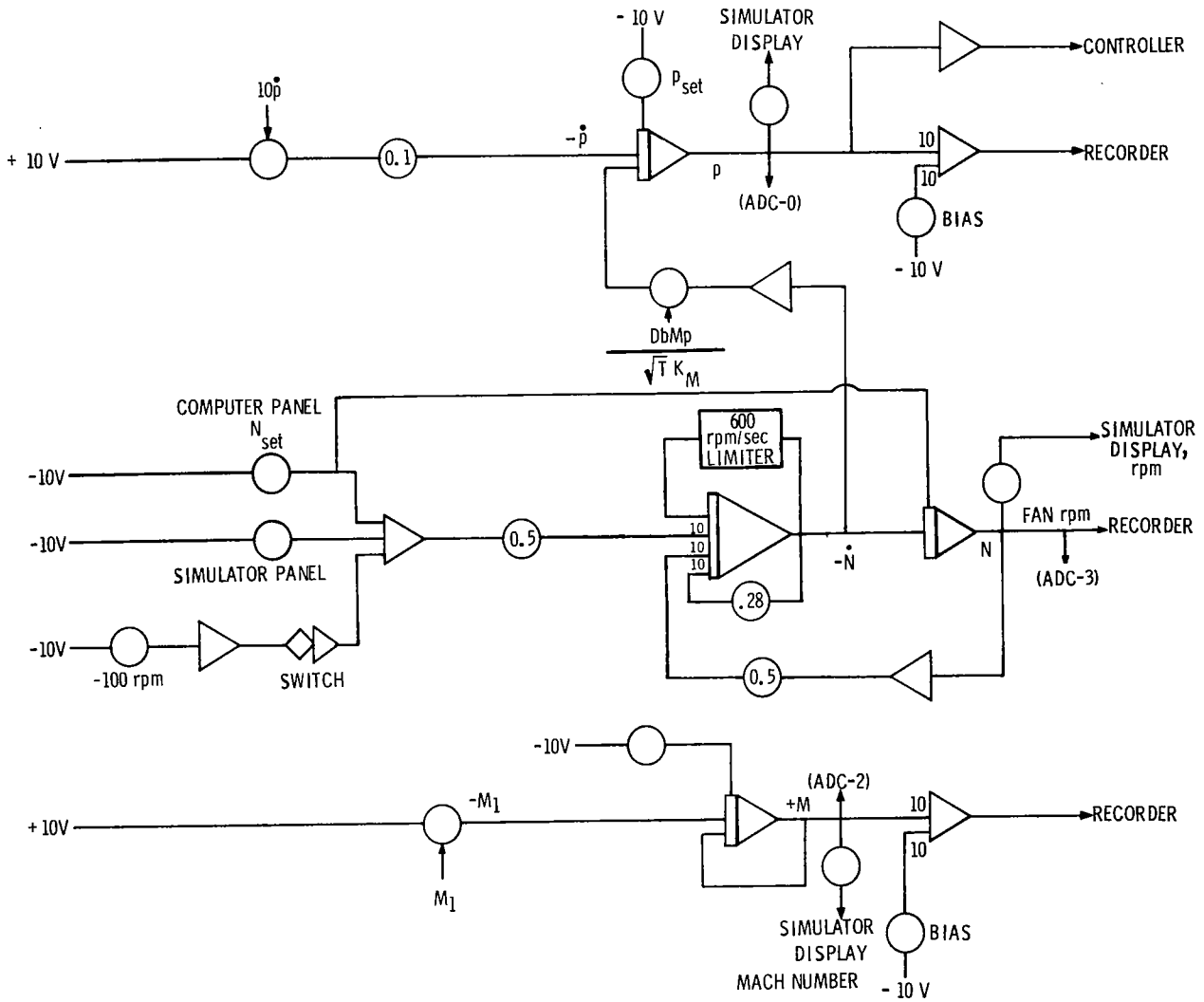

(b) Pressure, fan, and Mach number dynamics.

Figure 6.- Continued.

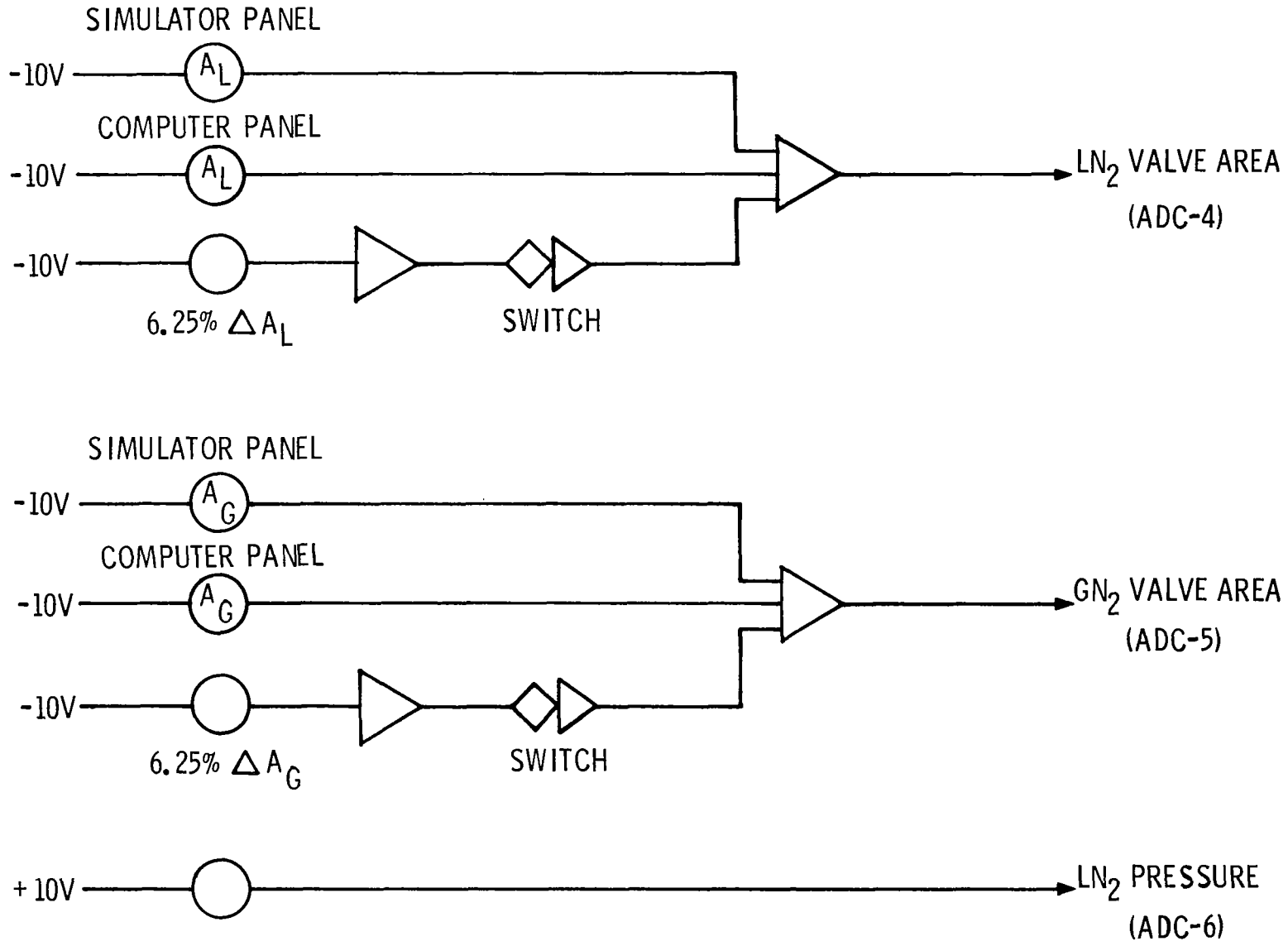

(c) Simulator analog block diagram.

Figure 6.- Continued.

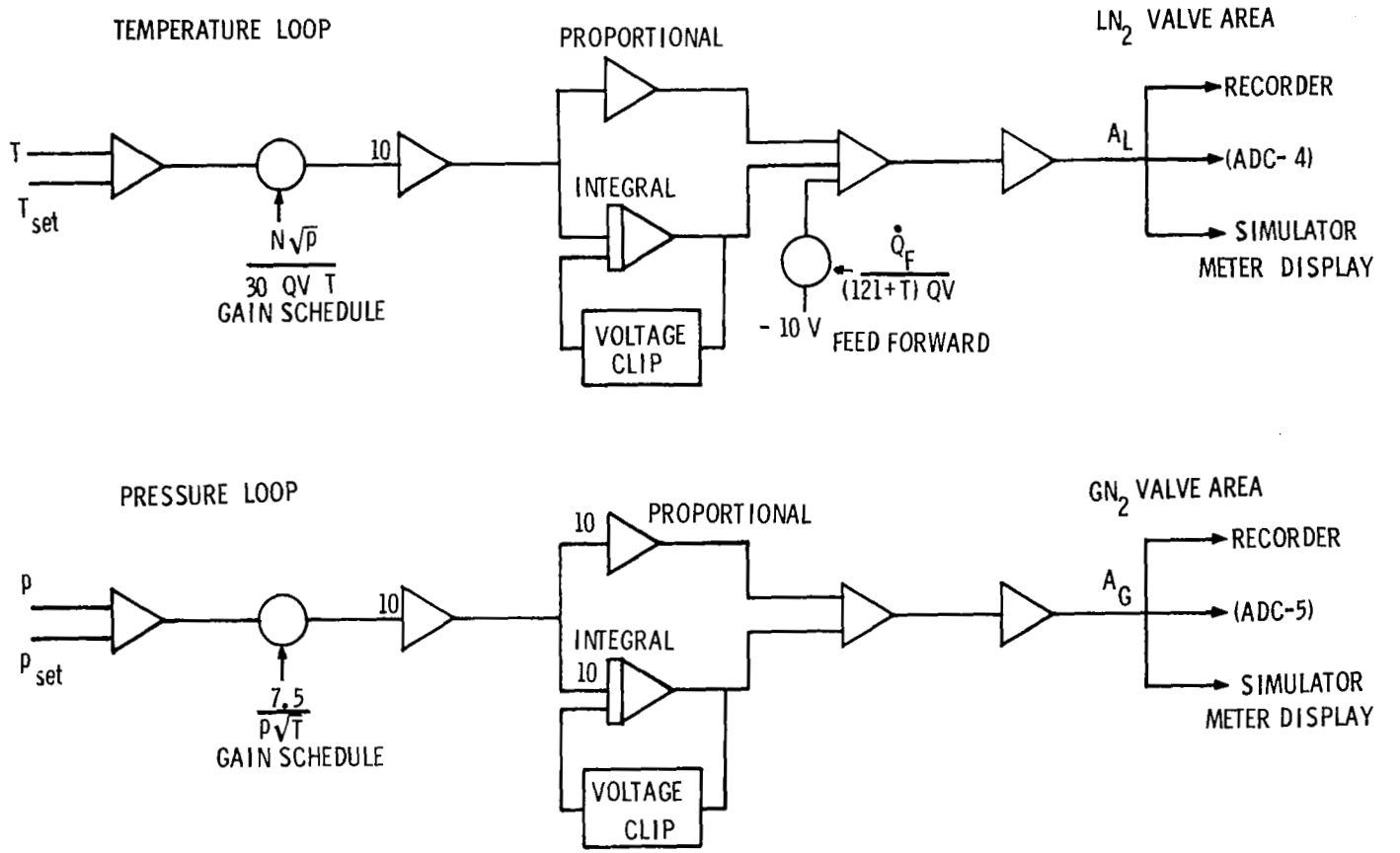

(d) Closed-loop controllers for temperature and pressure.

Figure 6.- Concluded.

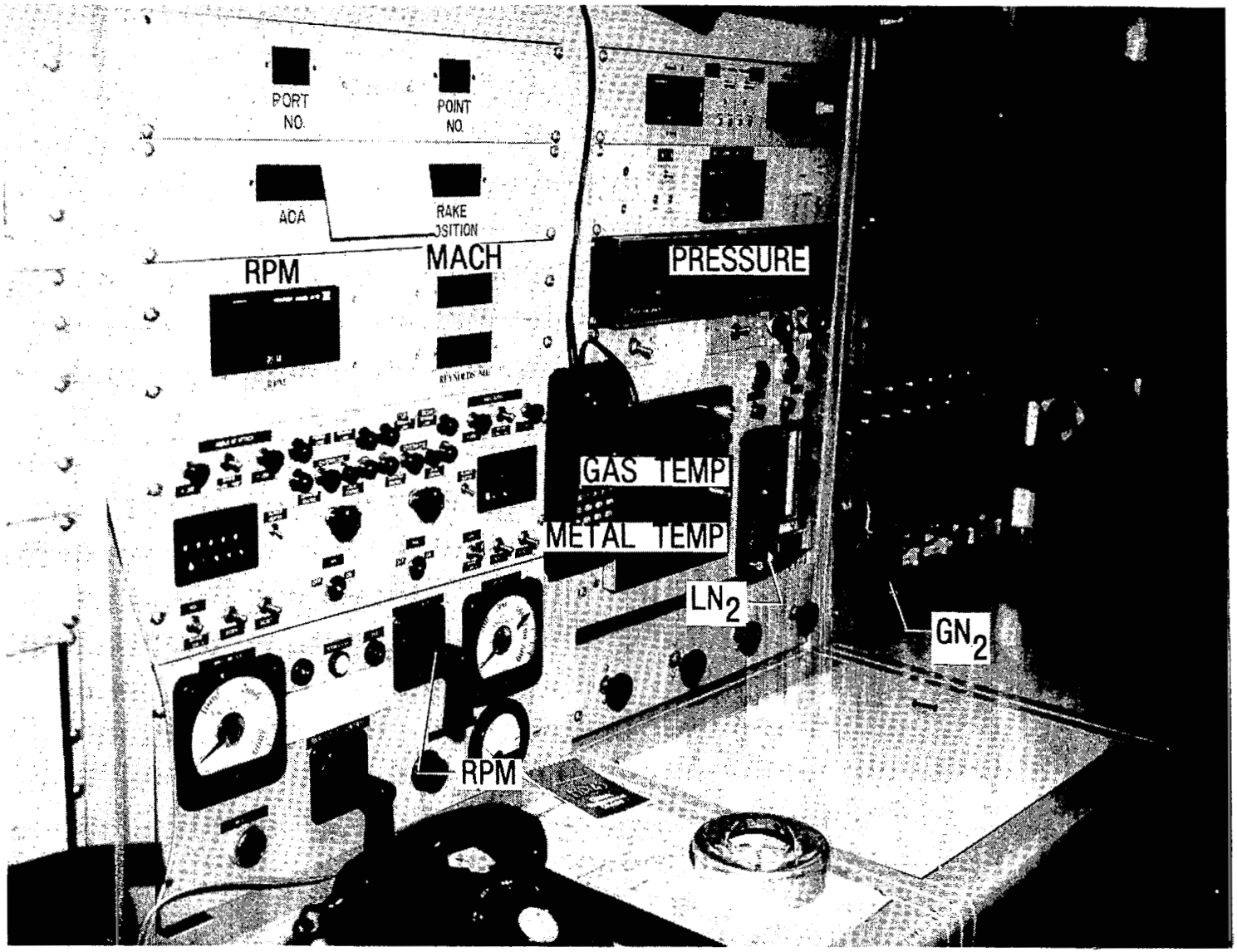

L-79-1666.1

Figure 7.- Control panel 0.3-m TCT.

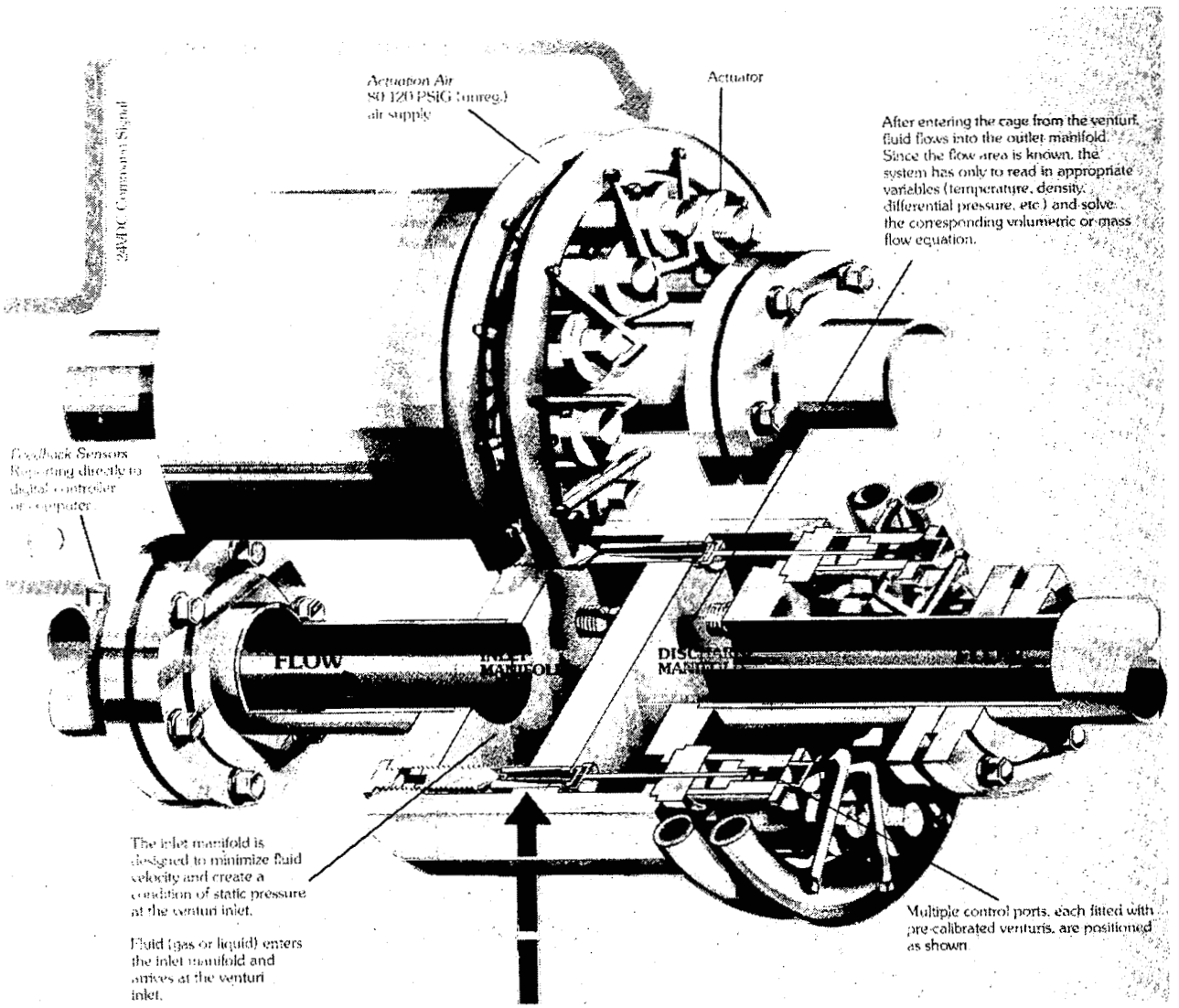

Figure 8.- Digital control valve. (1 atm = 14.7 psi.)

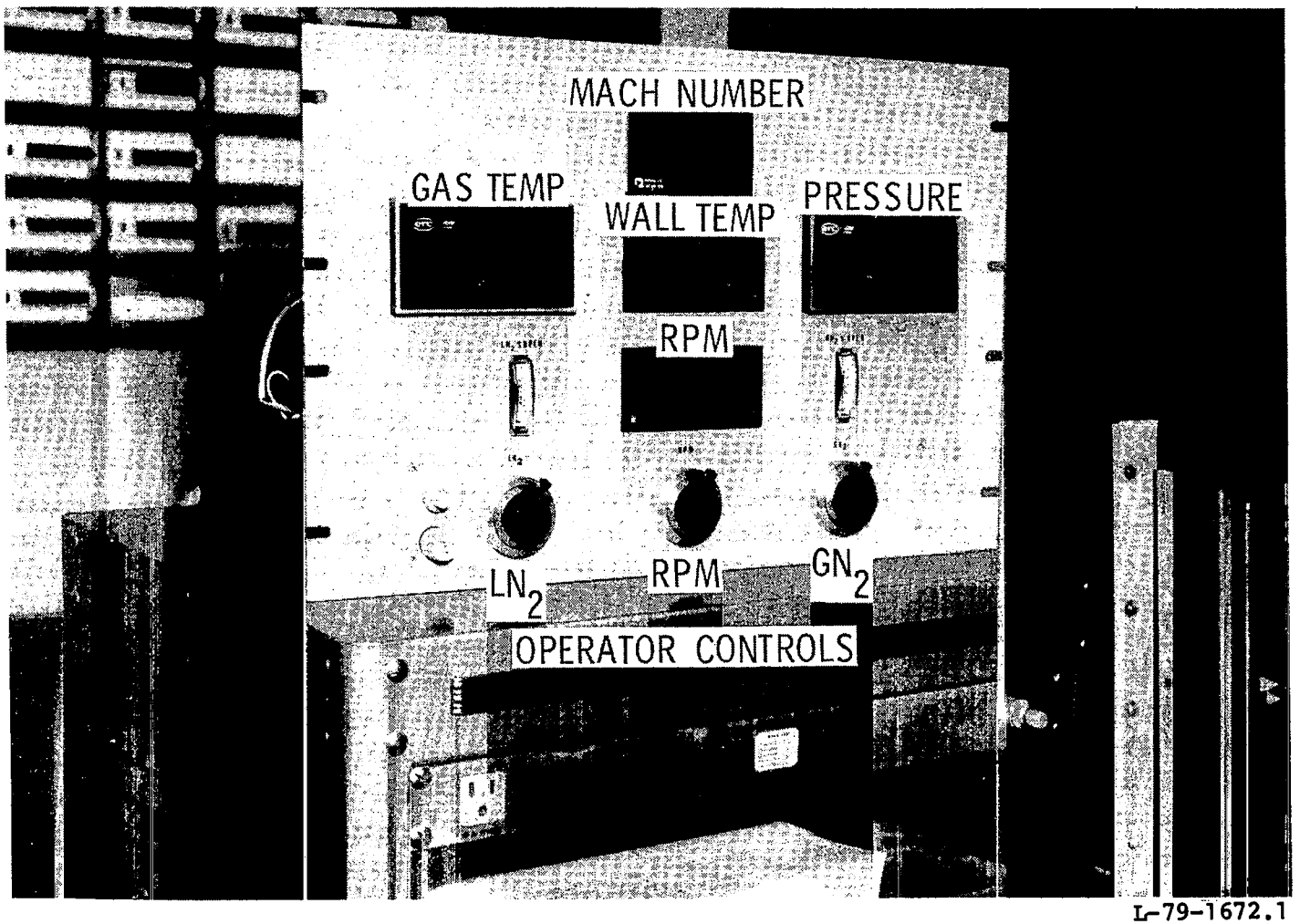

Figure 9.- Control panel for hybrid-computer simulation.

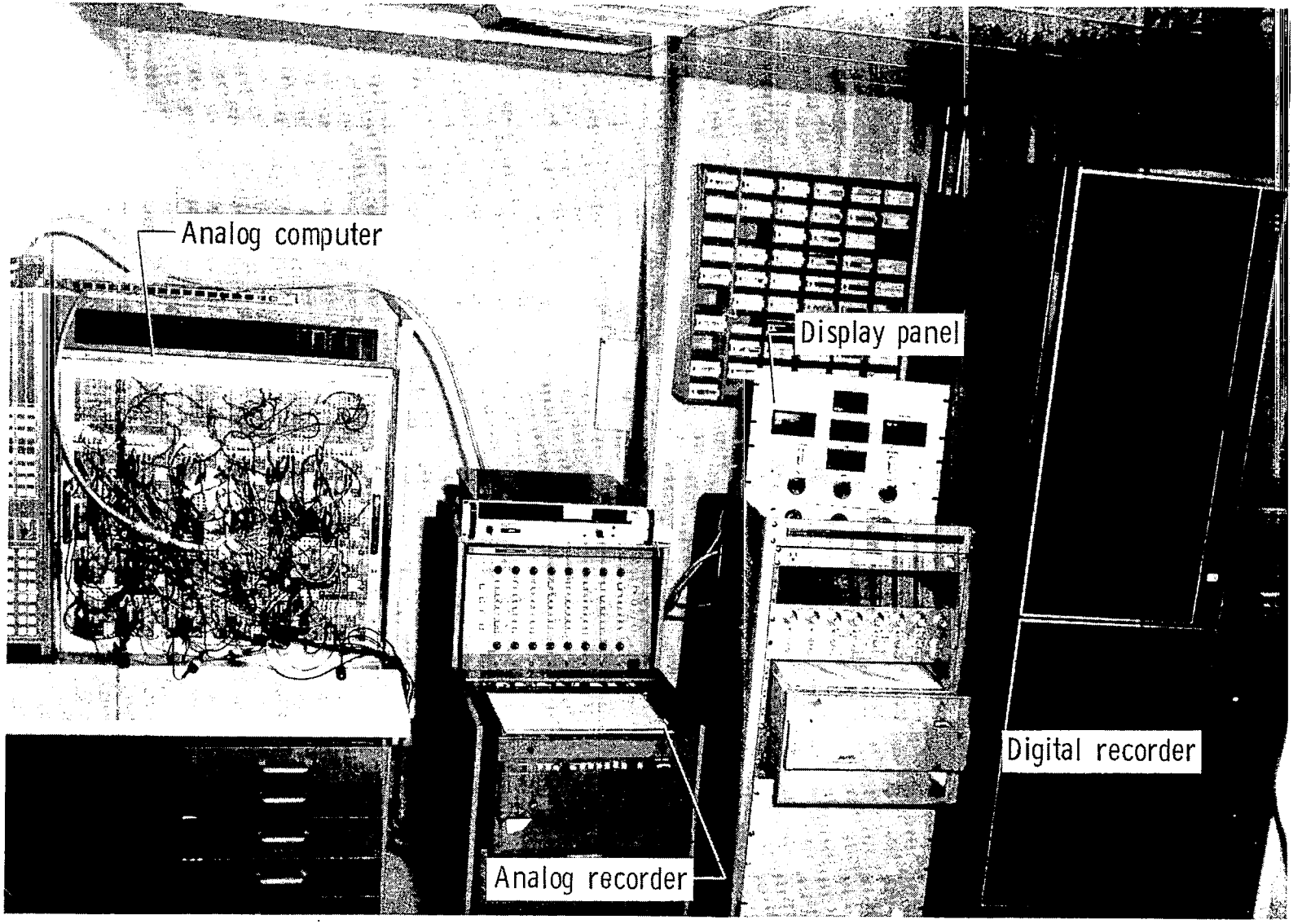

L-79-4845.1

Figure 10.- Simulator instrumentation.

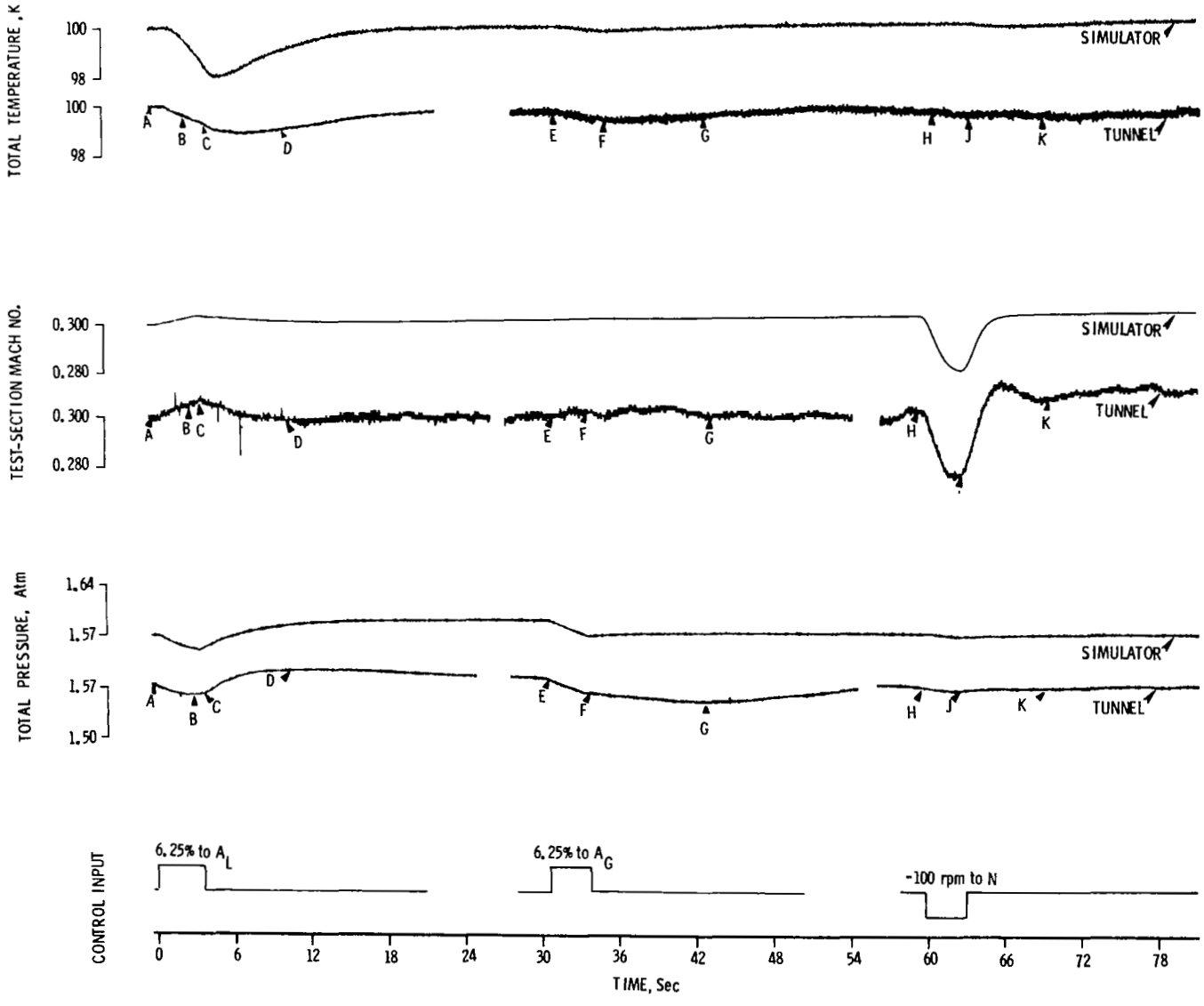

Figure 11.- Simulator and tunnel transient response data at T = 100 K, M = 0.3, and p = 1.57 atm.

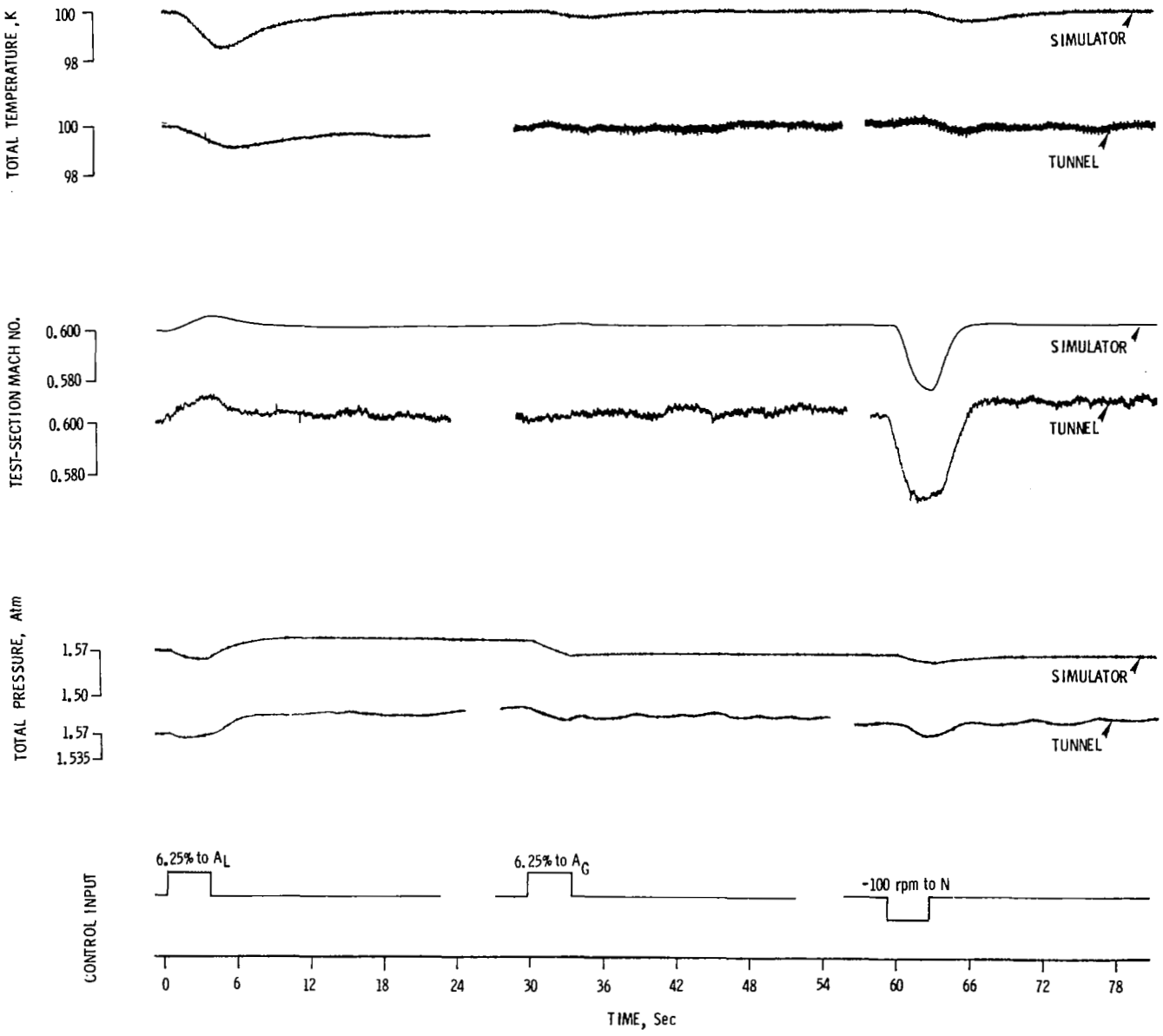

Figure 12.- Simulator and tunnel transient response data at T = 100 K, M = 0.6, and p = 1.57 atm.

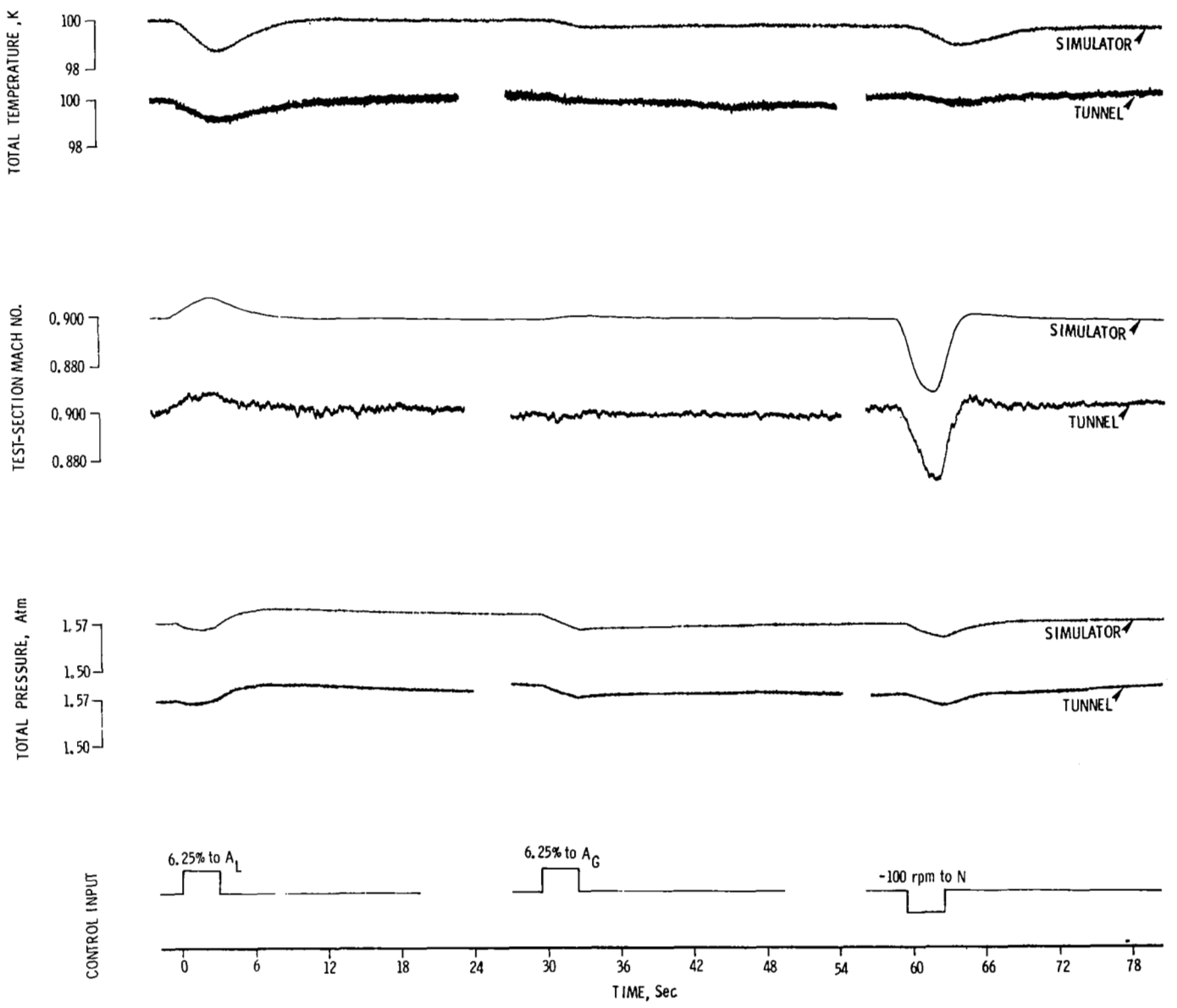

Figure 13.- Simulator and tunnel transient response data at T = 100 K, M = 0.9, and p = 1.57 atm.

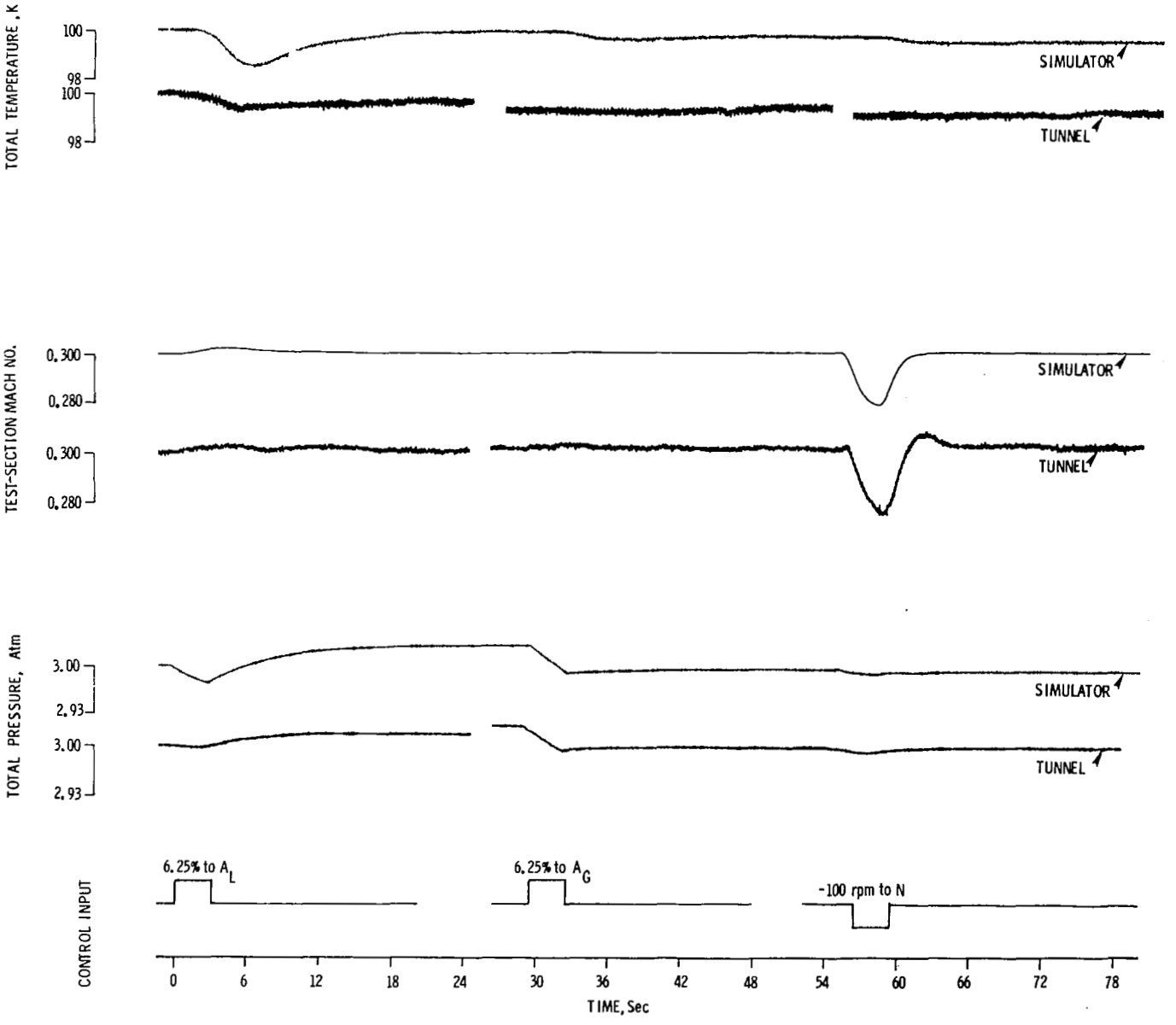

Figure 14.- Simulator and tunnel transient response data at T = 100 K, M = 0.3, and p = 3.00 atm.

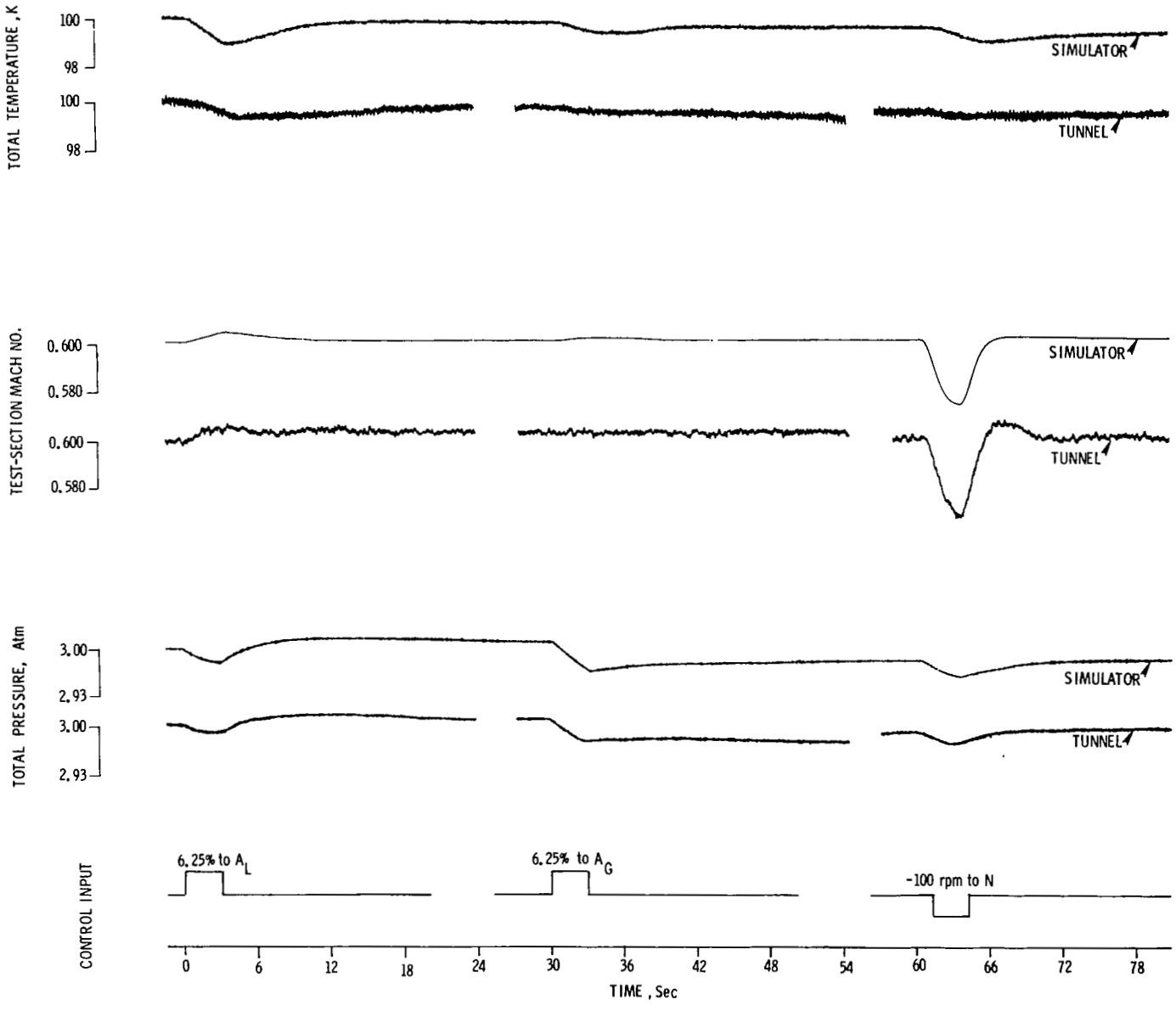

Figure 15.- Simulator and tunnel transient response data at T = 100 K, M = 0.6, and p = 3.00 atm.

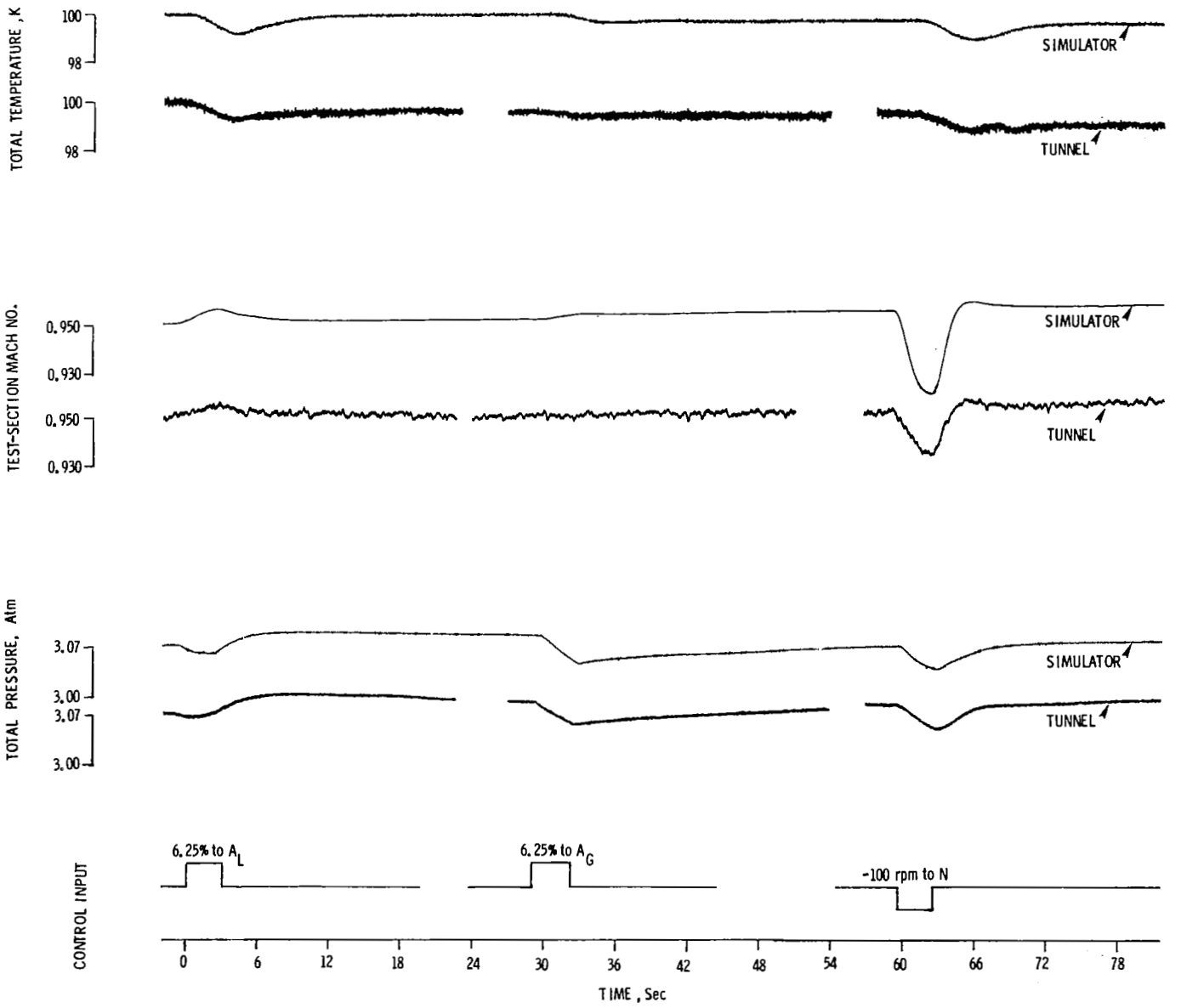

Figure 16.- Simulator and tunnel transient response data at T = 100 K, M = 0.95, and p = 3.07 atm.

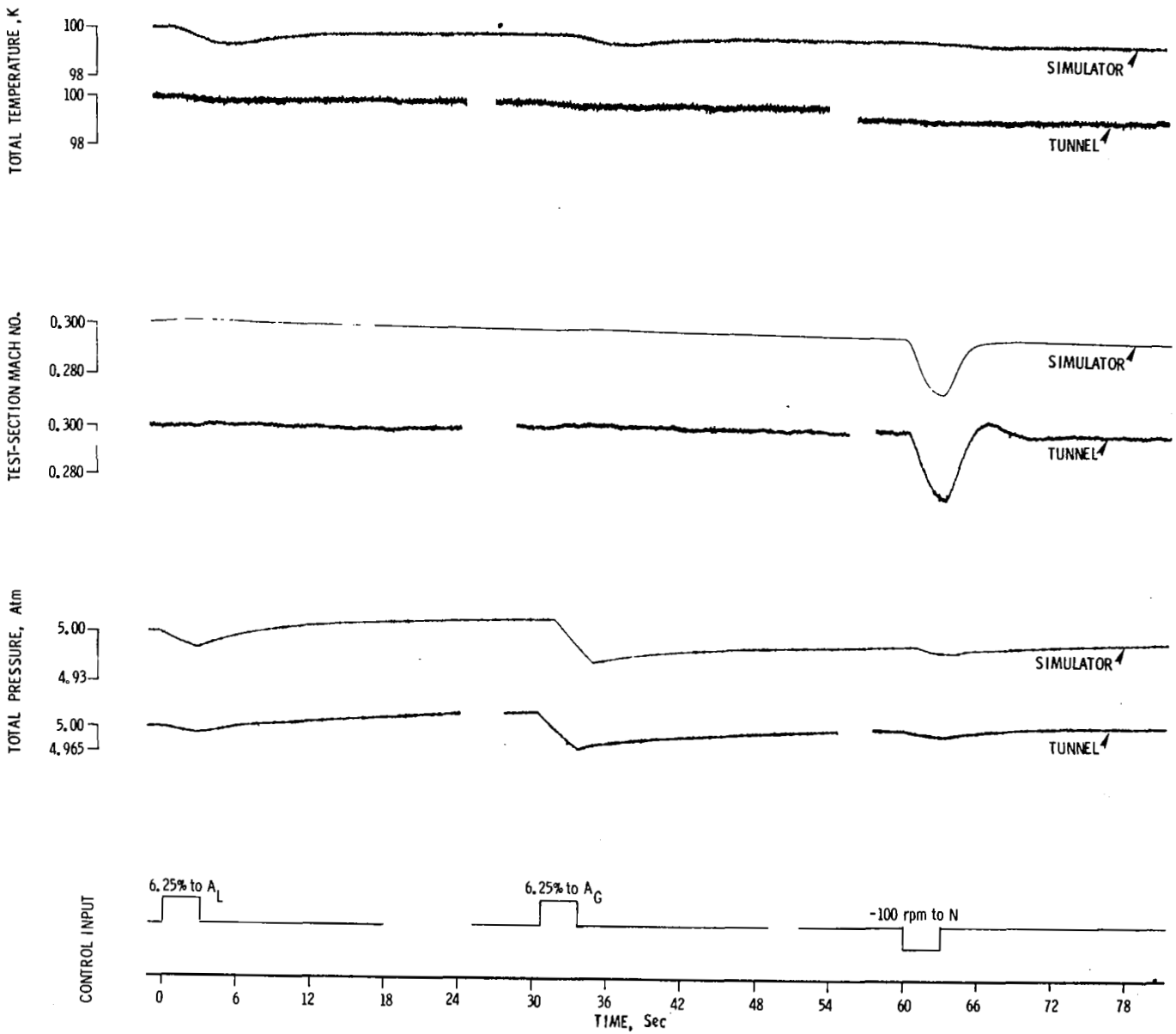

Figure 17.- Simulator and tunnel transient response data at T = 100 K, M = 0.3, and p = 5.00 atm.

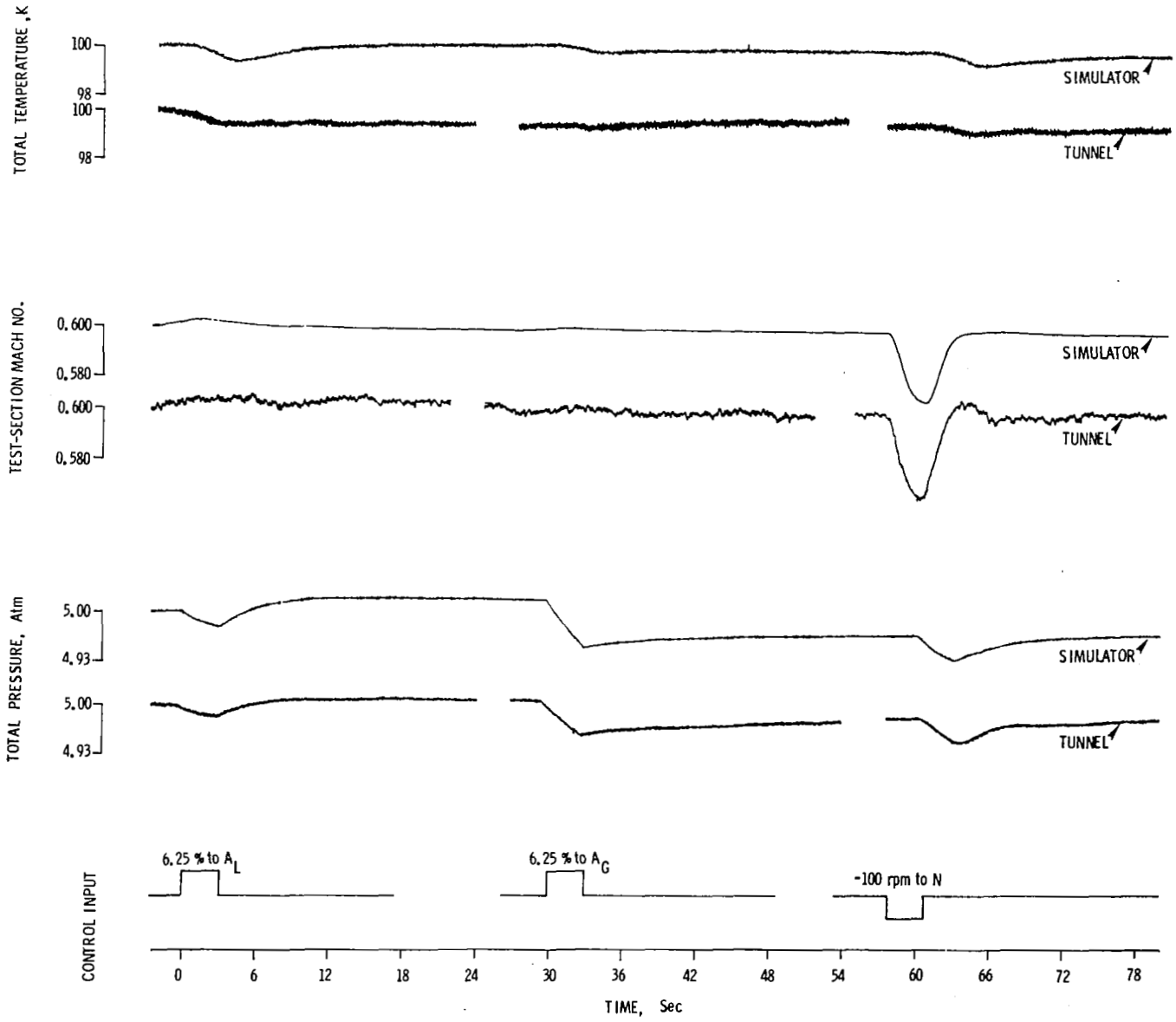

Figure 18.- Simulator and tunnel transient response data at T = 100 K, M = 0.6, and p = 5.00 atm.

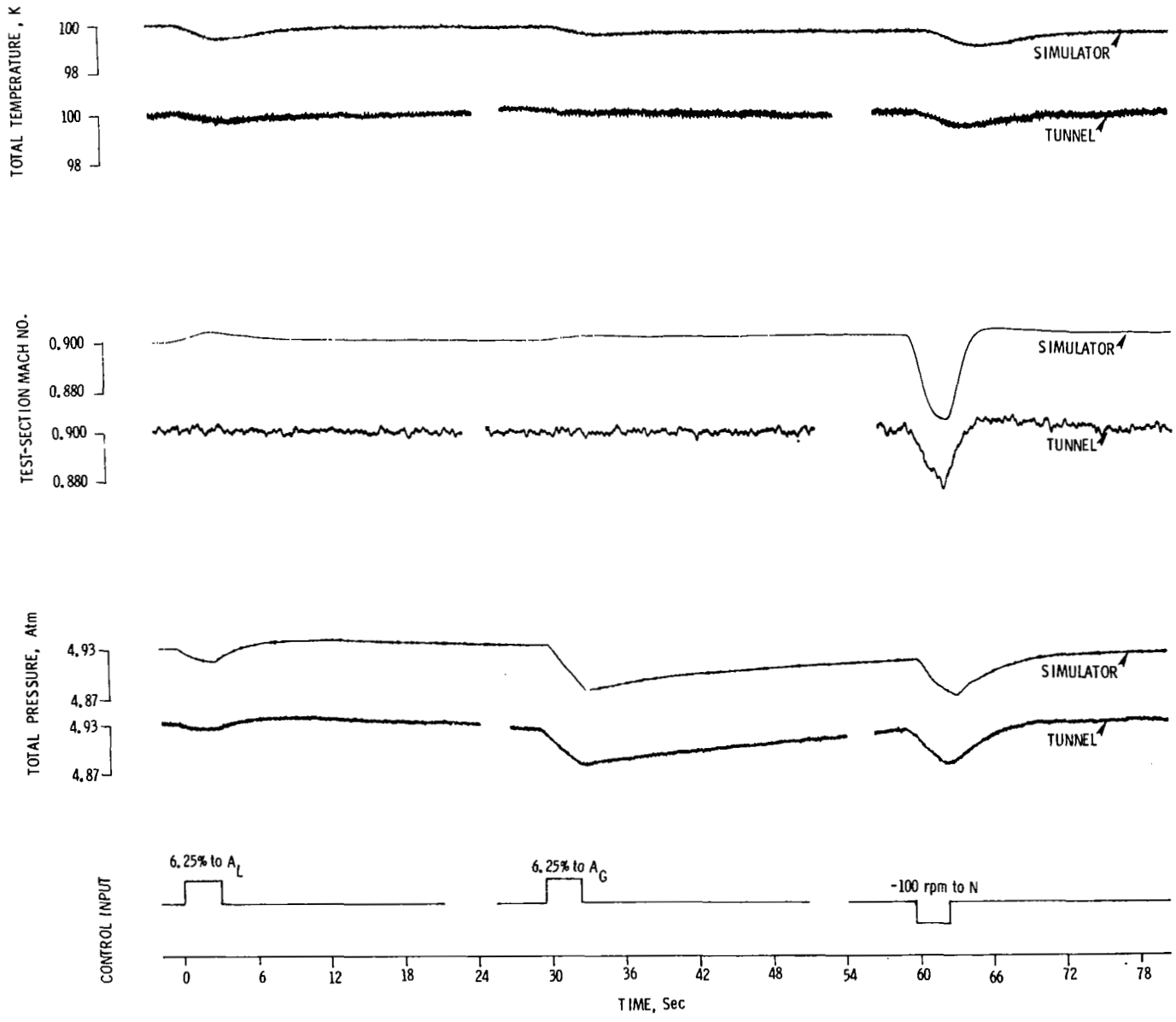

Figure 19.- Simulator and tunnel transient response data at T = 100 K, M = 0.9, and p = 4.93 atm.

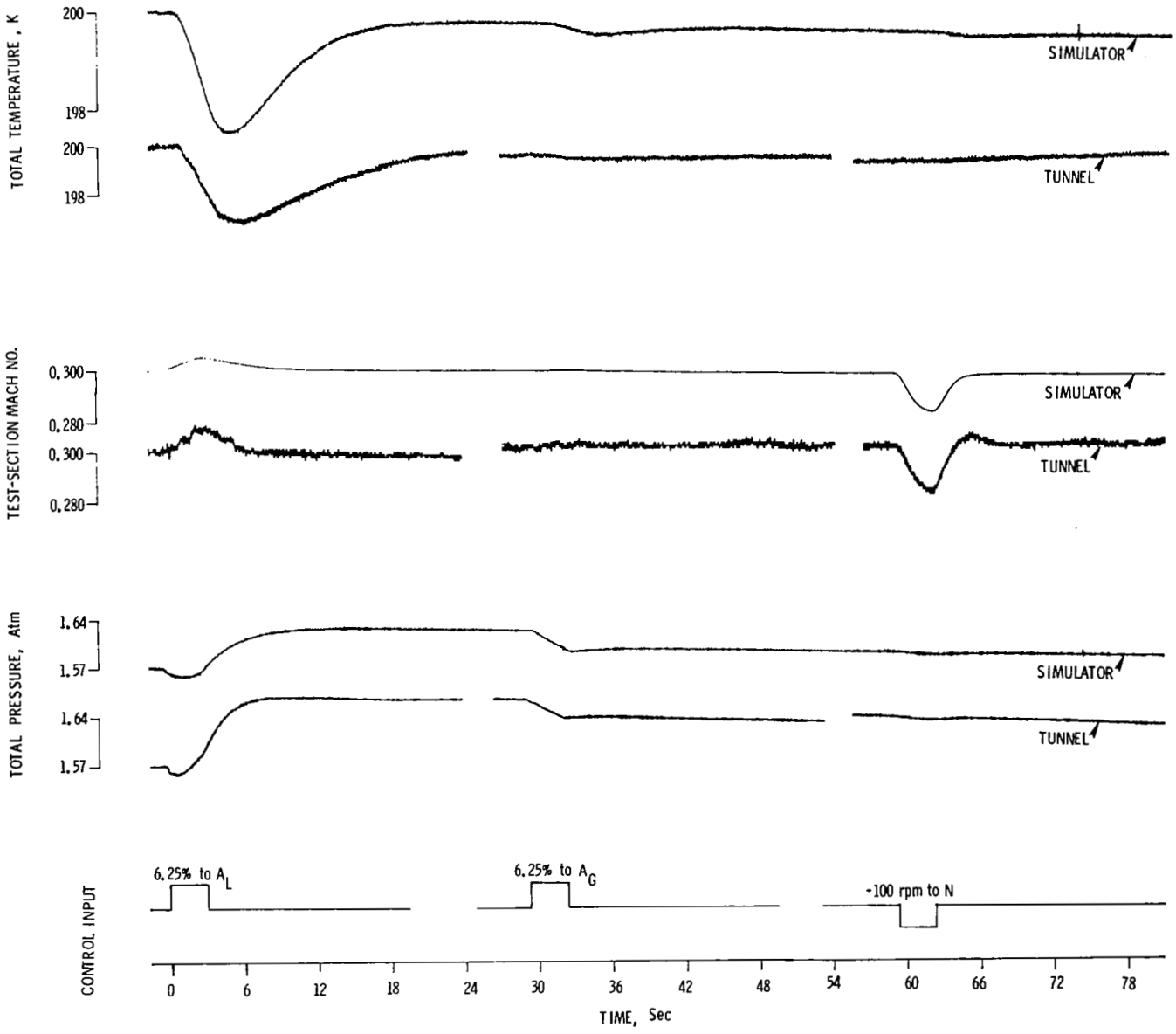

Figure 20.- Simulator and tunnel transient response data at T = 200 K, M = 0.3, and p = 1.57 atm.

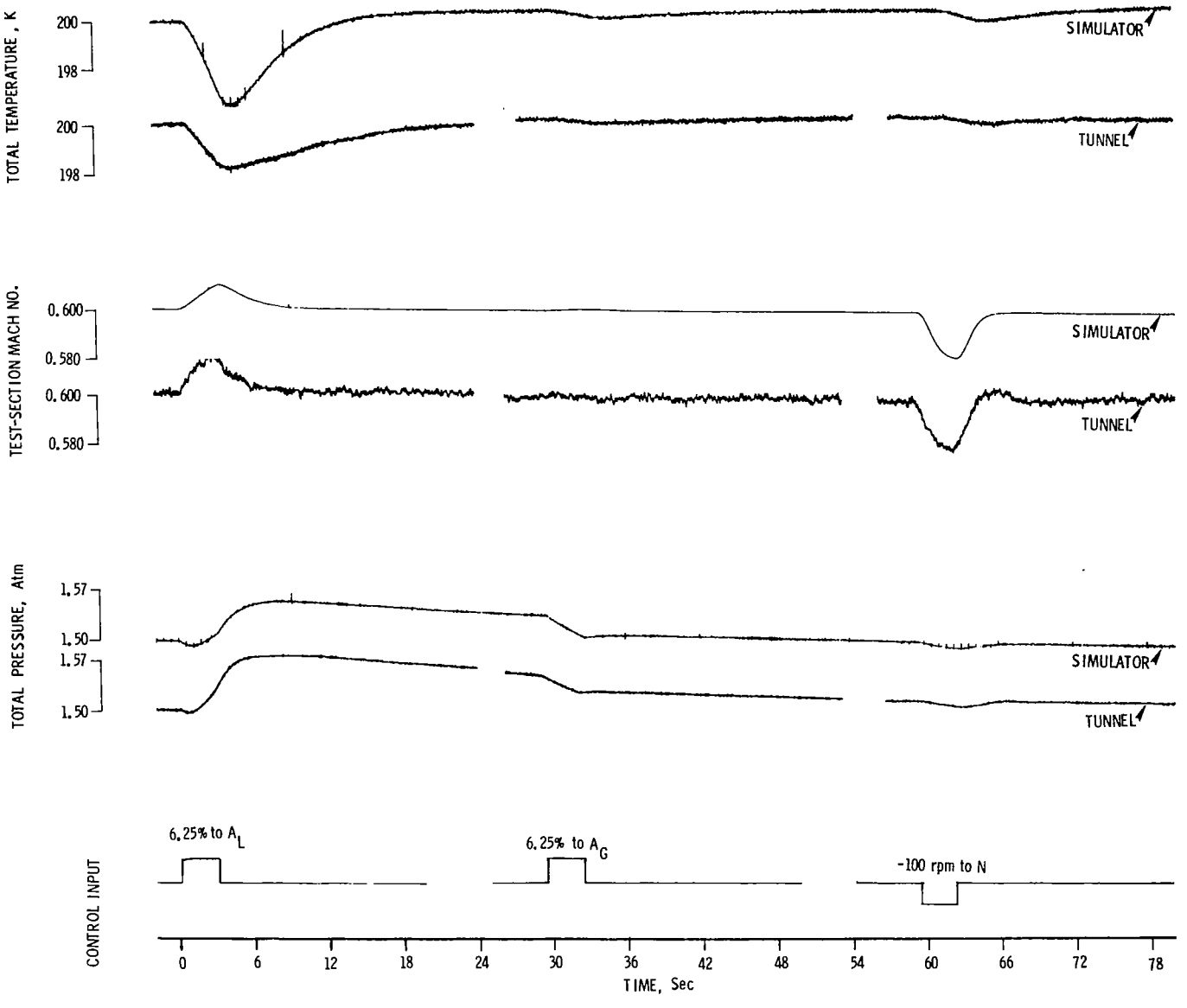

Figure 21.- Simulator and tunnel transient response data at T = 200 K, M = 0.6, and p = 1.50 atm.

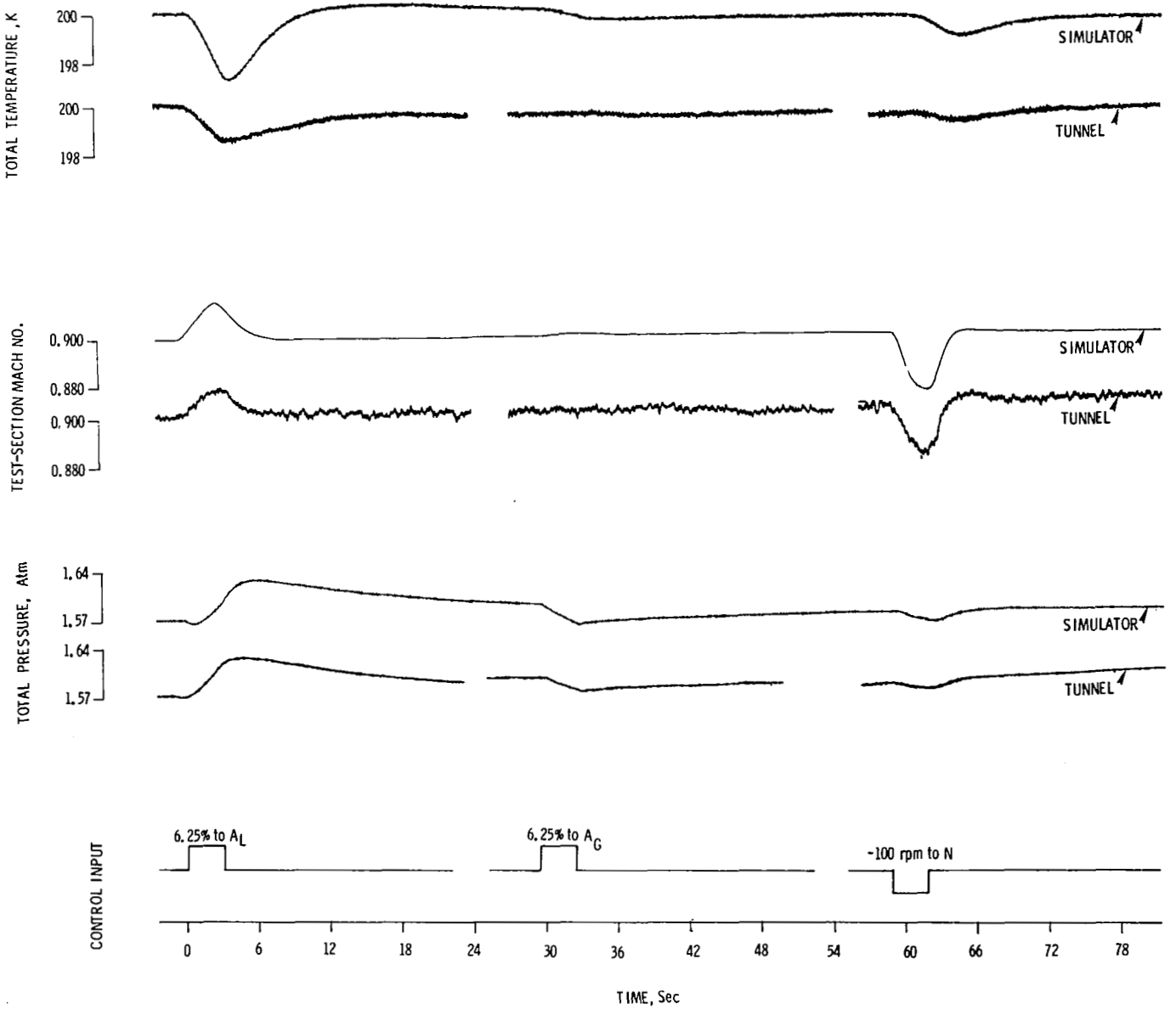

Figure 22.- Simulator and tunnel transient response data at T = 200 K, M = 0.9, and p = 1.57 atm.

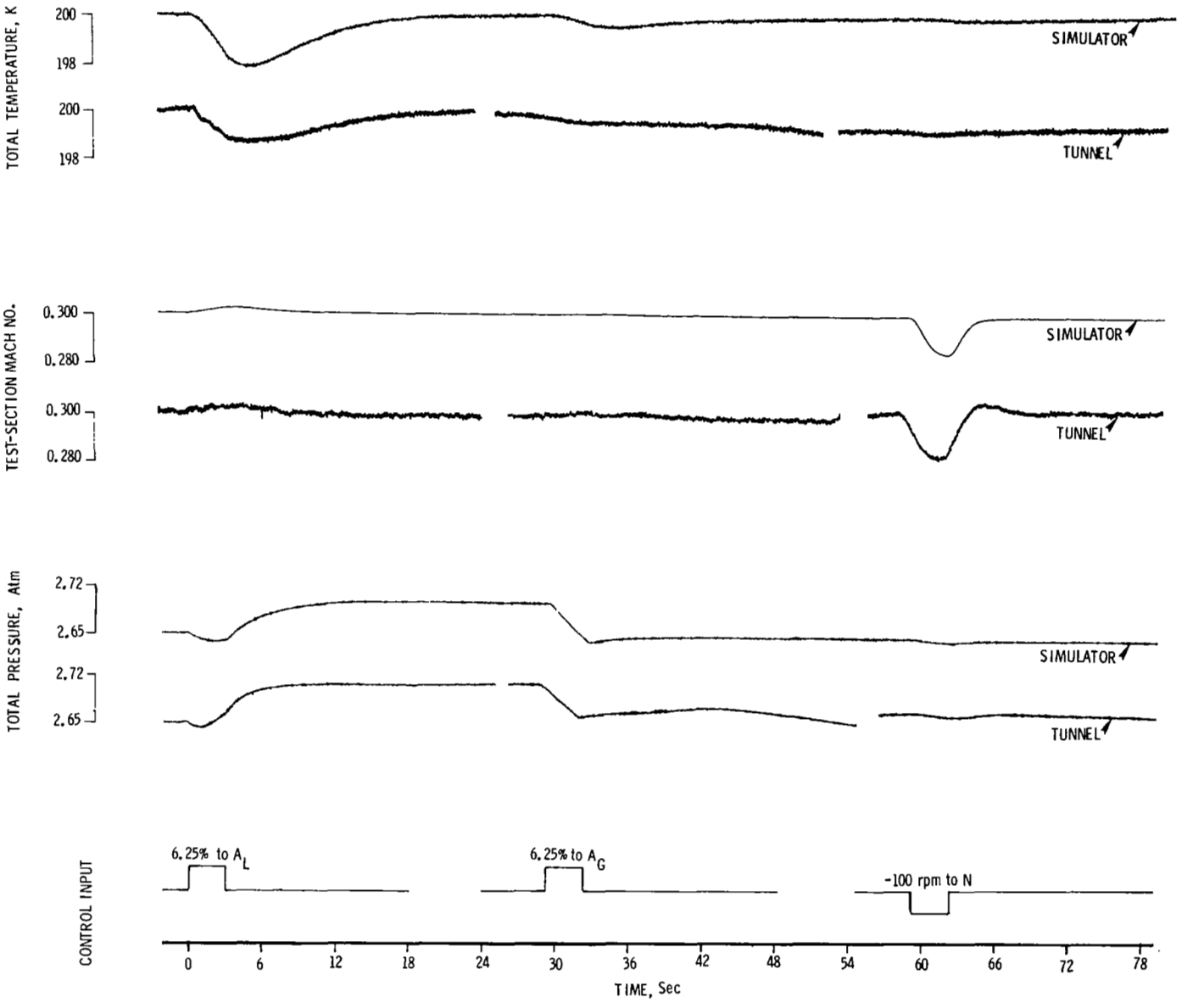

Figure 23.- Simulator and tunnel transient response data at T = 200 K, M = 0.3, and p = 2.65 atm.

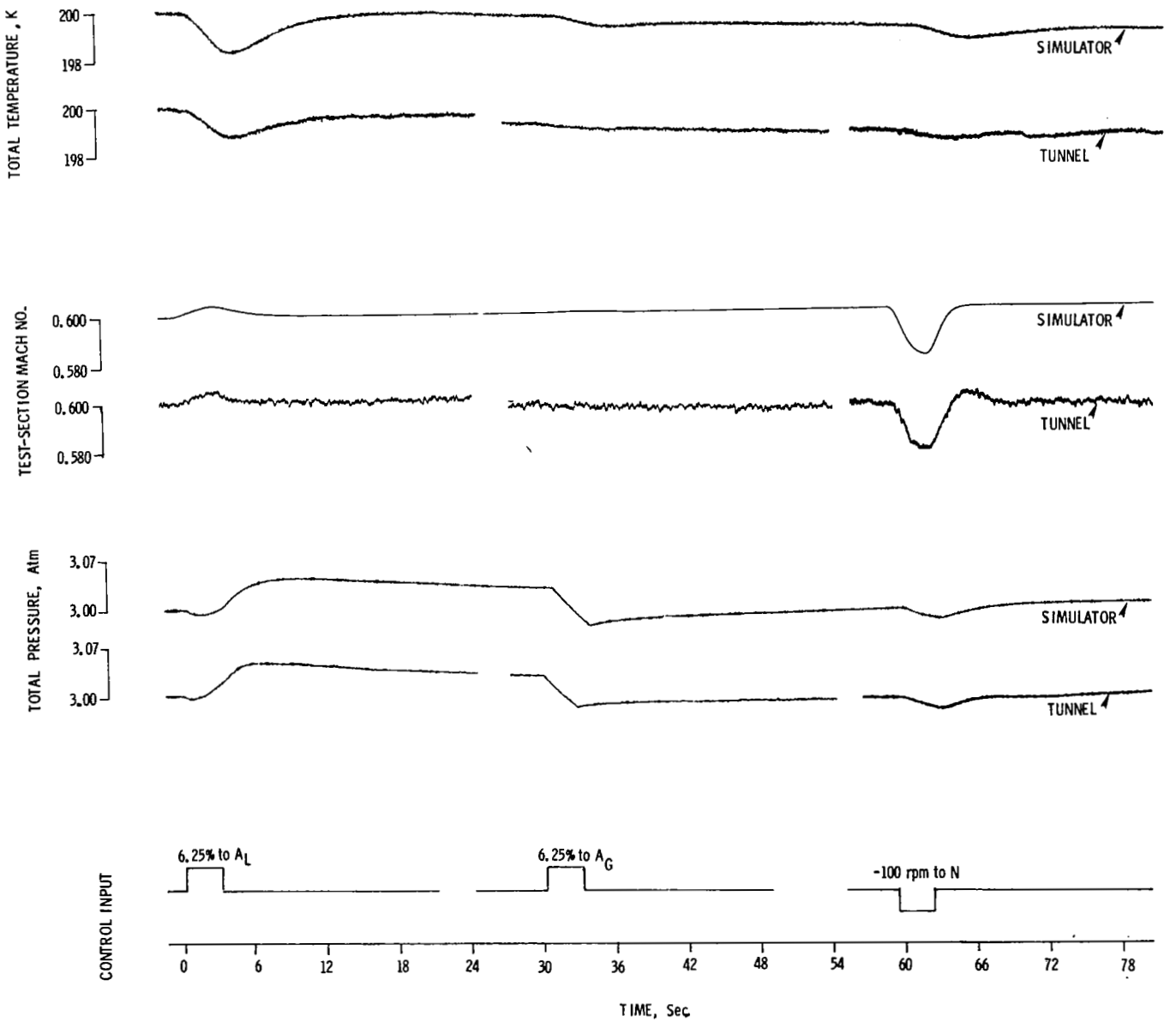

Figure 24.- Simulator and tunnel transient response data at T = 200 K, M = 0.6, and p = 3.00 atm.

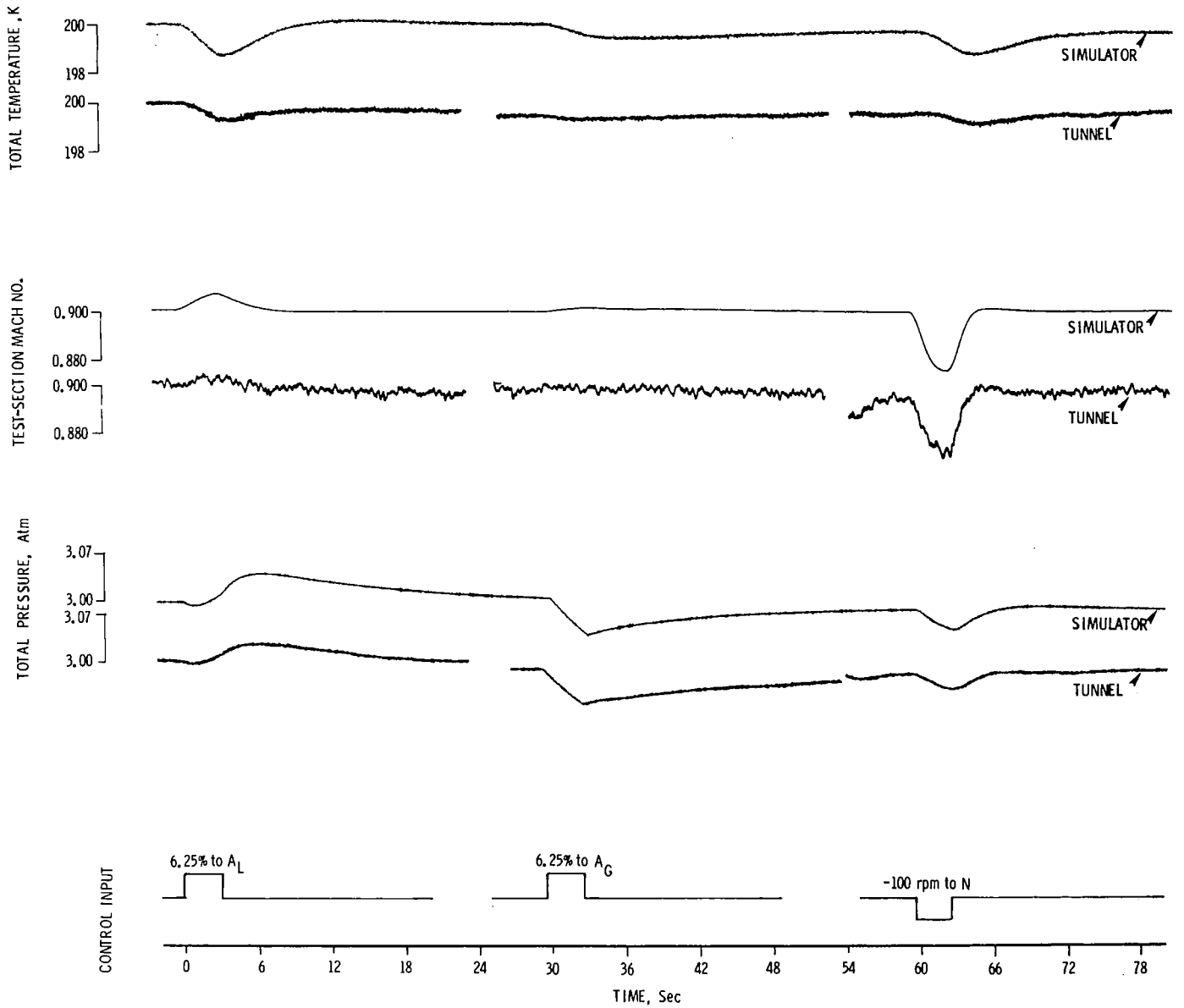

Figure 25.- Simulator and tunnel transient response data at T = 200 K, M = 0.9, and p = 3.00 atm.

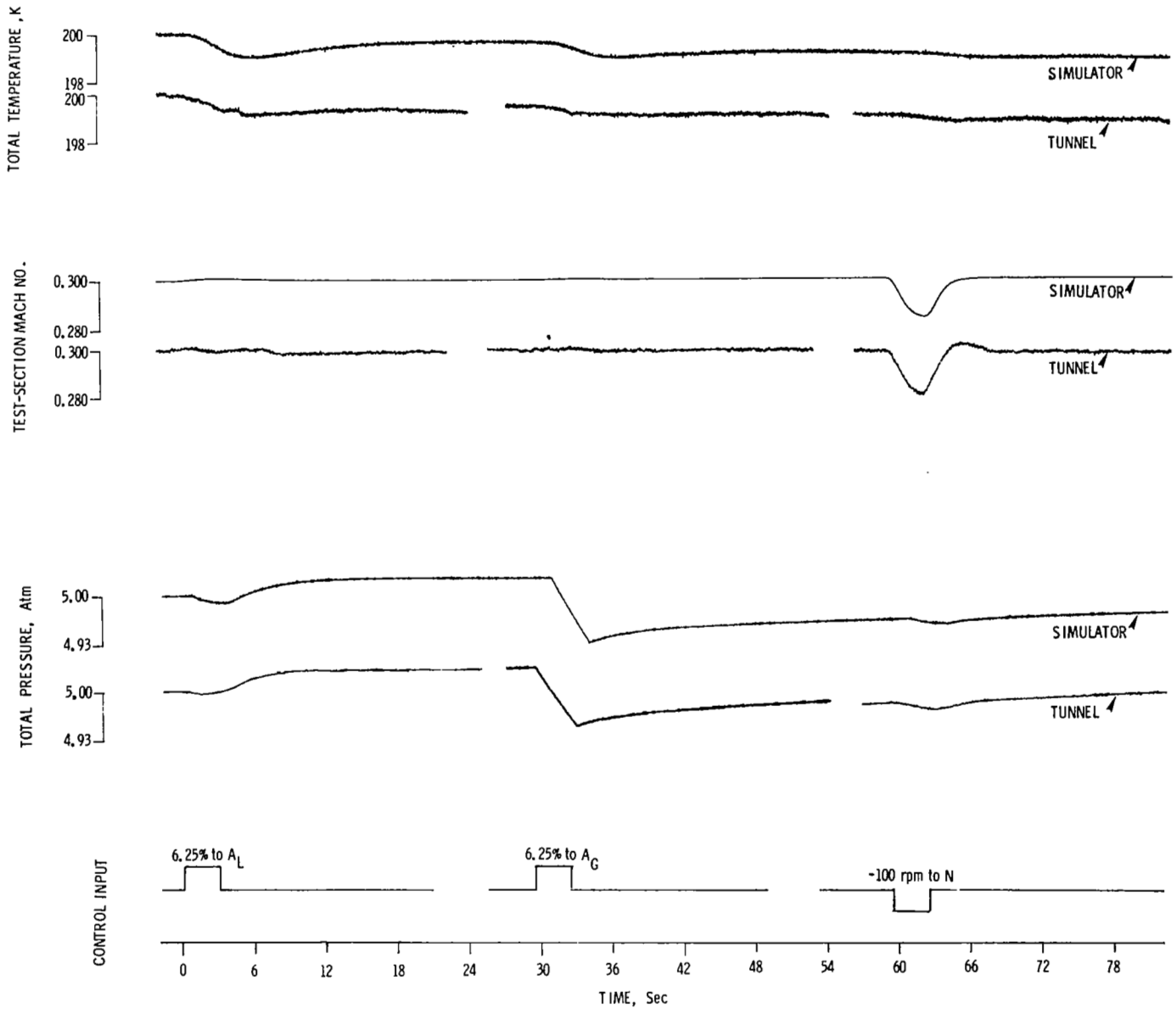

Figure 26.- Simulator and tunnel transient response data at T = 200 K, M = 0.3, and p = 5.00 atm.

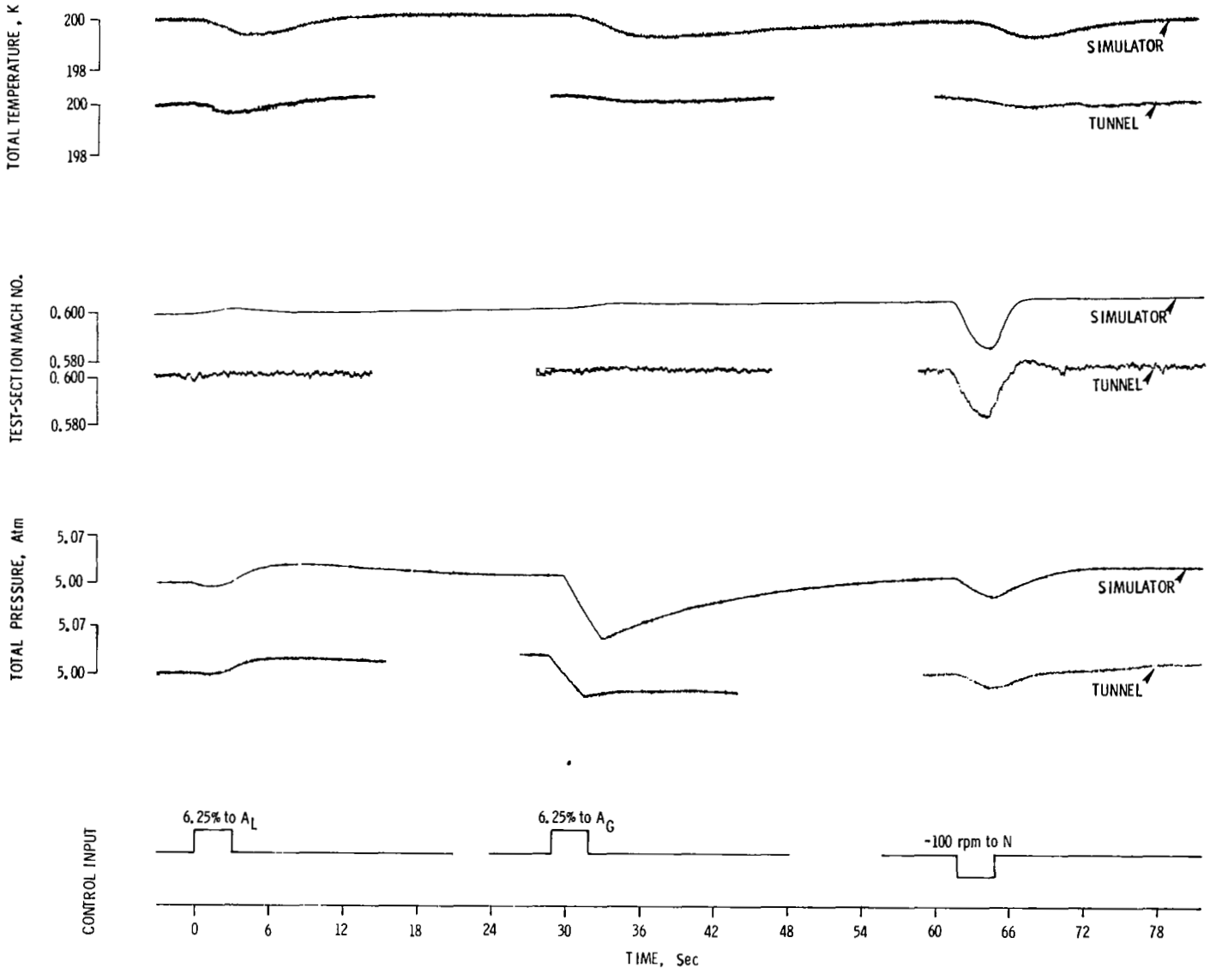

Figure 27.- Simulator and tunnel transient response data at T = 200 K, M = 0.6, and p = 5.00 atm.

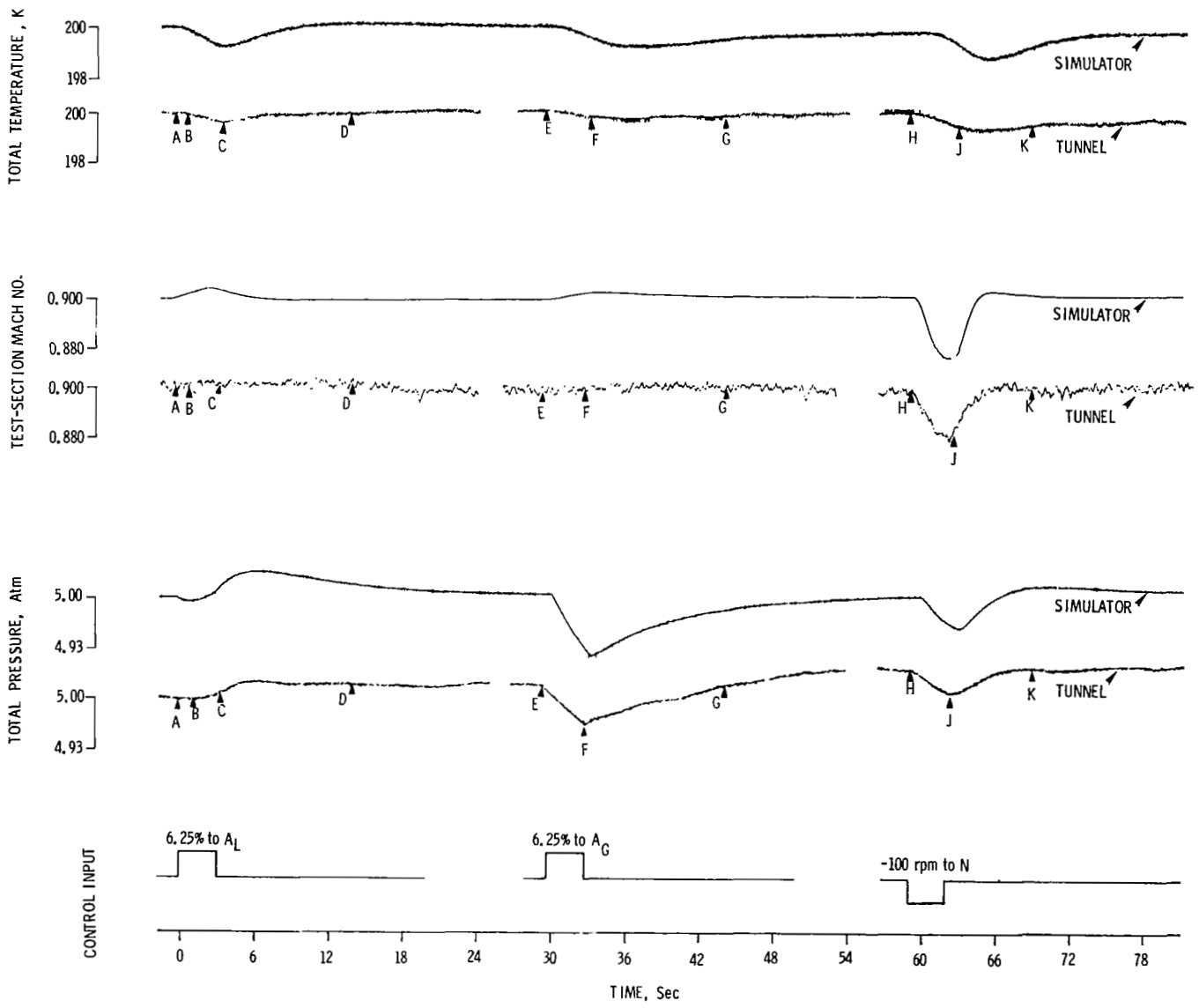

Figure 28.- Simulator and tunnel transient response data at T = 200 K, M = 0.9, and p = 5.00 atm.

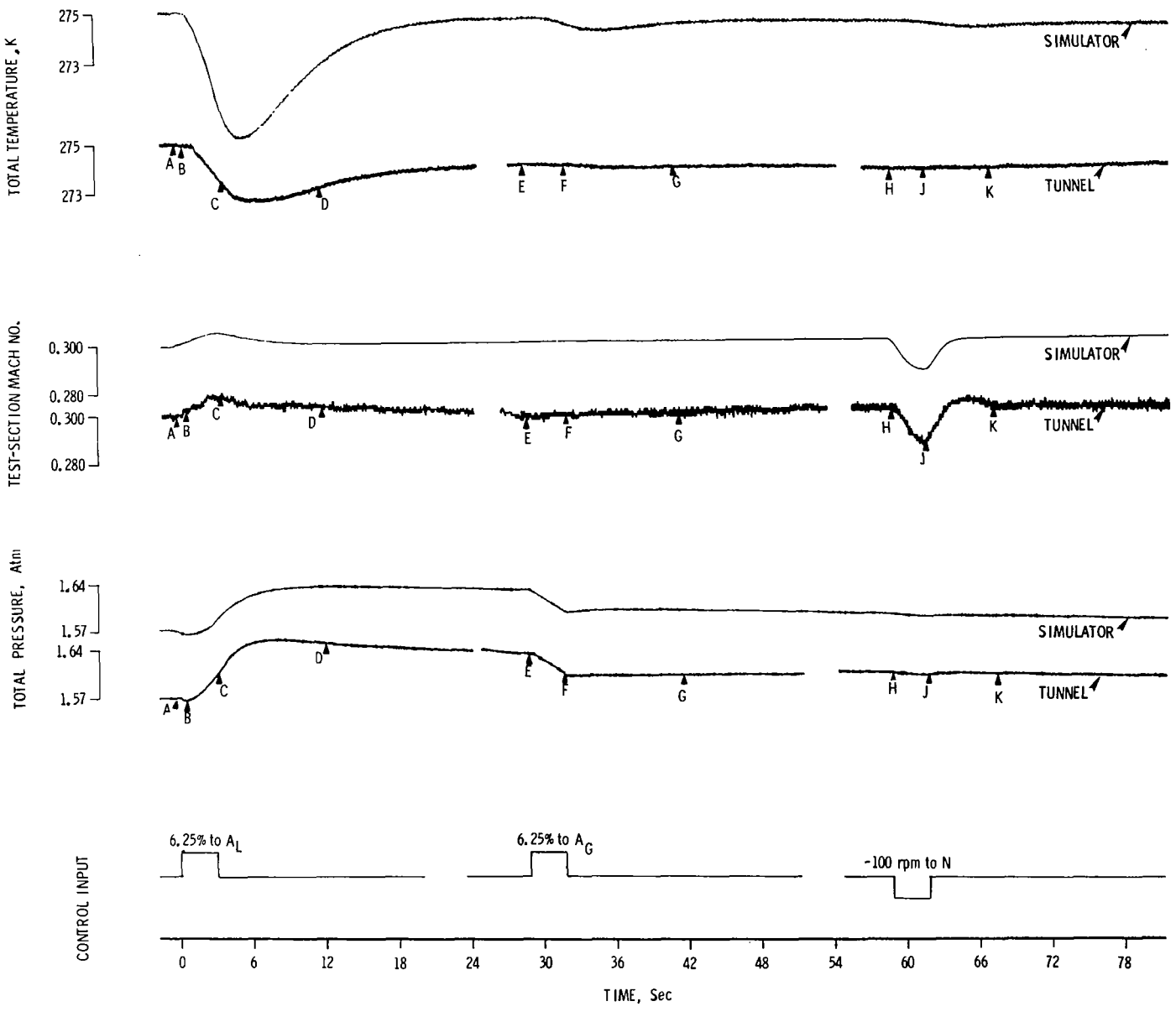

Figure 29.- Simulator and tunnel transient response data at T = 275 K, M = 0.3, and p = 1.57 atm.

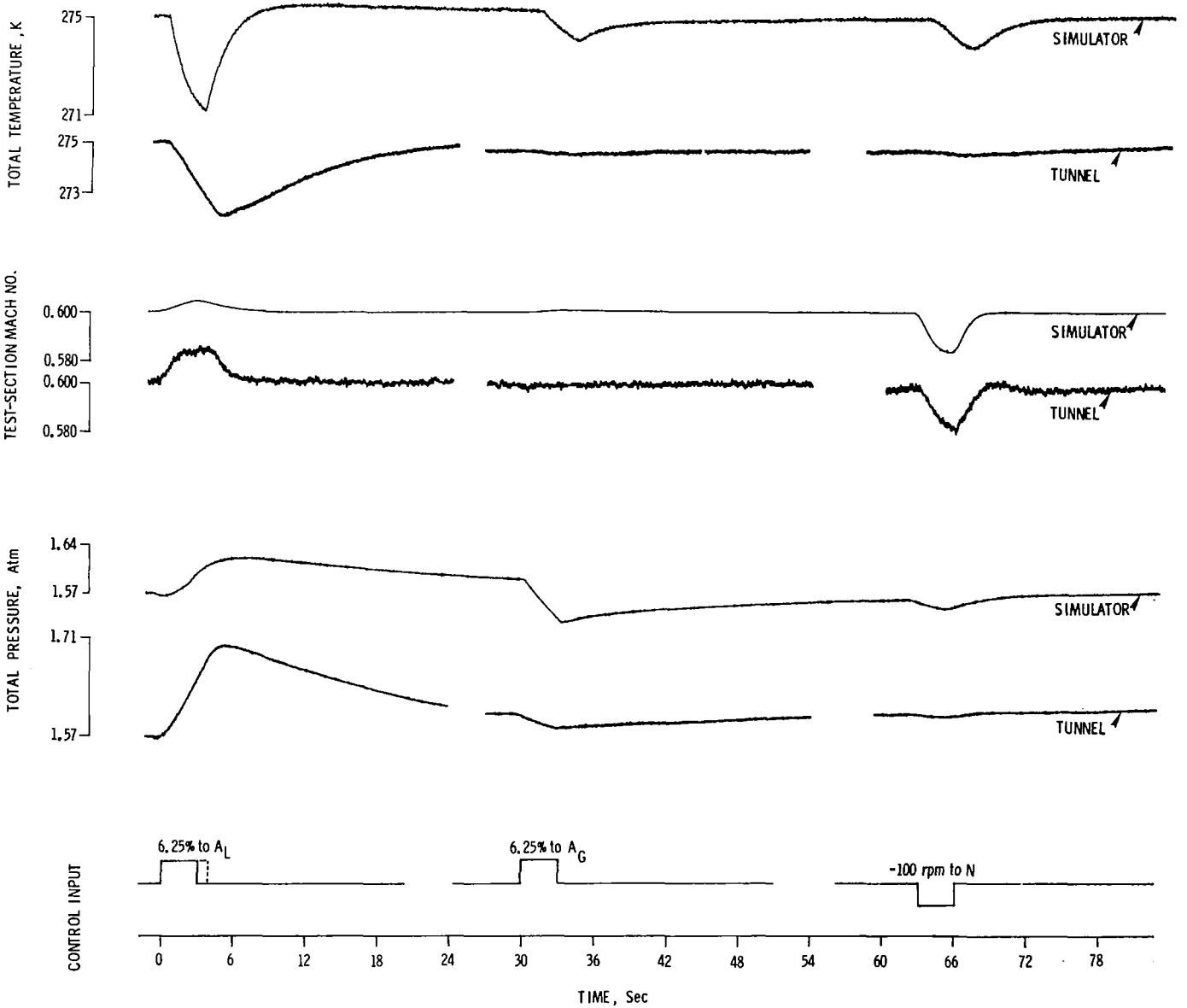

Figure 30.- Simulator and tunnel transient response data at T = 275 K, M = 0.6, and p = 1.57 atm.

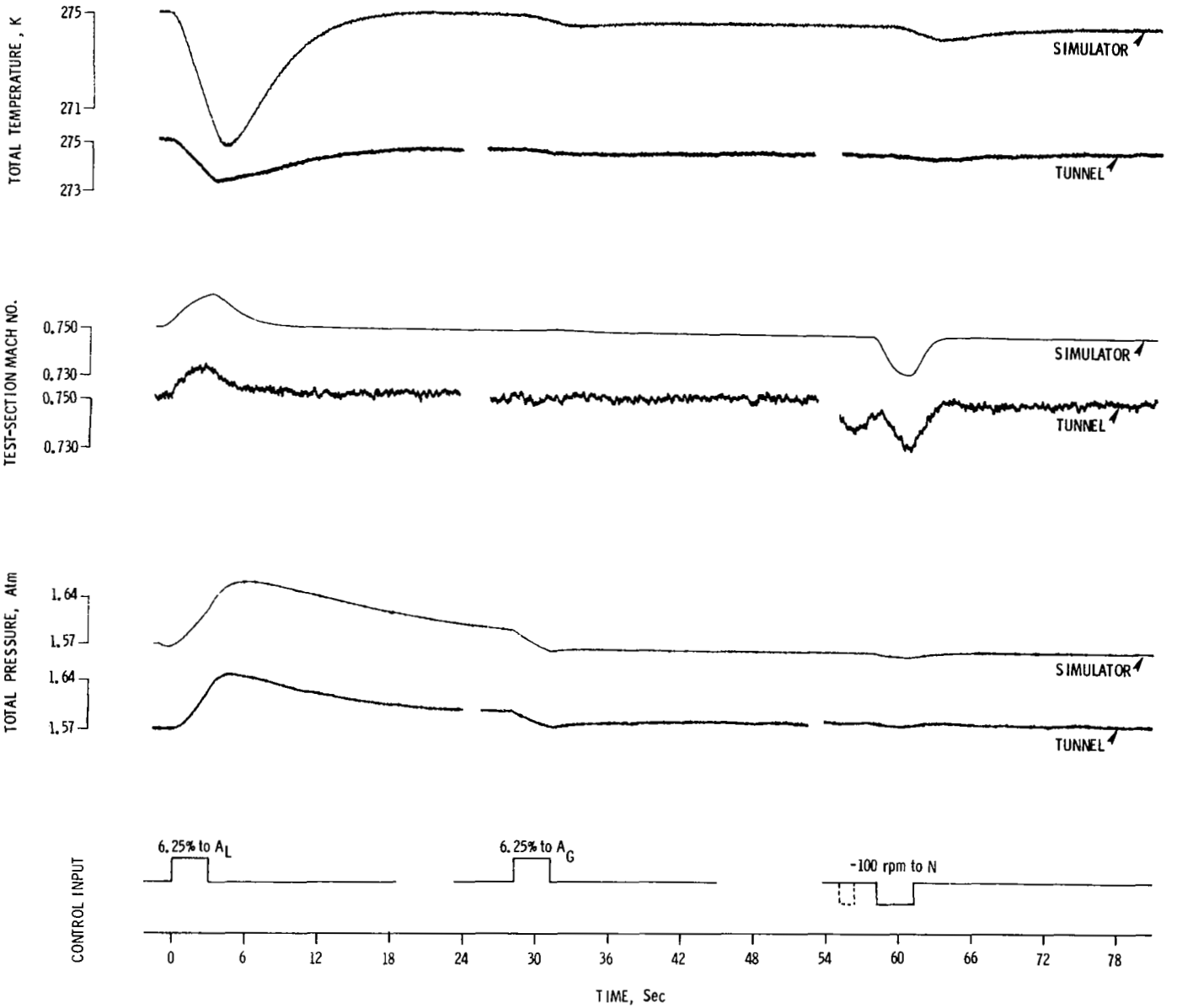

Figure 31.- Simulator and tunnel transient response data at T = 275 K, M = 0.75, and p = 1.57 atm.

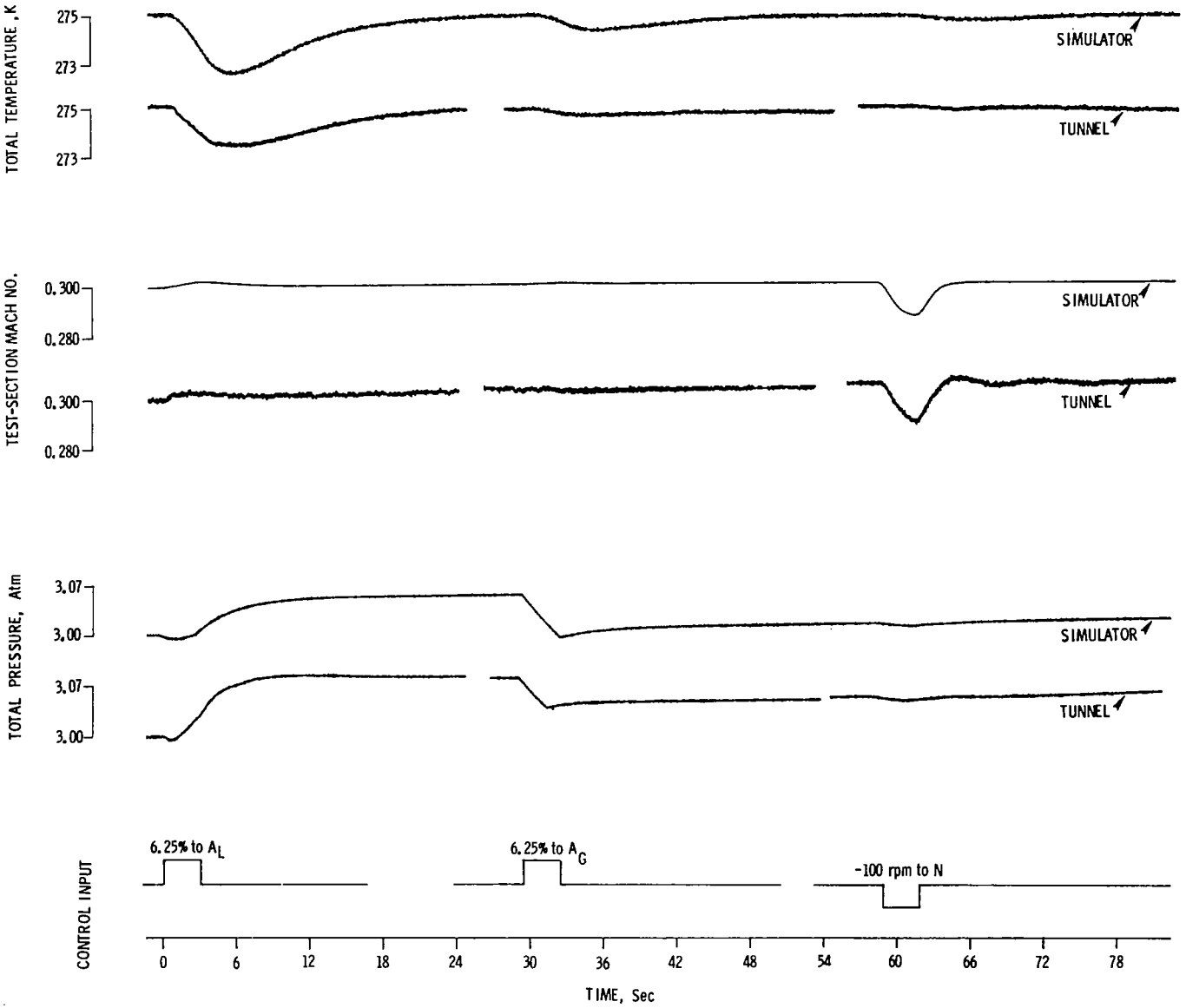

Figure 32.- Simulator and tunnel transient response data at T = 275 K, M = 0.3, and p = 3.00 atm.

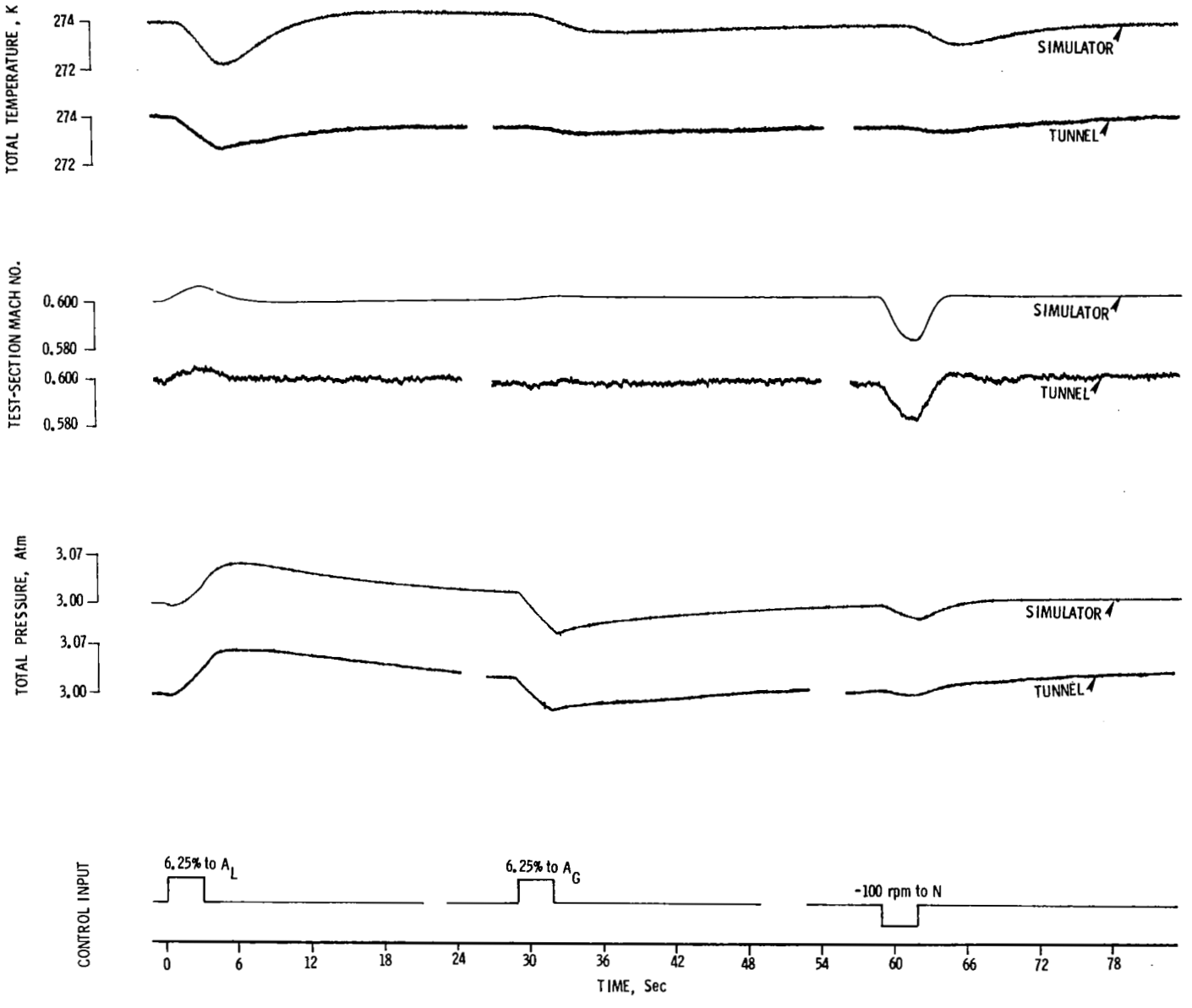

Figure 33.- Simulator and tunnel transient response data at T = 274 K, M = 0.6, and p = 3.00 atm.

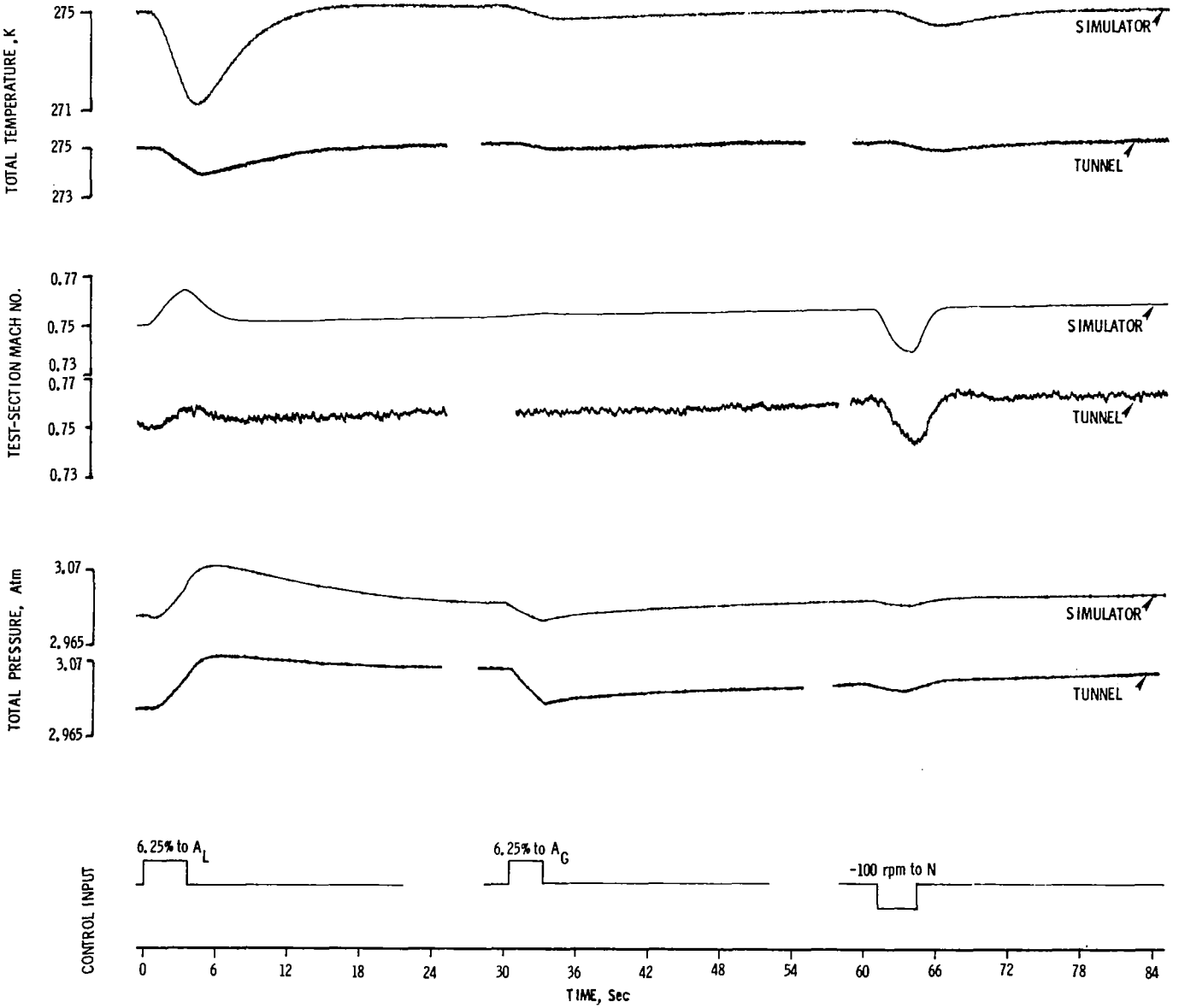

Figure 34.- Simulator and tunnel transient response data at T = 275 K, M = 0.75, and p = 3.00 atm.

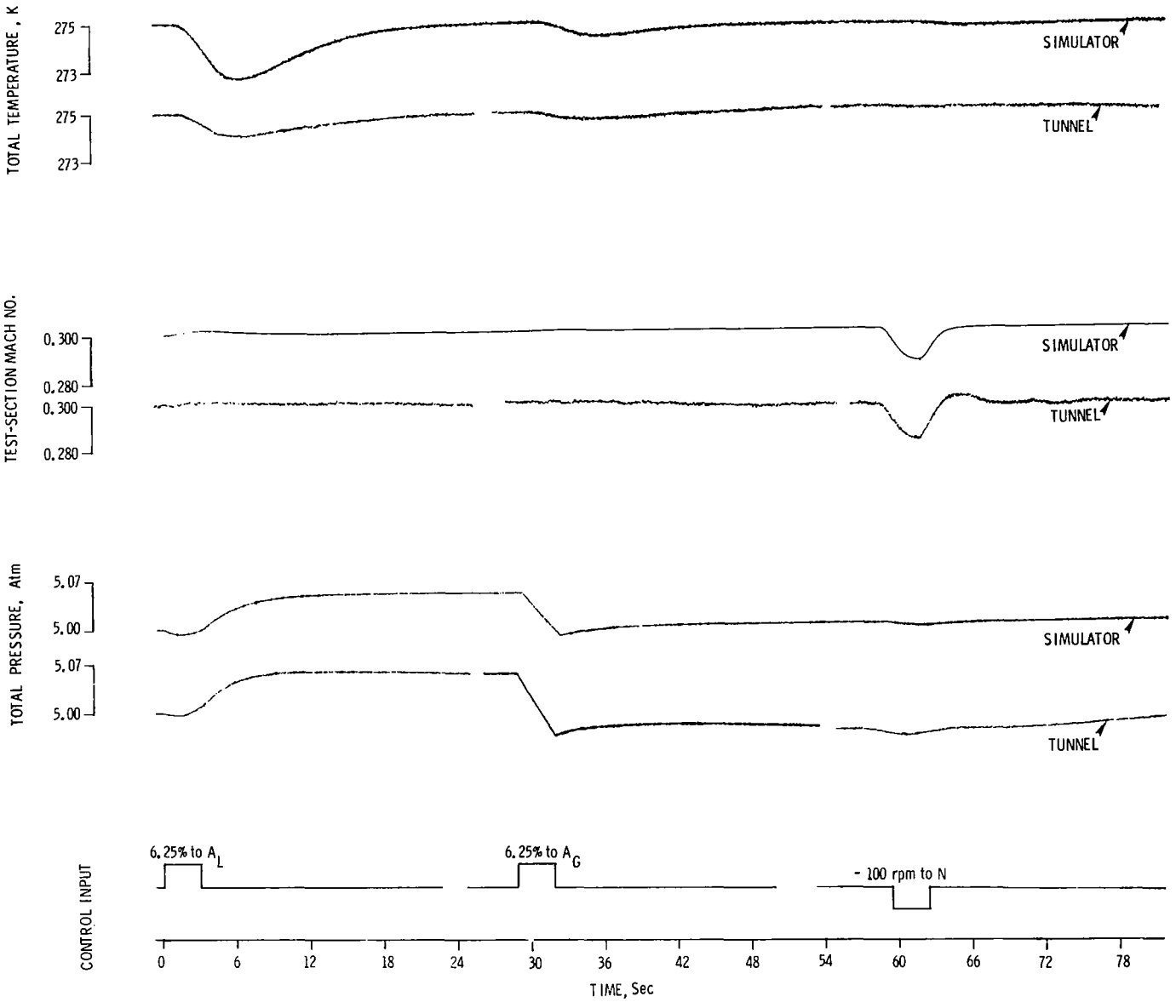

Figure 35.- Simulator and tunnel transient response data at T = 275 K, M = 0.3, and p = 5.00 atm.

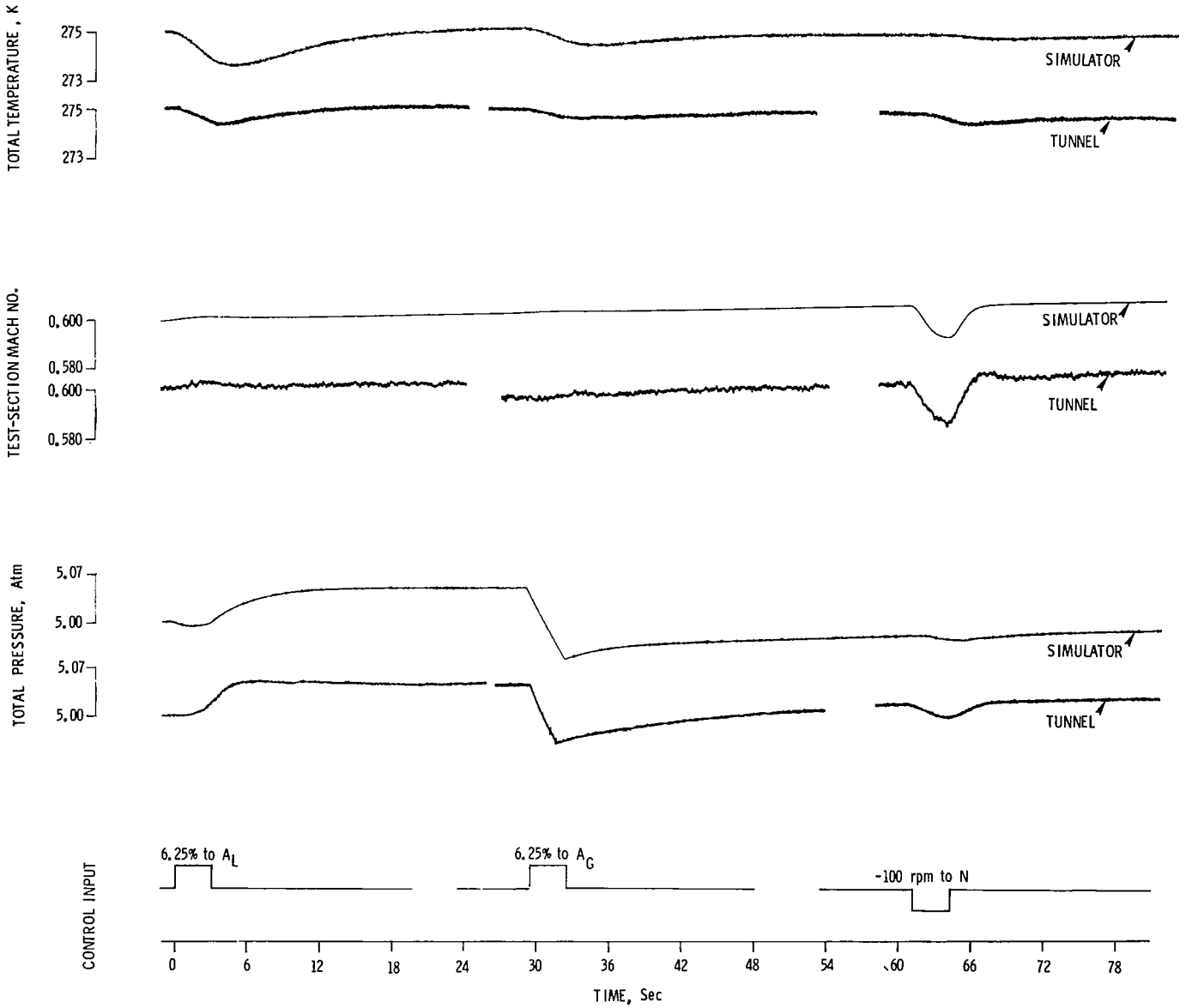

Figure 36.- Simulator and tunnel transient response data at T = 275 K, M = 0.6, and p = 5.00 atm.

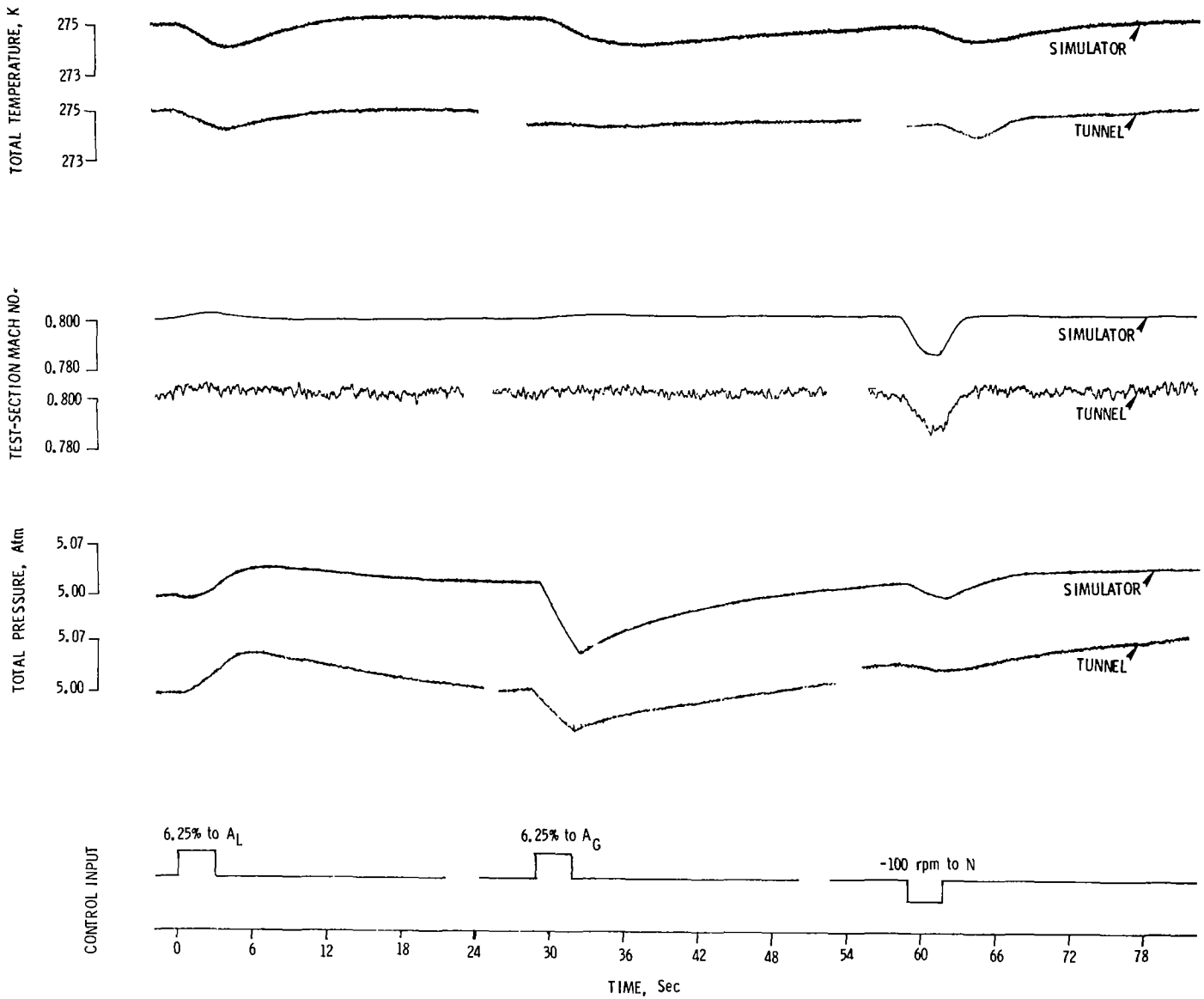

Figure 37.- Simulator and tunnel transient response data at T = 275 K, M = 0.8, and p = 5.00 atm.

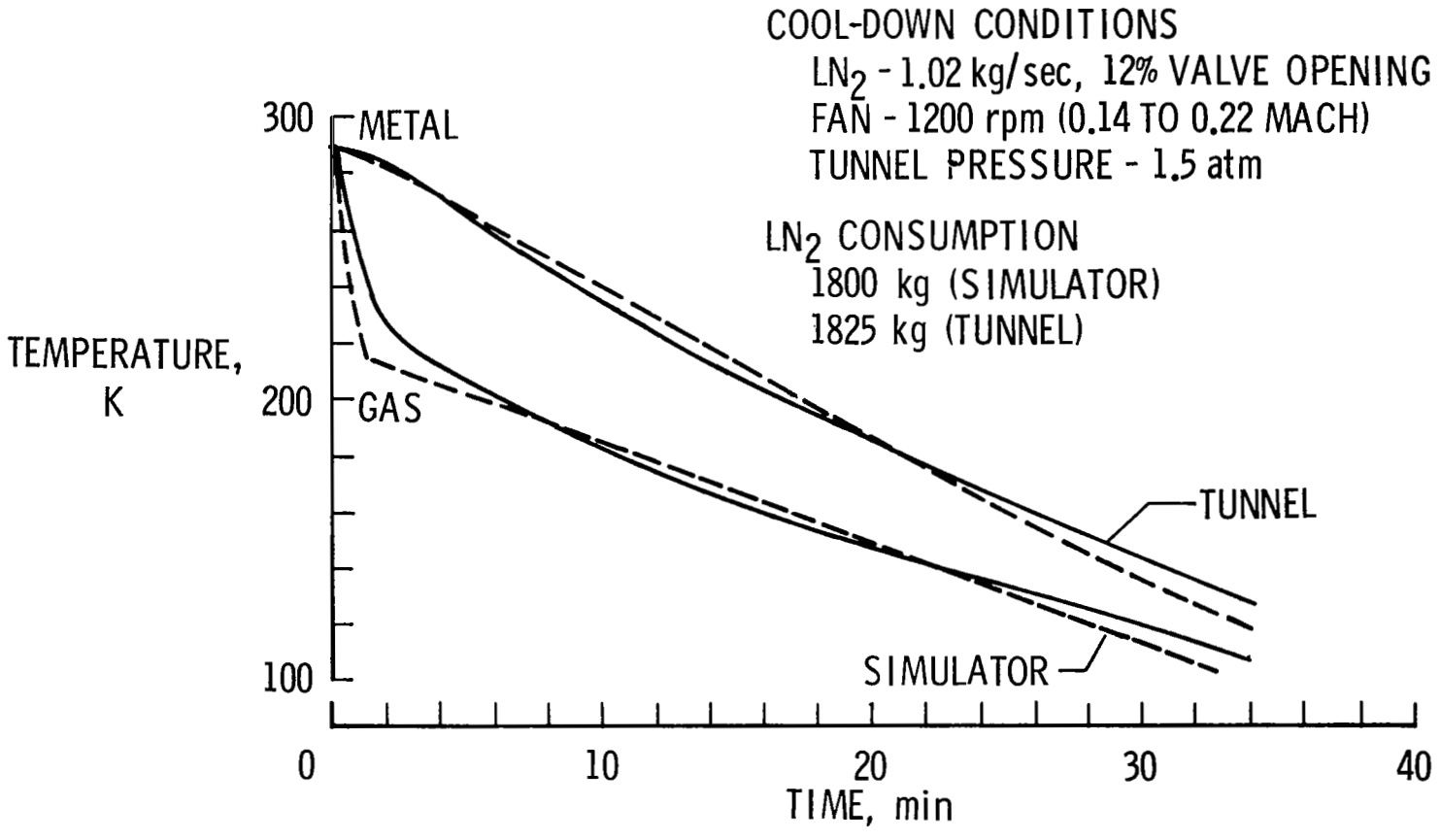

Figure 38.- Cool-down profile for tunnel and simulator.

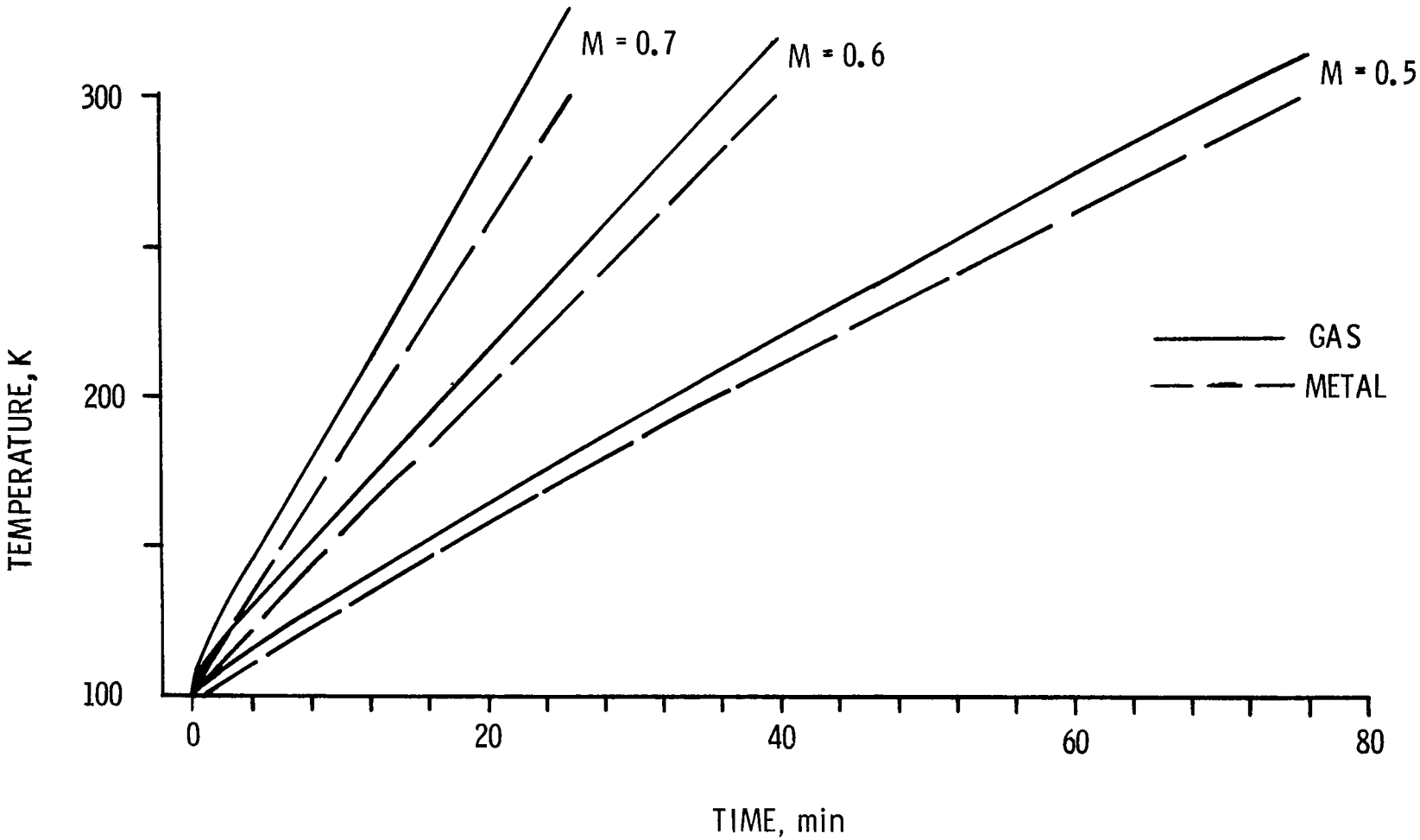

Figure 39.- Simulator warm-up profiles at a pressure of 2.00 atm. LN_2 valve closed at 0.

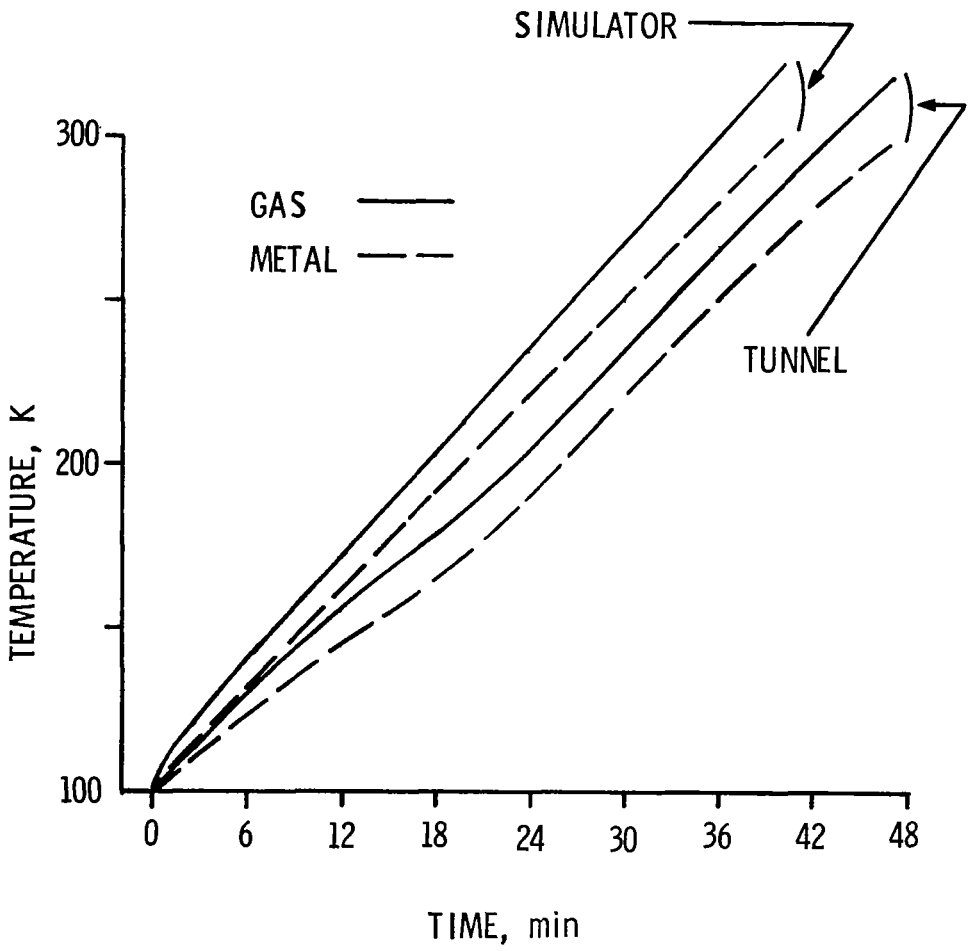

WARM-UP CONDITIONS :

SIMULATOR

Mach no. held constant at 0.6
Total pressure held constant at 2 atm

TUNNEL

Mach no. held at approx. 0.6
Total pressure held at approx. 2 atm

Figure 40.- Comparison of tunnel and simulator warm-up profiles. LN_2 valve closed at 0.

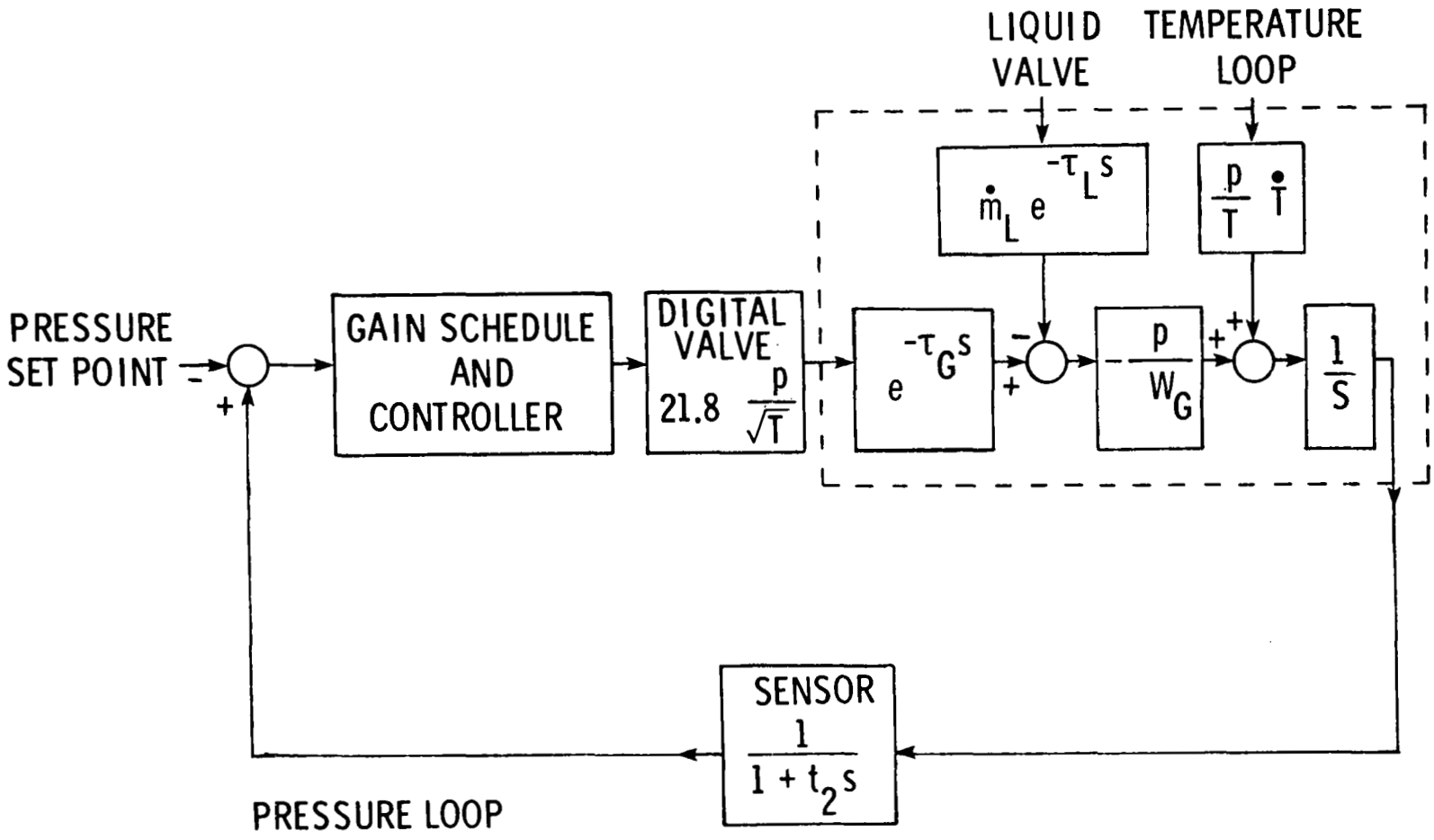

Figure 41.- Pressure-loop schematic for 0.3-m TCT control.

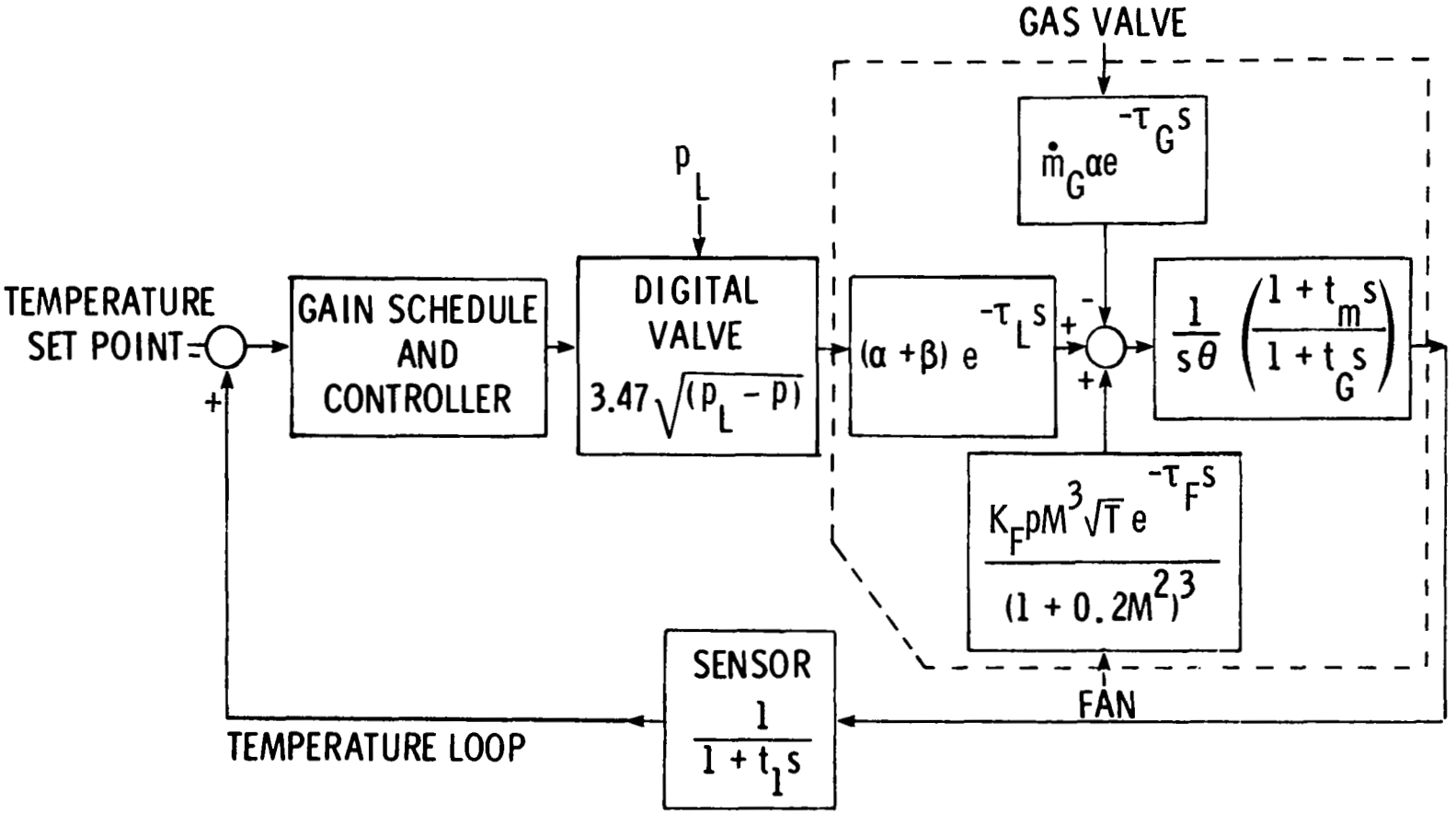

Figure 42.- Temperature-loop schematic for 0.3-m TCT control.

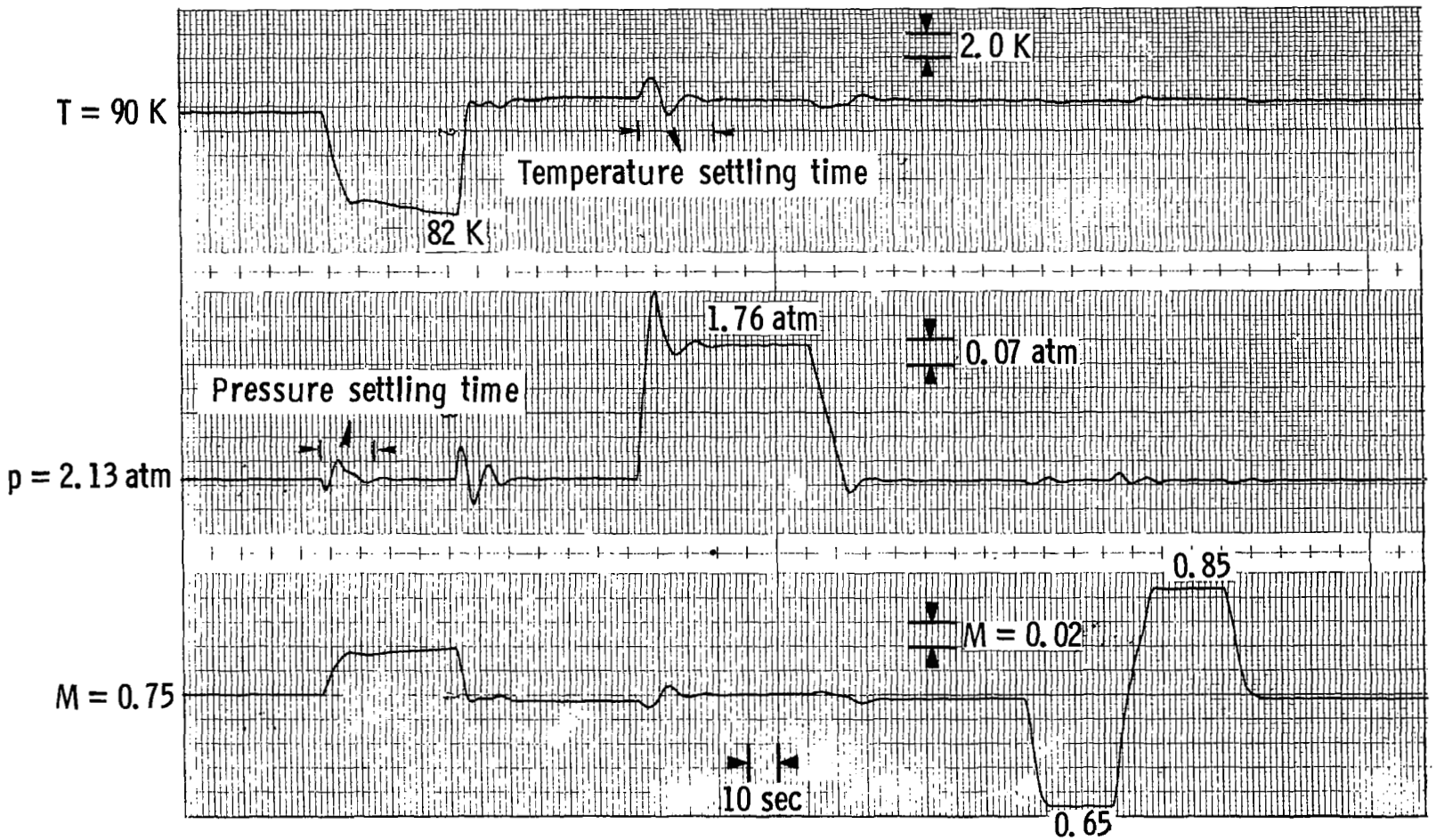

(a) Low tunnel temperature.

Figure 43.- Simulator temperature and pressure closed-loop responses.

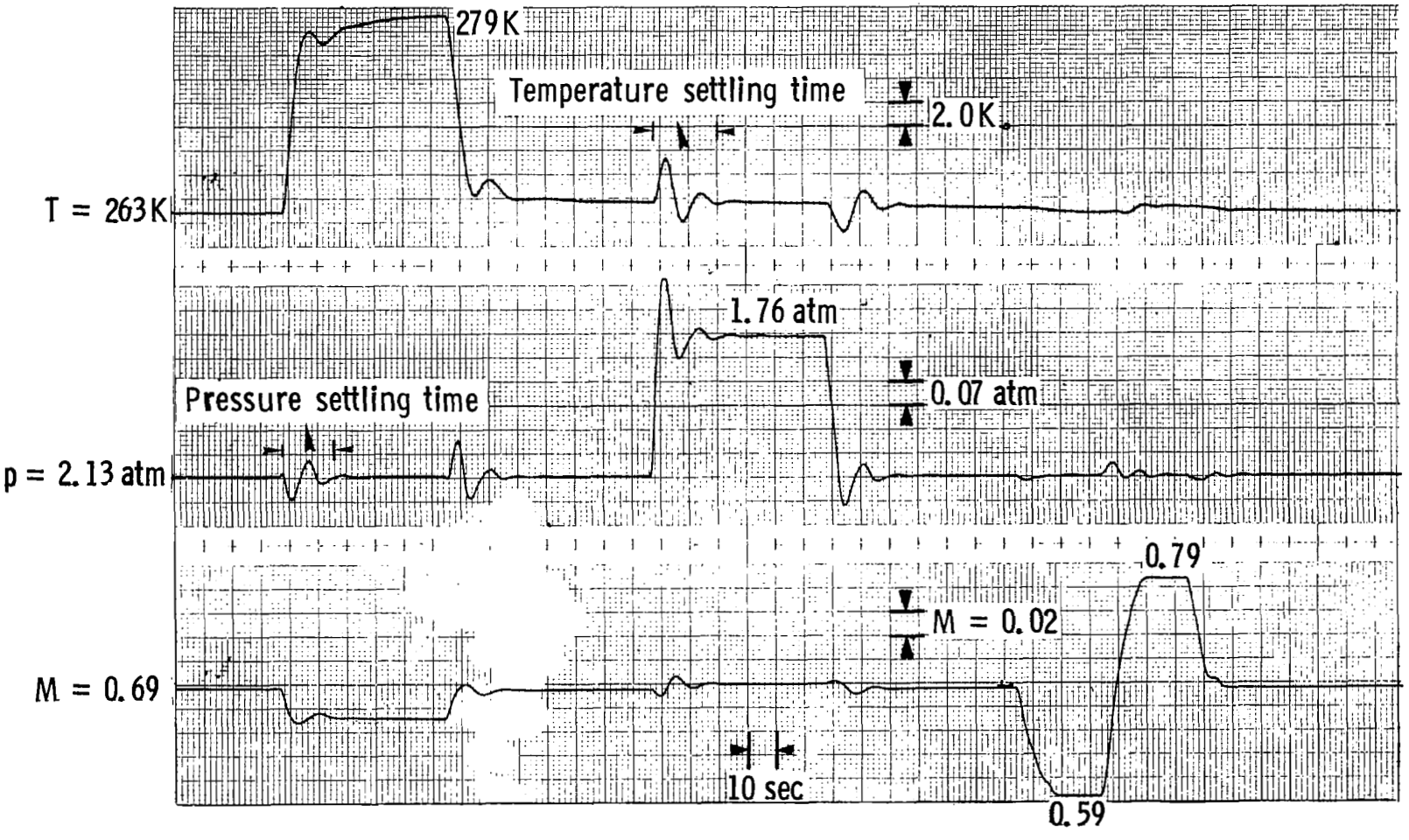

(b) High tunnel temperature.

Figure 43.- Concluded.

1. Report No.	2. Government Accession No.	3. Recipient's Catalog No.
NASA TP-1695		

4. Title and Subtitle	5. Report Date
DEVELOPMENT AND VALIDATION OF A HYBRID-COMPUTER SIMULATOR FOR A TRANSONIC CRYOGENIC WIND TUNNEL	September 1980
	6. Performing Organization Code
7. Author(s)	8. Performing Organization Report No.
Jerry J. Thibodeaux and S. Balakrishna	L-13691
	10. Work Unit No.
9. Performing Organization Name and Address	505-31-53-01
NASA Langley Research Center Hampton, VA 23665	11. Contract or Grant No.
	13. Type of Report and Period Covered
12. Sponsoring Agency Name and Address	Technical Paper
National Aeronautics and Space Administration Washington, DC 20546	14. Sponsoring Agency Code

15. Supplementary Notes

Jerry J. Thibodeaux: Langley Research Center, Hampton, Virginia.
S. Balakrishna: Old Dominion University, Norfolk, Virginia.

16. Abstract

A study has been undertaken to model the cryogenic-wind-tunnel process, to validate the model by the use of experimental data from the Langley 0.3-Meter Transonic Cryogenic Tunnel, and to construct an interactive simulator of the cryogenic tunnel using the validated model. Additionally, this model has been used for designing closed-loop feedback control laws for regulation of temperature and pressure in the 0.3-meter cryogenic tunnel.

The global mathematical model of the cryogenic tunnel that has been developed consists of coupled, nonlinear differential governing equations based on an energy-state concept of the physical cryogenic phenomena. Process equations and comparisons between actual tunnel responses and computer-simulation predictions are given. Also included are the control laws and simulator responses obtained using the feedback schemes for closed-loop control of temperature and pressure.

17. Key Words (Suggested by Author(s))	18. Distribution Statement
Cryogenics Cryogenic wind tunnels Control systems Control of cryogenic wind tunnels Test facilities	Unclassified - Unlimited Subject Category 09

19. Security Classif. (of this report)	20. Security Classif. (of this page)	21. No. of Pages	22. Price
Unclassified	Unclassified	81	A05

For sale by the National Technical Information Service, Springfield, Virginia 22161

NASA-Langley, 1980

5 1 1U,A, 081580 S00903DS
DEPT OF THE AIR FORCE
AF WEAPONS LABORATORY
ATTN: TECHNICAL LIBRARY (SUL)
KIRTLAND AFB NM 87117